UNIVERSITAT DE BARCELONA

Dynamics of cellular decision making processes

David Palau Ortin

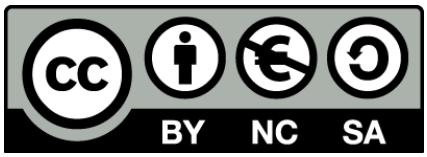

Universitat de Barcelona (UB)

Ph. D. Thesis

Dynamics of cellular decision making processes

Author:
David Palau Ortin

Advisor:
Dra. Marta Ibañes Miguez
Tutor:
Prof. José María Sancho Herrero

Programa de Doctorat de Física

November 2015

Grup de Física No Lineal
Departament d'Estructura i Constituents de la Matèria
Facultat de Física

"My dear, here we must run as fast as we can, just to stay in place. And if you wish to go anywhere you must run twice as fast as that."

Red Queen
(*Through the Looking-Glass*, Lewis Carroll)

Agraïments

El record d'aquesta etapa de la meva vida romandrà marcat per grans vivències i grans persones. No voldria deixar passar l'oportunitat d'agraïr a una part d'aquestes persones sense les quals aquesta tesi no hagués estat possible.

El meu primer agraïment cap a la meva directora de tesi, Marta Ibañes. Moltes gràcies, Marta, per la confiança dipositada en mi. Per tota la paciència i atenció dedicada. Per a generar un entorn de treball immillorable. Per ensenyar-me a valorar les idees d'un mateix amb confiança i, al mateix temps, escepticisme. Per tota la formació científica i personal que de tu n'he extret. Gràcies.

También a mi tutor de tesis y colaborador José María Sancho. Por tu sabiduría, por tu diligencia. Y muchas gracias por compartir la aventura de los patrones.

Als doctorands amb qui he compartit directora. A en David Frigola, a en Juan C Luna, a la Irina i a en Pau Formosa. Moltes gràcies, Pau, per tots els consells, per tota l'atenció i, especialment, per totes les teves qualitats humanes que fan que treballar o conversar amb tu sigui un autèntic plaer. Muchas gracias, Irina, por todos los ánimos y apoyo ofrecido, y por tu compañía en el despacho.

A Ana Caño (CSIC) del Centre for Research in Agricultural Genomics por todo su conocimiento y motivación. Muchas gracias, Ana, a ti y a tu grupo, por compartir conmigo vuestros conocimientos e inquietudes sobre el mundo de las plantas. Moltes gràcies a en Pep, a la Norma i a la Mary Paz entre d'altres.

Gràcies, Alfred Cortés (ICREA) del Institute for Global Health per permetre'm col·laborar amb tu, per la teva paciència i coneixement al a introduir-me al món de la malària.

A tot el departament per contribuir a un bon entorn de treball. A les secretaries del departament, per la vostra feina. Un especial agraïment als membres del Grup de Física No Lineal per compartir la vostra recerca. Gracias a ti, Rubén, por tu talento para el humor.

A totes les persones amb qui he compartit despatx durant aquesta etapa. En especial, a en Carles, a en Guillermo, a en Xavi i a en Marc. Gràcies pels "bons dies", per les converses i pel bon entorn de treball generat.

Aquesta etapa no s'hagués esdevingut de no ser per tots els anys previs de formació i motivació. Grans professors i companys d'estudi hi han contribuït. M'agradaria agrair a tots aquells professors que, amb la seva pedagogia i saviesa, han incrementat el meu propi coneixement i han alimentat la meva motivació per aquest. Gràcies a tots ells, als de les primeres etapes de la meva vida, als de la Carrera i als del Màster.

A tots els companys de la carrera. Esmentant-ne alguns, a l'Eulàlia, a la Núria, a l'Àlex, al Cristian i al Fran

A tots els companys del Màster, una etapa que em va acabar engrescant a iniciar la recerca d'aquesta Tesi.

A aquelles persones la relació amb les quals ha transcendit molt més enllà de l'entorn acadèmic on les he conegut. A l'Elisa, amb qui he compartit pis i de qui m'he nodrit de la seva forma de veure el món. A la Maria Martí, per la teva afectuositat. A en Cristian, pel teu sentit de l'humor. A en Pau (Piu!), per la teva sensatesa. A Pacheco, por tu nobleza. A Laura Casares, zope, por tu apoyo y por dejarte ganar de vez en cuando a algun juego de mesa.

A tu Mario, per la teva racionalitat i per la teva lleial amistat. A tu, Sara, per la capacitat d'arrancar-me un somriure fins i tot el més gris dels dies. En especial a tu, Frigola, per la moltíssima ajuda incondicional que sempre m'has ofert. Pel gran amic que hi ha dins teu. A ti, Juan, compañero de piso y amigo, por todas las bromas que acompañan mi dia a dia. A ti Dani, compañero en muchas facetas, por estar siempre allí. I a tu Lorena, tot l'afecte i suport que trobo en tu. Per ratolins.

A tots els científics, a tots els professors, a tots els divulgadors. A tots aquells que han contribuït i a tots els que contribueixen a crear un món en el que es pugui fer recerca.

A totes les novel·les i cançons que m'han acompanyat durant aquest temps. A la literatura, a la música i a la resta d'arts.

Al Kung Fu. Al meu sifu, José Pinto. Al Dr. Rafa i a la resta de germans del Hung Gar.

A tots els amics de tota la vida. Pel suport, pels ànims i pel vostre afecte. Gràcies Martin per les converses. A tu, Xavi, pel teu reconfortant sentit de l'humor. A tu, Ivette, per la confiança que sempre m'has tingut. I a tu, Balaguer, entre moltes altres coses, per la teva contagiosa obstinació a perseguir els somnis.

A la meva família. Per tots els vostres consells. Pels valors que m'heu transmès. Per tota la vostra estima incondicional. Gràcies, mama, papa, Cristina, iaio, iaia, tieta, padrí i padrina. Moltíssimes gràcies.

The realization of this Thesis would not have been possible without the financial support I had during these years: the FPU fellowship (FPU-AP2010-4656) supported by the Ministry of Education (2011) and the Ministry of Education, Culture and Sports (2011-2015); FIS2009-13360-C03-01 and FIS2012-37655-C02-02, Ministerio de Ciencia y Educación and Ministerio de Economia y Competitividad; 2009SGR14 and 2014SGR878, Generalitat de Catalunya; traveling grants of the Physics Faculty of the University of Barcelona).

A ma germana.

Contents

Part I

INTRODUCTION

Chapter 1

Introduction to cellular decision making

How do cells decide to perform a certain function instead of another? How a wide range of different cell types arises from a single one in order to form a multicellular organism? The dynamics of these biological processes involves networks of interactions and the integration of external stimuli. Nonlinear behaviours underlie these processes. Furthermore, these cellular decisions take place in cellular environments where the discrete nature of biochemical reactions and thermal fluctuations are relevant. Both nonlinearities and stochasticity motivate the study of cellular decision making using approaches from the field of Physics.

The cell is the unit of life of the living beings. Cells, either as unicellular organisms or as part of a tissue of a multicellular organism, can perform different functions thanks to their capability of changing their expression state. The transport of molecules, vesicle formation, enzyme synthesis are some examples of these functions (Alberts et al., 2008). These functions are not necessary permanently active, and their activation is triggered by intracellular or extracellular stimuli.

The turning on and off of some of these functions can be univocally determined by the environment: i.e., in the face of a certain condition, cells perform a certain specific response. However, cells can also show multiple behaviours under the

same stimulus or environment. Hence, two types of processes by which cells can change of state can be distinguished: those where the response is completely determined by the signals perceived by the cells (induced change) (Alberts et al., 2008), and those where the different responses under the action of signals have a probabilistic rule (cellular decision making) (Perkins and Swain, 2009; Balazsi et al., 2011).

Cellular decision making processes are ruled by stochastic dynamics since, under the same conditions, cells can choose between different states (defined through the functions the cell performs or by its expression profile). These decisions can happen spontaneously due to stochastic effects, or being induced by intra, extra or intracellular stimuli that interact with the dynamics of the cell.

The main goal of this thesis is to understand general aspects of cellular decision making processes from a theoretical point of view. To do so, we make use of Dynamical Systems tools in order to connect the properties of the decision with the relevant dynamical behaviour of the system while it is being made. This dynamical behaviour is dependent on signals that modify some parameters that control the interaction between the variables involved in the decision. We analyse the properties of cellular decisions in two systems: a system with cell-autonomous dynamics (Chapters 3 and 4), and a system of interacting cells in which the decision is made jointly by all the tissue (Chapter 5). Despite the strong difference in spatial coupling, both systems share similarities in the circuit architecture of the interactions that describe the dynamics. Before focusing on our results on cellular decisions, in Chapter 2 we review some general aspects of a genetic circuit that exhibits this type of architecture and on decision making processes. Finally, we tackle a particular question that arises in a decision made by the parasite that causes malaria in humans (Chapter 6).

This chapter reviews the biological concepts that underlie cellular decision making processes, giving some examples of cellular decisions (Section 1.1). Furthermore, it introduces a theoretical approach to study cellular decision making in order to understand general aspects of theses processes (Section 1.2).

1.1 Cell states, signals and stochasticity

A cell state can be defined by certain levels of gene expression that determine which proteins are being produced and at which rate. Proteins are macromolecules that perform many functions within cells. These functions include catalysis of metabolic reactions, DNA regulation, response to external stimuli, and transport of molecules (Alberts et al., 2008).

The protein levels of a cell depend on how the genetic information is regulated. The protein synthesis involves two main steps that are described by the Central Dogma of Molecular Biology: *Transcription* and *Translation* (Alberts et al., 2008). Several factors can regulate these two processes, e.g., RNA interference, chromatin modifications or transcription factors. Transcription factors are proteins that, alone or as part of a complex, promote – activate – or block – inhibit – the reading of specific genes. According to this, the synthesis of a certain protein can be regulated by the action of other proteins (including itself). These interactions define a network that is described by the biochemical regulation between the different proteins encoded in the genetic information of the cell. For instance, taking into account that the production of transcription factors is also regulated by transcription factors, a transcriptional network with the genes as nodes and the interactions between their products as edges can be defined (Alon, 2007b; Tyson and Novak, 2010). The dynamics resulting from these regulations are relevant for cell state transitions and cellular decision making processes.

1.1.1 Cell-autonomous decisions

Several cellular decisions have been studied in very different biological systems, where cells integrate stimuli to make the decision (Losick and Desplan, 2008; Balazsi et al., 2011). We denominate *cell-autonomous decision* the cellular decision that is independent of the choice of the other cells of the population. Cell-autonomous decisions are recurrently observed in unicellular organisms, but the development of multicellular organisms also poses some examples of them (Losick and Desplan, 2008; Balazsi et al., 2011). Given a certain stimulus, the responses each cell performs are determined by probabilities – that do not depend on the state of the other cells. Consequently, if all the cells are

under the effect of the same signal, the resultant cell population gives rise to a stochastic pattern where all the final cell types involved in the decision are distributed randomly (Losick and Desplan, 2008). Otherwise, if the external signal is heterogeneous, cells can be distributed cell-autonomously according to a spatially ordered pattern (Wolpert, 1969), for instance. In this case, although the cells exhibit different responses, this variety of responses is a readout of the variety of the signal (induced change). So, these processes can not be classified as cellular decision making.

Cell-autonomous decision making has been deeply studied in bacteria. Different cell states have been characterized in *B. subtilis* (Kearns and Losick, 2005; Maamar and Dubnau, 2005; Suel et al., 2006; Maamar et al., 2007; Suel et al., 2007; Lopez et al., 2009) and *E. coli* (Balaban et al., 2004; Lewis, 2007) in response to different environmental stress conditions. In higher order organisms, the maturation process of *Xenopus laevis* oocytes is a paradigmatic example of a two fate cell-autonomous decision, where an homogeneous population of immature oocytes gives rise – driven by a progesterone signal – to a heterogeneous population where some oocysts have become mature and the others have not (Ferrell and Machleder, 1998; Xiong and Ferrell, 2003). A similar phenomenon happens in HL60 cells (neutrophil precursor cells in mammals), where DMSO signal (dimethyl sulfoxide) induces a cell-autonomous decision whereby some HL60 cells differentiate into neutrophils (Chang et al., 2006). Despite the fact that cell-autonomous decisions are common in single cell systems, tissue formation also sets some examples of them. For instance, photoreceptor cells that compose the complex eye of *Drosophila melanogaster* larva choose between either become yellow or pale (Mikeladze-Dvali et al., 2005; Wernet et al., 2006; Vasiliauskas et al., 2009; Graham et al., 2010). This decision gives rise to a stochastic pattern where these two cell types are randomly distributed. The choice of olfactory receptors in the walls of the nasal cavity in mouse form a stochastic pattern as well (Mombaerts, 2004).

Plasmodium falciparum, one of the parasites that causes malaria in humans, also poses an example of cell-autonomous decision making. During the bloodstream stage of this parasite, it presents to states: *merozoite* and *gametocyte*. Each merozoite proliferates in the blood and, at each proliferation cycle, it stochastically chooses between remaining as a merozoite or becoming a gametocyte-committed cell (Bousema and Drakeley, 2011; Kafsack et al., 2014). In this

thesis we are going to study this example of cell-autonomous decision.

Although bacteria are unicellular organisms, they have a mechanism of communication between them that can modulate the changes of state of the other bacteria of the colony. This prokaryotic mechanism of communication is called *quorum sensing* and it relies on the production, spreading through diffusion and sensing of small biomolecules. Bacteria integrate these molecules to know the size of the colony and use this number – as an external signal – to decide their fate. Several decisions are controlled by a quorum sensing mechanism: competence activation, sporulation and virulence among others (Bassler and Losick, 2006; Lopez et al., 2009). Because of this mechanism of communication, these decisions may not be classified as entirely cell-autonomous.

1.1.2 Pattern formation

In multicellular organisms, cells are usually arranged according to certain spatial distributions to form tissues. The functions and the shapes of these tissues depend on the spatial arrangement of different cell types. In this thesis, we name *patterns* these spatial distributions of cell types. We have already reported in the previous section that stochastic patterns can arise from autonomous cellular decisions (Losick and Desplan, 2008). However, pattern formation typically requires some spatial information or cell-to-cell communication.

Several strategies are recurrently used for pattern formation in development (Salazar-Ciudad et al., 2003; Morelli et al., 2012; Rue and Garcia-Ojalvo, 2013). One early question that arised in pattern formation is which mechanism can let the cells know their spatial position. Lewis Wolpert in 1969 proposed a mechanism by which cells could know their spatial position according to gradients of certain diffusive molecules (morphogens) (Wolpert, 1969, 1971). Morphogen gradients are present during several development processes and they are usually generated through diffusion from a source of cells in the boundaries of the tissue (Gilbert, SF, 2006). Cells change of fate according to the concentration of morphogen they detect, with a threshold-like mechanism, for instance. Therefore, the fate reached by a cell is completely determined by the signal it receives (e.g. the morphogen concentration). In other words, for a given signal value, a cell does not choose among distinct cell fates (it is an induced change).

Despite the fact that diffusion can typically homogenize heterogeneities, Alan Turing, in 1952, pointed that it can also drive pattern formation (Turing, 1952; Murray, 2002). According to Turing's study, reaction-diffusion systems of interacting chemical species that have different diffusion coefficients can destabilize the homogeneous starting state and give rise to a pattern. Two decades later (1971), Meinhardt and Gierer extended the mechanism (also so-called as Gierer-Meinhardt patterns) by identifying two key ingredients: a short range activator and a long range inhibitor (Gierer and Meinhardt, 1972; Meinhardt, H, 1982).

Another mechanism that drives pattern formation is by direct cell-to-cell communication. Patterns that arise from this mechanism are fine-grained and are produced by the interaction between membrane molecules in neighbouring cells. Lateral inhibition is a paradigmatic example of this interaction where a cell prevents its adjacent cells to choose its own fate. Notch signalling pathway has been identified as a recurrent lateral inhibition mechanism that gives rise to pattern formation during animal development (Collier et al., 1996; Eddison et al., 2000; Oates et al., 2012; Neves et al., 2012; Formosa-Jordan et al., 2013; Petrovic et al., 2014; Hamada et al., 2014). This lateral inhibition mechanism amplifies the stochastic differences between statistically identical cells in order to give rise to two distinct cell types.

Some patterning processes take place in a more complex manner, with different mechanisms – like those mentioned above – working together (see, for instance,(Salazar-Ciudad et al., 2003; Formosa-Jordan et al., 2012; Marcon and Sharpe, 2012; Green and Sharpe, 2015)).

1.1.3 Signals, multistability and network motifs

The probability of each choice of a cellular decision is often controlled by a signal that induces this decision. These inductive signals can have different origins. For instance, changing environments drive unicellular organisms to make decisions about their current state (McClean et al., 2007; Acar et al., 2008; Kuchina et al., 2011). For these unicellular organisms, the response in front of this external information may be crucial in order to optimize their survival or to improve the competence of each individual. Furthermore, cells within multicellular organisms also receive inductive signals that make them decide too about changing their current state (Chang et al., 2006, 2008; Kalmar

et al., 2009). This occurs during differentiation of developing organisms. In this section we describe how a signal can affect the system in order to drive a change of state.

In the 40's, Conrad H. Waddington proposed the epigenetic landscape metaphor to illustrate cell differentiation processes during development (Waddington, 1957). The Waddington landscape idea describes a developing cell as a ball rolling down a landscape, from the top of the hill down into the valley. During this process, several bifurcations take place, representing cellular decisions during development. The bottom of each valley would corresponds to a cell state, while the valley describes the basin of attraction of this cell state. According to Waddington landscape metaphor, the number of available cell states increases during development (from monostability to multistability).

Stuart Kauffman showed that interactions between genes produce attractors of the dynamics (Kauffman, 1969a,b). He showed that even a very large network only exhibits a few number of stable dynamics. These results suggest that the network of interactions that regulates gene expression within cells converges to few different attractors, defining several but not infinite number of different cell states.

According to the interpretations of Kauffman and Waddington on cell states, cellular decision making can be described as a transition that modifies the number of valleys of the landscape – in the metaphor of Waddington – or the number of stable behaviours of a network – in the Kauffman interpretation.

The multistability present in the above interpretations and required for cellular decision making arises from the circuitry or wiring of interactions and from the nonlinearity of these interactions, when viewed in terms of multiple attractors of the dynamics of interacting elements. These nonlinearities arise from the type of biochemical reactions taking place.

Topological analysis of the transcriptional networks of *E. coli* and yeast has shown that there are some molecular circuits with recurrent architectures (Alon, 2007b). These sub-grafs are called *network motifs* and their isolation and their study can be important in order to understand the behaviour of a transcription network as a whole. Since the study of transcriptional networks started, several network motifs have been characterized (Tyson et al., 2003; Alon, 2007a; Davidson, 2010).

One of the simplest and most abundant network motif is negative auto-regulation (negative feedback loop) in which a transcription factor represses its own production. It has been shown – both theoretically and experimentally – that this motif can perform two important regulatory functions: to reduce fluctuations and to accelerate the response to a signal(Alon, 2007a). Another very frequent network motif is positive auto-regulation (positive feedback loop), where a gene product promotes its own expression. The dynamical features exhibited by this second motif are somehow opposite to those of negative auto-regulation, i.e, it increases response times and fluctuations (Alon, 2007a). Another important property of the positive auto-regulation architecture is the capability to perform a bistable response when nonlinearities in the dynamics are strong enough (Alon, 2007a).

Crosslinked interactions, in which two transcription factors are involved, each one promoting or inhibiting the production of the second one, have been also characterized and found in transcriptomes (Gardiner, 2005; Mikeladze-Dvali et al., 2005; Kalmar et al., 2009). Negative cross-regulation – also known as mutual inhibition – is an example of these architectures. In this circuit, each gene product inhibits the expression of the other gene. So, each species promotes its own production by inhibiting its inhibitor. The mutual inhibition motif corresponds to a positive feedback loop architecture, like positive auto-regulation, and so, it can elicit bistable responses as well (Ackers et al., 1982; Tian and Burrage, 2006).

Crossed inhibition circuits have been also characterized in tissues where each cell interacts with its neighbours. Lateral inhibition is an example whereby a cell of the tissue prevents expression of a certain protein in the adjacent cells (Artavanis-Tsakonas et al., 1999; Schwanbeck et al., 2011; Andersson et al., 2011). These interactions are driven in several differentiation processes in animals by Notch pathway. When all cells interact with each other through lateral inhibition, spontaneous symmetry breaking driving periodic patterning, arising from small variability between cells, can occur (Collier et al., 1996; Wearing and Sherratt, 2001; O'Dea, R. D. and King, J. R., 2011, 2012). Spontaneous pattern formation arises from the linear destabilization of the homogeneous solution, where all the cells of the tissue are in the same state (Murray, 2002; Cross and Greenside, 2009). Additionally to this crossed inhibition (trans interaction), it has been also studied theoretically the different solutions of the

system when a kind of auto-activation (cis interaction) is present (Sprinzak et al., 2010, 2011; Formosa-Jordan and Ibañes, 2014).

1.1.4 Stochasticity in cellular decisions

Molecular reactions that rule cellular decisions, as many cellular processes, take place in a stochastic environment due to thermal fluctuations. Because of this noise, cells, even under the same exact conditions, can behave differently. This noise has been classified in two types according to its source: *intrinsic* and *extrinsic* noise. Intrinsic noise is the dynamical noise produced by the randomness associated to the reactants meeting in the molecular reactions. Low copy numbers of the species involved in the reactions increases this noise. The extrinsic noise comes from differences between cells in concentration and localization of the substances involved in gene regulation (Elowitz et al., 2002). Heterogeneous populations can be originated by an identical signal because of these sources of stochasticity (Ishimatsu et al., 2013).

While some cellular processes are performed by mechanisms that reduce the effects of noise (Becskei and Serrano, 2000; Koseska et al., 2009; Sokolik et al., 2015), others make use of it and take advantage of this stochasticity to drive the cellular decision (Mombaerts, 2004; Balaban et al., 2004; Acar et al., 2005; Wernet et al., 2006; Maamar et al., 2007; Suel et al., 2007; Acar et al., 2008; Losick and Desplan, 2008; Beaumont et al., 2009; Balazsi et al., 2011; Weber and Buceta, 2011, 2013; Kafsack et al., 2014). For instance, noise can increase the sensibility of some decisions as a kind of stochastic resonance (Wiesenfeld and Moss, 1995; Maamar et al., 2007; Suel et al., 2007). In pattern formation processes that arise from destabilization of a homogeneous state of the tissue, noise is essential to drive the small differences required to trigger patterning. These small differences are then amplified by the specific pattern formation mechanism (Meyer and Roeder, 2014). This coexistence of different cell types in an organized pattern within a tissue gives rise to complex structures, such as organs, that perform emergent behaviours. Also from the perspective of the individual cells, stochasticity contributes favourably to cellular decision making by allowing for multiple responses under the same conditions. It has been studied that stochastic differentiation takes place when cells are unable to fully adapt to their environment. This happens when they have to decide between

two mutually exclusive functions that, nevertheless, are both crucial for survival. Parasites that cause malaria, for instance, have to choose between the proliferating state or the transmissible differentiated state in the bloodstream stage. This decision is driven by a purely stochastic epigenetic mechanism (Kafsack et al., 2014) whereby the parasite population is heterogeneously distributed between these two states. A similar case is found in Cyanobacterias. It requires both photosynthesis and nitrogen fixation and both functions are exclusive. They solve this dilemma by dedicating a cell subpopulation entirely to nitrogen fixation while the rest performs the photosynthesis (Wolk, 1996). It remains unclear if this decision is purely cell-autonomous. Galactose switch in yeast offers an example where the probabilistic behaviour of the decision is observed along time by a stochastic switching (Acar et al., 2008; Frigola et al., 2012). In this example, cells are exposed to a mixture of low glucose and high galactose and so they choose between either utilizing the limited amount of glucose or growing on galactose (Acar et al., 2005). Another stochastic-driven phenomenon is bet hedging (Balaban et al., 2004; Losick and Desplan, 2008; Beaumont et al., 2009). This strategy consists in hedging the range of responses in order to ensure that a certain subpopulation could survive if the environment conditions suddenly change. This mechanisms have been studied in deep in bacteria (Balaban et al., 2004; Beaumont et al., 2009).

1.2 Methodological approach of cellular decision making

In the last decade, the new techniques of visualization that have provided quantitative data in several biological processes, in combination with new genetic tools, have both strongly promoted a cross-communication with theoretical approaches coming from disciplines such as Physics. This new approach, characterized by mathematical and computational modelling of biological systems together with quantitative data, to unravel the complexities of living organisms has been defined as Systems Biology (Alon, 2007b). Systems Biology addresses the study of complex biological systems using a holistic approach which focuses on the emergent properties of the system. Multidisciplinariety is also a common, even defining, feature of Systems Biology, using tools that were traditionally associated to other disciplines such as Mathematics or Physics.

As many other processes approached by Systems Biology, using the tools of Dynamical Systems (Strogatz, 1994), cell-autonomous decision making driven by signals have been studied from the theoretical point of view (Guantes and Poyatos, 2008; Huang et al., 2007; Huang, 2009; Verd et al., 2014; Hong et al., 2011, 2012; Pfeuty, 2012; Pfeuty and Kaneko, 2009; Machens et al., 2005). According to it, cellular decisions may be described as transitions between different attractors of the dynamics. The number of attractors available to a system is determined by its set of parameter values as well as by its interactions (network or circuit architecture). Changes in the value of some of these parameters (control parameters), can result in changes in the attractors of the system: some attractors can disappear, some new attractors can appear and/or the attractors can change their state variable values. In this context, cell state transitions can be driven by signals which change a control parameter and, hence, the number of attractors of the system (Huang et al., 2007; Guantes and Poyatos, 2008; Pfeuty and Kaneko, 2009; Hong et al., 2011; Ferrell, 2012; Hong et al., 2012). These changes of the number of attractors driven by inductive signals have been also experimentally observed in systems where both monostable or bistable regimes are found (Ishimatsu et al., 2013; Bhalla et al., 2002). In decision making processes driven by signals, the temporal profile of these stimuli is also relevant to determine the final response of the system (Werner et al., 2005; Wong and Wang, 2006; Nene and Zaikin, 2012; Nené et al., 2012; Nené and Zaikin, 2013; Palau-Ortin et al., 2015).

Deterministic differential equations describe the dynamics of a system and the stable states in a regime where the noise contributions are negligible. However, cellular decision making processes take place in a noisy environment, where fluctuations are inherently associated to their dynamics. Hence, cellular decision making processes, where noise is relevant, have to be modelled using stochastic methods to describe the dynamics. There are different methods to model stochastic systems (Gardiner, 2005; Van Kampen, 2007). In this section we are going to briefly review three stochastic methods: Markov chains, Master equations and Stochastic differential equations.

A Markov chain is a random process that describes the probability of discrete variables (e.g. number of cells, number of molecules) over discrete time variable (i.e. step, cycle, etc). Any Markov chain verifies the so-called Markov property that claims that the next state depends on the current state and not on

the sequence of events that preceeded it (Van Kampen, 2007; Wilkinson et al., 2006). This stochastic description is typically used for purely stochastic processes whose temporal variable is discrete (see Chapter 6 of this thesis). Systems with continuous-time evolution can be described by the continuous-time version of the Markov chain model (Wilkinson et al., 2006).

Master equations are used to describe stochastic processes continuous in time of discrete (or continuous)-state variables (e.g. number of molecules) that can be modelled by the probabilistic switching between states (Van Kampen, 2007). The equations are the variation over time of the conditional probability that the system occupies one state at a given time provided it was in a given state in a previous time. The dynamics are markovian. Daniel Gillespie presented in 1976 an algorithm to implement biochemical reactions in terms of how the number of molecules changes over time according to the probability per unit of time each reaction has to occur (Gillespie, 1977). This method is a kind of kinetic Monte Carlo method for simulating the dynamics of discrete numbers of reactants.

Langevin equation are stochastic differential equations – proposed by Paul Langevin in 1908 – that describe the time-evolution of a system by adding a perturbational term (noise term) to the deterministic version of the equation. Langevin equations model processes where both the variable that defines the system state and the temporal variable are continuous (Van Kampen, 2007). The dynamics of the noise term is faster than the dynamics of the system variables and it is responsible of the stochastic nature of the Langevin equations. Gaussian noises with no auto-correlation between any two time interval describe also markovian processes.

In this Thesis all these methods have been used and hence it constitutes an example of how these different stochastic procedures can describe cellular decision making processes.

Chapter 2

An exploration of the mutual inhibition with auto-activation motif

2.1 Introduction

In this Chapter we present an exploration of a simple network motif that involves two molecular species, X and Y. These species are regulated by mutual inhibition with auto-activation. Consequently, from the point of view of each gene of the motif, they are in a double positive feedback loop architecture (Fig. 2.1). The main feature of this motif is the richness of the different stability regimes it exhibits (Guantes and Poyatos, 2008). In addition, this motif underlies several cell state transitions in different organisms and systems (Huang et al., 2007; Guantes and Poyatos, 2008; Kalmar et al., 2009; Strasser et al., 2012; Hong et al., 2012; Ishimatsu et al., 2013; Lu et al., 2013; Verd et al., 2014).

The motivation of this Chapter is to review the dynamics of a transcriptional mutual-inhibition with auto-activation motif in order to introduce the cellular decision making studies included in Chapters 3 and 4. The focus is on multi-stability, since it is a key ingredient to characterize decisions driven by signals that change a parameter value. Furthermore, this Chapter reviews previous

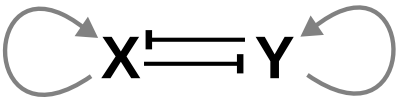

Figure 2.1 Mutual inhibition with auto-activation motif. Schematic representation of the interactions between two molecular species, X and Y. They interact through mutual-inhibition (blunt black arrows) and have a positive auto-regulation (grey arrows). The network motif without auto-activation is also called toggle switch. Hence, the mutual inhibition with auto-activation motif can be named: toggle switch with auto-activation.

studies of cellular decision making that have been done in the framework of this motif (Huang et al., 2007; Guantes and Poyatos, 2008; Nene and Zaikin, 2012; Nené et al., 2012). To this end we make use of a stochastic model for this circuit motif. An adiabatic approximation of a set of biochemical reactions that can account for the deterministic dynamics of this model is presented, comparing two different derivations. Then, we computationally explore results known about cellular decision making to contextualize our studies in Chapters 3, 4 and 5.

2.2 From reactions to equations

Different biochemical reactions can drive the same network motif. For instance, there are several ways a reactant (X) can inhibit another one (Y). To name a few:

- by binding the promoter sites of the inhibited reactant (Y) and reducing its expression. Since this mechanism blocks the transcription of the sequence that encodes the gene (Y), it is so-called *transcriptional inhibition*.
- by activating a pathway which drives degradation of the inhibited reactant protein (Y). This mechanism is a *post-translational* inhibition, since neither the transcription nor the translation of the gene is affected but its product.
- by sequestering and by forming a non-functional heterodimer (X-Y). This inhibition also takes place after translation (*post-translational*).

We focus our study in genetic interactions through gene products (proteins) and promoter binding sites (i.e. second example of the list). So, the products of the genes (X and Y) act as transcription factors.

In the toggle switch with positive auto-regulation (Fig. 2.1), in addition to the cross-inhibition between both reactants, each reactant strengthens its own expression attaching to their promoter binding sites. In this scenario, different mechanisms of integrating the inhibitory and auto-activatory regulations have been characterized by different authors. Specifically, the activator and the inhibitor can share the same promoter binding sites (Guantes and Poyatos, 2008; Nené et al., 2012), or they can have specific independent binding sites (Huang et al., 2007). We implemented the motif with the first interpretation: The activator and the inhibitor bind the same promoter sites. Yet, the results are not expected to depend strongly on the chosen interpretation.

The model implemented describes the motif of mutual inhibition with positive auto-regulation as described by Guantes and Poyatos (2008). In this model, there are two proteins (X and Y) that dimerize (cooperativity of second order) interacting with the free binding sites of the promoter of the genes encoding these proteins (P_x and P_y). Different complexes arise as a result of these bindings: P_xX_2, P_yY_2, P_xY_2 and P_yX_2. The interaction of these proteins with the promoter regions changes the production rate of the mRNAs encoding proteins X and Y (M_x and M_y) with respect to the basal mRNA transcription rate. Specifically, the following reactions have been taken into account, as described by Guantes and Poyatos (2008):

- Promoter–TF binding/unbinding:

$$\begin{aligned} P_x + 2X &\underset{K_-}{\overset{K_+}{\rightleftharpoons}} P_xX_2 \\ P_y + 2Y &\underset{K_-}{\overset{K_+}{\rightleftharpoons}} P_yY_2 \\ P_y + 2X &\underset{K_-/\sigma}{\overset{K_+}{\rightleftharpoons}} P_yX_2 \\ P_x + 2Y &\underset{K_-/\sigma}{\overset{K_+}{\rightleftharpoons}} P_xY_2 \end{aligned} \tag{2.1}$$

- mRNA dynamics:

$$\begin{array}{cccccc} P_x & \xrightarrow{\beta_x} & P_x + M_x & P_y & \xrightarrow{\beta_y} & P_y + M_y \\ P_x X_2 & \xrightarrow{\rho\,\beta_x} & P_x X_2 + M_x & P_y Y_2 & \xrightarrow{\rho\,\beta_y} & P_y Y_2 + M_y \\ M_x & \xrightarrow{\delta_m} & \emptyset & M_y & \xrightarrow{\delta_m} & \emptyset \end{array} \tag{2.2}$$

- Protein dynamics:

$$\begin{array}{cccccc} M_x & \xrightarrow{\gamma} & M_x + X & M_y & \xrightarrow{\gamma} & M_y + Y \\ X & \xrightarrow{\delta} & \emptyset & Y & \xrightarrow{\delta} & \emptyset, \end{array} \tag{2.3}$$

where for the sake of simplicity, the same values for the rates (K_+, K_-, σ, ρ, δ_m, γ, δ) for both X and Y proteins have been considered. All bindings of the transcription factors to promoters are considered, for simplicity, to occur at the same rate. σ measures the ratio between the dissociation rates of a binding mediating auto-activation over the one mediating cross-inhibition. Notice that dimerizations are not taken into account as independent reactions (e.g. $X+X \rightarrow X_2$) and, instead, they are included in the promoter binding reactions (reactions (2.1)). The auto-activation strength is controlled by ρ parameter ($\rho > 1$).

Reactions (2.1)-(2.3) are translated into ordinary differential equations (ODE) according to the mass action-kinetics,

$$
\begin{cases}
\frac{d[X]}{dt} &= \gamma\,[M_x] - \delta\,[X] + 2\,K_-([P_xX_2] + \frac{[P_yX_2]}{\sigma}) - \\
&\quad -2\,K_+\,V^2\,[X]^2\,([P_x^T] + [P_y^T] - [P_xX_2] - [P_xY_2] - \\
&\quad -[P_yY_2] - [P_yX_2]) \\
\frac{d[Y]}{dt} &= \gamma\,[M_y] - \delta\,[Y] + 2\,K_-([P_yY_2] + \frac{[P_xY_2]}{\sigma}) - \\
&\quad -2\,K_+\,V^2\,[Y]^2\,([P_x^T] + [P_y^T] - [P_xX_2] - [P_xY_2] - \\
&\quad -[P_yY_2] - [P_yX_2]) \\
\frac{d[M_x]}{dt} &= \beta_x([P_x^T] + (\rho - 1)\,[P_xX_2] - [P_xY_2]) - \delta_m\,[M_x] \\
\frac{d[M_y]}{dt} &= \beta_y([P_y^T] + (\rho - 1)\,[P_yY_2] - [P_yX_2]) - \delta_m\,[M_y] \\
\frac{d[P_xX_2]}{dt} &= K_+\,V^2\,[X]^2\,([P_x^T] - [P_xX_2] - [P_xY_2]) - K_-\,[P_xX_2] \\
\frac{d[P_yY_2]}{dt} &= K_+\,V^2\,[Y]^2\,([P_y^T] - [P_yY_2] - [P_yX_2]) - K_-\,[P_yY_2] \\
\frac{d[P_xY_2]}{dt} &= K_+\,V^2\,[Y]^2\,([P_x^T] - [P_xX_2] - [P_xY_2]) - K_-\,\frac{[P_xY_2]}{\sigma} \\
\frac{d[P_yX_2]}{dt} &= K_+\,V^2\,[X]^2\,([P_y^T] - [P_yY_2] - [P_yX_2]) - K_-\,\frac{[P_yX_2]}{\sigma},
\end{cases}
\tag{2.4}
$$

with all the variables in concentrations by dividing the number of molecules by the cell volume (V) re-scaled through Avogadro's number and where we considered that there is a fixed number of binding sites for each promoter (P_x^T and P_y^T),

$$
\begin{cases}
P_x^T &= P_x + P_xX_2 + P_xY_2 \\
P_y^T &= P_y + P_yY_2 + P_yX_2\,.
\end{cases}
\tag{2.5}
$$

Protein dynamics in cells are commonly slower than those of mRNA (Garcia-Ojalvo, 2011). In addition, the dynamics of binding and unbinding are faster than translation processes. We assume a clear time scale separation between these processes in order to perform an adiabatic approximation. To do so,

we first define the dynamics of total proteins X and Y. This is because the dynamics of free proteins (see Eqs. (2.4)) involve both fast and slow processes, whereas those of the total protein amounts are only slow. These new variables are:

$$\begin{cases} [X_{total}] &= [X] + 2\Big([P_xX_2] + [P_yX_2]\Big) \\ [Y_{total}] &= [Y] + 2\Big([P_yY_2] + [P_xY_2]\Big) \end{cases} \tag{2.6}$$

The model of Eqs. (2.4) is re-written according to these two new variables as:

$$\begin{cases} \frac{d[X_{total}]}{dt} &= \gamma\,[M_x] - \delta\Big([X]_{total} - 2\,[P_xX_2] - 2\,[P_yX_2]\Big) \\ \frac{d[Y_{total}]}{dt} &= \gamma\,[M_y] - \delta\Big([Y]_{total} - 2\,[P_yY_2] - 2\,[P_xY_2]\Big) \\ \frac{d[M_x]}{dt} &= \beta_x([P_x^T] + (\rho-1)\,[P_xX_2] - [P_xY_2]) - \delta_m\,[M_x] \\ \frac{d[M_y]}{dt} &= \beta_y([P_y^T] + (\rho-1)\,[P_yY_2] - [P_yX_2]) - \delta_m\,[M_y] \\ \frac{d[P_xX_2]}{dt} &= K_+\,V^2\left([X_{total}] - 2\,[P_xX_2] - 2\,[P_yX_2]\right)^2([P_x^T] - \\ & \quad -[P_xX_2] - [P_xY_2]) - K_-\,[P_xX_2] \\ \frac{d[P_yY_2]}{dt} &= K_+\,V^2\left([Y_{total}] - 2\,[P_yY_2] - 2\,[P_xY_2]\right)^2([P_y^T] - \\ & \quad -[P_yY_2] - [P_yX_2]) - K_-\,[P_yY_2] \\ \frac{d[P_xY_2]}{dt} &= K_+\,V^2\left([Y_{total}] - 2\,[P_yY_2] - 2\,[P_xY_2]\right)^2([P_x^T] - \\ & \quad -[P_xX_2] - [P_xY_2]) - K_-\,\frac{[P_xY_2]}{\sigma} \\ \frac{d[P_yX_2]}{dt} &= K_+\,V^2\left([X_{total}] - 2\,[P_xX_2] - 2\,[P_yX_2]\right)^2([P_y^T] - \\ & \quad -[P_yY_2] - [P_yX_2]) - K_-\,\frac{[P_yX_2]}{\sigma}, \end{cases} \tag{2.7}$$

We choose $1/\delta$ as a characteristic slow time scale ($\delta \ll K_-$, K_+, β_x, β_y, δ_m, and $\gamma \sim \delta$). A dimensionless time t' is defined as $t' = t\,\delta$. We also define the quotient $\epsilon \equiv \frac{\delta}{K_-}$.

We rewrite Eqs. (2.7) by introducing ϵ and t',

$$
\begin{cases}
\dfrac{d[X_{total}]}{dt'} &= \dfrac{\gamma}{\delta}\,[M_x] - [X_{total}] + 2\,[P_xX_2] + 2\,[P_yX_2] \\
\dfrac{d[Y_{total}]}{dt'} &= \dfrac{\gamma}{\delta}\,[M_y] - [Y_{total}] + 2\,[P_yY_2] + 2\,[P_xY_2] \\
\epsilon\,\dfrac{d[M_x]}{dt'} &= \dfrac{\beta_x}{K_-}([P_x^T] + (\rho-1)\,[P_xX_2] - [P_xY_2]) - \dfrac{\delta_m}{K_-}\,[M_x] \\
\epsilon\,\dfrac{d[M_y]}{dt'} &= \dfrac{\beta_y}{K_-}([P_y^T] + (\rho-1)\,[P_yY_2] - [P_yX_2]) - \dfrac{\delta_m}{K_-}\,[M_y] \\
\epsilon\,\dfrac{d[P_xX_2]}{dt'} &= K\,V^2\left([X_{total}] - 2\,[P_xX_2] - 2\,[P_yX_2]\right)^2([P_x^T] - \\
&\quad -[P_xX_2] - [P_xY_2]) - [P_xX_2] \\
\epsilon\,\dfrac{d[P_yY_2]}{dt'} &= K\,V^2\left([Y_{total}] - 2\,[P_yY_2] - 2\,[P_xY_2]\right)^2([P_y^T] - \\
&\quad -[P_yY_2] - [P_yX_2]) - [P_yY_2] \\
\epsilon\,\dfrac{d[P_xY_2]}{dt'} &= K\,V^2\left([Y_{total}] - 2\,[P_yY_2] - 2\,[P_xY_2]\right)^2([P_x^T] - \\
&\quad -[P_xX_2] - [P_xY_2]) - \dfrac{[P_xY_2]}{\sigma} \\
\epsilon\,\dfrac{d[P_yX_2]}{dt'} &= K\,V^2\left([X_{total}] - 2\,[P_xX_2] - 2\,[P_yX_2]\right)^2([P_y^T] - \\
&\quad -[P_yY_2] - [P_yX_2]) - \dfrac{[P_yX_2]}{\sigma},
\end{cases}
\tag{2.8}
$$

where $K \equiv \frac{K_+}{K_-}$ is the equilibrium constant. In the adiabatic limit we have $\epsilon \to 0$. By imposing this limit in Eqs. (2.8), the right-hand side of the last six equations becomes zero, and the two first equations for the total amounts are well-behaved. The adiabatic approximation on the last six equations set the equilibrium values of $[P_xX_2]$, $[P_xY_2]$, $[P_yY_2]$, $[P_yX_2]$, $[M_x]$ and $[M_x]$,

$$\begin{cases} [M_x] &= \dfrac{\beta_x}{\delta_m}\Big([P_x^T] + (\rho-1)[P_xX_2] - [P_xY_2]\Big) \\ [M_y] &= \dfrac{\beta_y}{\delta_m}\Big([P_y^T] + (\rho-1)[P_yY_2] - [P_yX_2]\Big) \\ [P_xX_2] &= \dfrac{[P_x^T]\,K\,V^2\,[X]^2}{1+K\,V^2\,[X]^2+\sigma\,K\,V^2\,[Y]^2} \\ [P_yY_2] &= \dfrac{[P_y^T]\,K\,V^2\,[Y]^2}{1+K\,V^2\,[Y]^2+\sigma\,K\,V^2\,[X]^2} \\ [P_xY_2] &= \dfrac{[P_x^T]\,K\,V^2\,\sigma\,[Y]^2}{1+K\,V^2\,[X]^2+\sigma\,K\,V^2\,[Y]^2} \\ [P_yX_2] &= \dfrac{[P_y^T]\,K\,V^2\,\sigma\,[X]^2}{1+K\,V^2\,[Y]^2+\sigma\,K\,V^2\,[X]^2}, \end{cases} \tag{2.9}$$

expressed in terms of X and Y as in Eqs. (2.4).

We now want to extract $\frac{d[X]}{dt'}$ and $\frac{d[Y]}{dt'}$. To this end, we take into account that (using the definition in Eq. (2.6)),

$$\begin{cases} \dfrac{d[X]}{dt'} &= \dfrac{d[X_{total}]}{dt'} - 2\,\dfrac{d[P_xX_2]}{dt'} - 2\,\dfrac{d[P_yX_2]}{dt'} \\ \dfrac{d[Y]}{dt'} &= \dfrac{d[Y_{total}]}{dt'} - 2\,\dfrac{d[P_yY_2]}{dt'} - 2\,\dfrac{d[P_xY_2]}{dt'}. \end{cases} \tag{2.10}$$

$\frac{d[X_{total}]}{dt'}$ and $\frac{d[Y_{total}]}{dt'}$ are obtained from the two first equations in (2.8) by replacing the equilibrium expressions of $[P_xX_2]$, $[P_xY_2]$, $[P_yY_2]$, $[P_yX_2]$, $[M_x]$ and $[M_x]$ (Eqs. 2.9) into them. The time derivatives of the complexes with the bound promoters are obtained by derivating the equilibrium expressions (2.9) through application of the chain rule (e.g. $\frac{d[P_xX_2]}{dt'} = \frac{\partial[P_xX_2]}{\partial X}\frac{dX]}{dt'} + \frac{\partial[P_xY_2]}{\partial Y}\frac{dY]}{dt'}$). After some algebra, the following version of the model in the adiabatic approximation is obtained:

$$\left\{\begin{array}{rcl} \dfrac{dx}{dt'} & = & \dfrac{M_1(x,y)}{P_2(x,y)\,M_1(x,y)-P_1(x,y)\,M_2(x,y)}\left(\widetilde{\dfrac{dx}{dt'}}\right) \\ & & +\dfrac{-M_2(x,y)}{P_2(x,y)\,M_1(x,y)-P_1(x,y)\,M_2(x,y)}\left(\widetilde{\dfrac{dy}{dt'}}\right) \\ \dfrac{dy}{dt'} & = & \dfrac{-P_1(x,y)}{P_2(x,y)\,M_1(x,y)-P_1(x,y)\,M_2(x,y)}\left(\widetilde{\dfrac{dx}{dt'}}\right) \\ & & +\dfrac{P_2(x,y)}{P_2(x,y)\,M_1(x,y)-P_1(x,y)\,M_2(x,y)}\left(\widetilde{\dfrac{dy}{dt'}}\right), \end{array}\right. \tag{2.11}$$

where $x = V\sqrt{K}\,[X]$, $y = V\sqrt{K}\,[Y]$ are the protein concentrations in dimensionless units, $M_{1,2}(x,y)$ and $P_{1,2}(x,y)$ are defined as,

$$\left\{\begin{array}{rcl} M_1(x,y) & = & 1+\dfrac{4\sqrt{K}}{V}\,y\left(\dfrac{[P_y^T]\left(1+\sigma\,x^2\right)}{\left(1+y^2+\sigma\,x^2\right)^2}+\dfrac{[P_x^T]\,\sigma\left(1+x^2\right)}{\left(1+x^2+\sigma\,y^2\right)^2}\right) \\ M_2(x,y) & = & -\dfrac{4\,\sigma\sqrt{K}}{V}\,x^2\,y\left(\dfrac{[P_x^T]}{\left(1+x^2+\sigma\,y^2\right)^2}+\dfrac{[P_y^T]}{\left(1+y^2+\sigma\,x^2\right)^2}\right) \\ P_1(x,y) & = & -\dfrac{4\,\sigma\sqrt{K}}{V}\,y^2\,x\left(\dfrac{[P_y^T]}{\left(1+y^2+\sigma\,x^2\right)^2}+\dfrac{[P_x^T]}{\left(1+x^2+\sigma\,y^2\right)^2}\right) \\ P_2(x,y) & = & 1+\dfrac{4\sqrt{K}}{V}\,x\left(\dfrac{[P_x^T]\left(1+\sigma\,y^2\right)}{\left(1+x^2+\sigma\,y^2\right)^2}+\dfrac{[P_y^T]\,\sigma\left(1+y^2\right)}{\left(1+y^2+\sigma\,x^2\right)^2}\right) \end{array}\right. \tag{2.12}$$

and the expressions of $\left(\widetilde{\dfrac{dx}{dt'}}\right)$ and $\left(\widetilde{\dfrac{dy}{dt'}}\right)$ read

$$\left\{\begin{array}{rcl} \left(\widetilde{\dfrac{dx}{dt'}}\right) & = & a_x\,\dfrac{1+\rho\,x^2}{1+x^2+\sigma\,y^2}-x \\ \left(\widetilde{\dfrac{dy}{dt'}}\right) & = & a_y\,\dfrac{1+\rho\,y^2}{1+y^2+\sigma\,x^2}-y, \end{array}\right. \tag{2.13}$$

where a_x and a_y are defined as,

$$a_i = \frac{\beta_i \, \gamma \, V \, [P_i^T] \, \sqrt{K}}{\delta \, \delta_m}, \tag{2.14}$$

with $i \in \{x, y\}$.

Expression of Eqs. (2.13) corresponds to what we would have found if $\frac{d[P_x X_2]}{dt} = \frac{d[P_x Y_2]}{dt} = \frac{d[P_y Y_2]}{dt} = \frac{d[P_y X_2]}{dt} = \frac{d[M_x]}{dt} = \frac{d[M_y]}{dt} = 0$ had been considered in Eqs. (2.4). Notice that the version of the model of Eqs. (2.11) tends to the reduced version (Eqs. (2.13)) when $M_1(x, y) \to 1$, $M_2(x, y) \to 0$, $P_1(x, y) \to 0$ and $P_2(x, y) \to 1$.

In the following section we explore the agreement between the model of Eqs. (2.11) and the reduced version of the model described by the Eqs. (2.13).

2.3 The reduced version of the adiabatic approximation

We compare the two versions of the model: The version derived by the whole procedure, Eqs. (2.11), and its reduced version, Eqs. (2.13) (*reduced version*). We explored differences between both versions of the model for three parameter values that drive different number of stable solutions: three (tristability, Fig. 2.2A-B), two (bistability, Fig. 2.2C-D) and one (monostability, Fig. 2.2E-F). Results of Figure 2.2 reveal that there are no relevant differences between both versions of the model. These differences are reduced for low values of promoters (P_x^T and P_y^T).

Differences between both model versions are only significant along curves that can be identified as the nullclines (see the nullclines in Fig. 2.3A-C). These large differences come from the singularity where the derivative of either x or y tends to zero. These differences, however, do not affect the temporal evolutions of both model versions simulated through a Runge-Kutta of fourth order ($dt = 0.001$).

Taking into account that both versions of the model behave without any evident difference for a reasonable range of promoter values, we are going to approach the deterministic dynamics of the system through the reduced version of Eqs. (2.13). Unless specified, the results of the other sections of this chapter are generated using this model, already presented in (Guantes and Poyatos, 2008).

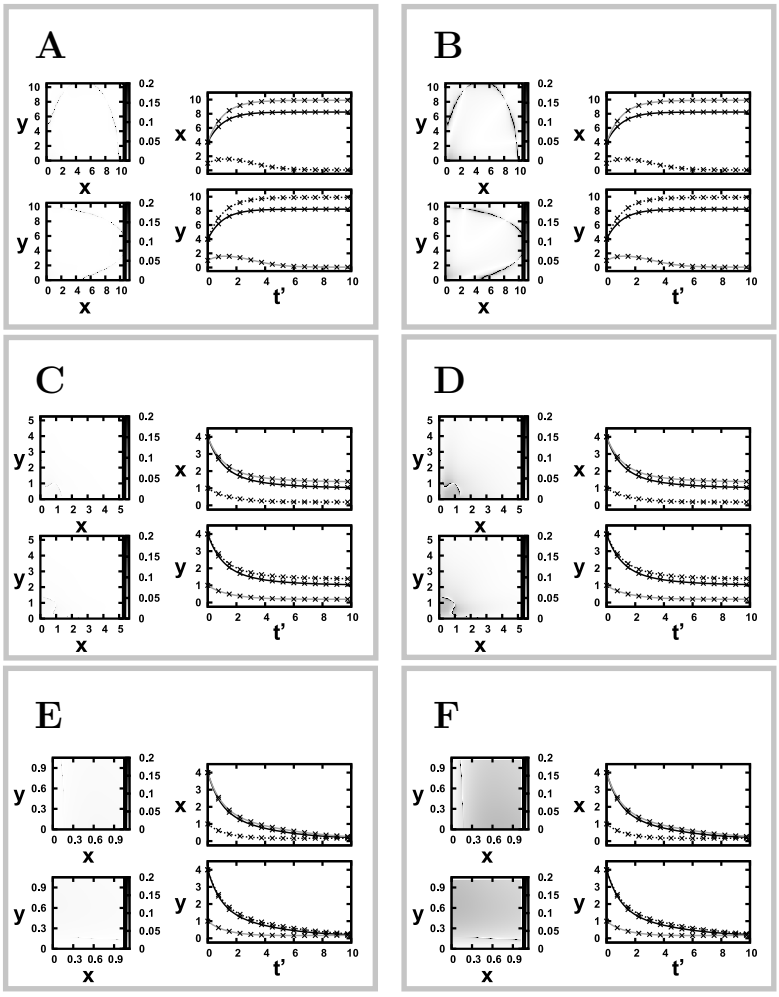

Figure 2.2 Comparison between two adiabatic reductions. (A-F, Left) Quotients (top) $\frac{dx}{dt'}/(\widetilde{\frac{dx}{dt'}})$ and (bottom) $\frac{dy}{dt'}/(\widetilde{\frac{dy}{dt'}})$ across the space of x and y values in greyscale (colour bar; black colour corresponds to values ≥ 0.2). $\frac{dx}{dt'}$ and $\frac{dy}{dt'}$ are defined as in Eq. (2.11), and $(\widetilde{\frac{dx}{dt'}})$ and $(\widetilde{\frac{dy}{dt'}})$ as in Eq. (2.13). (A-F, Right) Dynamics over time of each dimensionless variable, $x(t')$ and $y(t')$, comparing the two adiabatic reductions (lines for Eq. (2.11) and crosses for Eq. (2.13)) for three different initial conditions. (A,B) Tristable regime for $a_x = a_y = 1$. (C,D) Bistable regime for $a_x = a_y = 0.2$. (E,F) Monostable regime for $a_x = a_y = 0.14$. (A,C,E) for $P_x^T = 1$. (B,D,F) for $P_x^T = 1$. Other parameters of the simulations: $\sigma = 0.2$, $\rho = 10$, $\delta = 1$, $\gamma = 10$, $K = 10^{-5}$, $V = 10$. Grid size of the heat maps, 100×100.

2.4 Multistability

Taking into account that cellular decision making involves more than one available choice, multistability is a common feature of the mechanisms which control cellular decision making. Multistability is a property usually exhibited by nonlinear systems. It is known that Eqs. (2.13) exhibit multiple stable states for the same parameter values (Guantes and Poyatos, 2008). In these equations, the nonlinearities required for multistability come from the dimerization and from promoter saturation. Figure 2.3A-C shows the stationary behaviour of the reduced model (Eqs. (2.13)) for the three different values of a_x and a_y explored in Fig. 2.2: $a_x = a_y = 1$ (Fig. 2.3A), $a_x = a_y = 0.2$ (Fig. 2.3B) and $a_x = a_y = 0.14$ (Fig. 2.3C). x and y nullclines (Strogatz, 1994) ($dx/dt = 0$, $dy/dt = 0$) are shown. Stability of the stationary states of the system has been evaluated by computing the temporal evolution of the perturbed stationary solutions through a deterministic algorithm that numerically integrates the dynamics (4^{th} order Runge-Kutta with time step $dt = 0.001$). The basins of attraction denote the initial condition values of the phase portrait that evolve to a certain steady solution. The manifolds dividing the basins of attraction of Fig. 2.3A-C have been calculated by time reversal integrations started at the unstable points. The temporal evolutions simulated in Fig. 2.2 confirm that the final solution is determined by the initial condition as corresponding to the basins of attraction in Fig. 2.3. Notice also that unstable solutions can be reached due to the deterministic nature of the algorithm (Fig. 2.2C-D).

The number of attractors – and their values – of the dynamics is controlled by the parameter values. We explore a_x,a_y parameter values, which in Eqs. (2.13) are the dimensionless maximal production rates (Fig. 2.3D-E). The bifurcation diagram (Fig. 2.3D) shows the value of x at both the stable and unstable stationary solutions as parameter $a = a_x = a_y$ varies. The stability of the stationary solutions has been numerically checked as described above. Fig. 2.3E shows the number of stable stationary solutions across the a_x,a_y parameter space. Both Figs. 2.3D-E show different stability regimes of the model, where one, two or three solutions are stable. This parameter space is dynamically explored in Chapters 3 and 4.

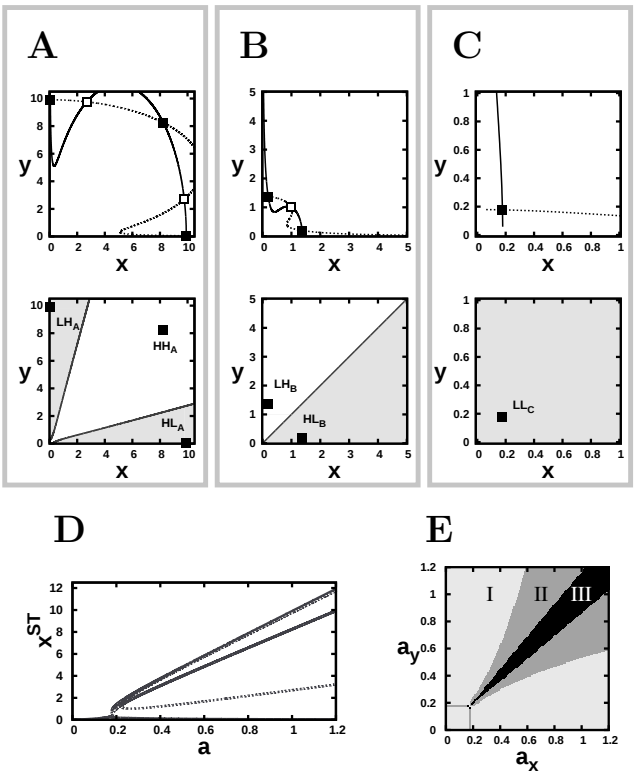

Figure 2.3 Exploring the multistability exhibited by the deterministic dynamics of the motif. (A) Tristable regime ($a_x = a_y = 1.0$), with three stable states: LH_A, HL_A, HH_A. (B) Bistable regime ($a_x = a_y = 0.2$), with two stable states: LH_B, HL_B. (C) Monostable regime ($a_x = a_y = 0.14$), with a single stable state: LL_C. (A-C,top) x-nullcline ($dx/dt = 0$, solid lines) and y-nullcline ($dy/dt = 0$, dashed lines). Stable (filled squares) and unstable (empty squares) states are depicted. (A-C,bottom) The basin of attraction (different colours) of each stable state (filled squares). Manifolds, separating the basins of attraction, are depicted when more than one basin is present (solid line). (D) Bifurcation diagram of X protein steady states with $a = a_x = a_y$ as a control parameter. Solid and dashed lines are the stable and unstable branches respectively. (E) Regions in the a_x–a_y parameter space with three (III, black), two (II, dark grey) or one (I, light grey) stationary stable solutions. This panel was generated by evaluating the number of stationary stable solutions for 150×150 a_x,a_y values ranging from 0.001 to 1.2 distributed in a square grid. Other parameters of the model in all panels are $\sigma = 0.2$ and $\rho = 10$.

2.5 A stochastic dynamics for the toggle switch with auto-activation

Cellular decision making involves different responses under the same conditions. This is because the reactions that rule cellular processes have a stochastic nature. The stochasticity arises from the discrete nature of matter, and involves the randomness of the meeting of the reactants for reactions to occur, low copy numbers of the species that participate in these reactions and binding/unbinding energies of reactions of the order of thermal energies of the cellular environment. Despite the fact that the deterministic model informs on the average behaviour of the system, a stochastic model adds details about the heterogeneous responses of a population of cells which evolve under the same conditions. Moreover, for low copy number of the reactants, transition probabilities of each reaction per unit of time can give a more accurate description of the system than reaction rates.

We considered a phenomenological stochastic model for the toggle switch with auto-activation, described by the following probabilities in terms of Gillespie algorithm (Gillespie, 1977):

$$\begin{cases} P_1(X \to X+1) &= \dfrac{\dfrac{a_x\, V}{\sqrt{k}}\, \dfrac{V^2 + k\rho X^2}{V^2 + kX^2 + k\sigma Y^2}}{W(X,Y)} \\ P_2(X \to X-1) &= \dfrac{X}{W(X,Y)} \\ P_3(Y \to Y+1) &= \dfrac{\dfrac{a_y\, V}{\sqrt{k}}\, \dfrac{V^2 + k\rho Y^2}{V^2 + kY^2 + k\sigma X^2}}{W(X,Y)} \\ P_4(Y \to Y-1) &= \dfrac{Y}{W(X,Y)}, \end{cases} \tag{2.15}$$

where X and Y are the molecule number of each specie ($X = x\frac{V}{\sqrt{k}}$ and $Y = y\frac{V}{\sqrt{k}}$) and k is the equilibrium constant ($k = K\,V^2$). The molecule number modification of each reaction is denoted between parentheses. $W(X,Y)$ is the normalization function that guarantees that $\sum_{i=1}^{4} P_i = 1$. According to the Gillespie algorithm, which reaction occurs next is decided stochastically from the above

probabilities. The time at which this reaction happens is determined stochastically too from an exponential distribution with characteristic time $1/W(X,Y)$.

This model sets a phenomenological stochastic description of the mutual inhibition between X and Y and their auto-activation. Additionally, it can be understood as the stochastic version of the adiabatic limit of reactions (2.1) and (2.3), given by Eqs. (2.13) (Rao and Arkin, 2003). This stochastic model is also used in Chapters 3 and 4. In the following, this stochastic model is used to review some properties of cellular decision making processes. Despite the stochastic simulations are performed with the molecule number of the proteins, X and Y, results of this chapter and of Chapters 3 and 4 are expressed with dimensionless units, x and y.

2.6 The motif as a model for cellular decision making studies

Due to not only the recurrence of the toggle switch with auto-activation motif in cellular decision making processes, but also the to richness of the different stability regimes exhibited by it, it has been theoretically studied by several authors in order to understand general aspects of these decisions (Guantes and Poyatos, 2008; Huang et al., 2007; Nené et al., 2012). In all these studies, the induction of the decision is driven by a signal that controls some parameters of the dynamics.

Huang et al. (2007) described the decision that takes place during blood cell differentiation through a mutual inhibition and auto-activation motif. The (myeloid) precursor cells decide between two fates: erythroid/megakaryocyte and myelomonocytic lineages. These two cell fates exhibit a low value of one protein and a high value of another one (PU.1 and GATA1), while the precursor cell has similar levels of both proteins. The authors explain the decision by means of two stability regimes. Initially, the precursor cells are in a steady state characterized by similar levels of both proteins (symmetric state). The decision inductor changes permanently the initial stability regime to a new bistable one where this symmetric steady state is destabilized and two new asymmetric stable states (each with only one of the two proteins in high amounts) are created.

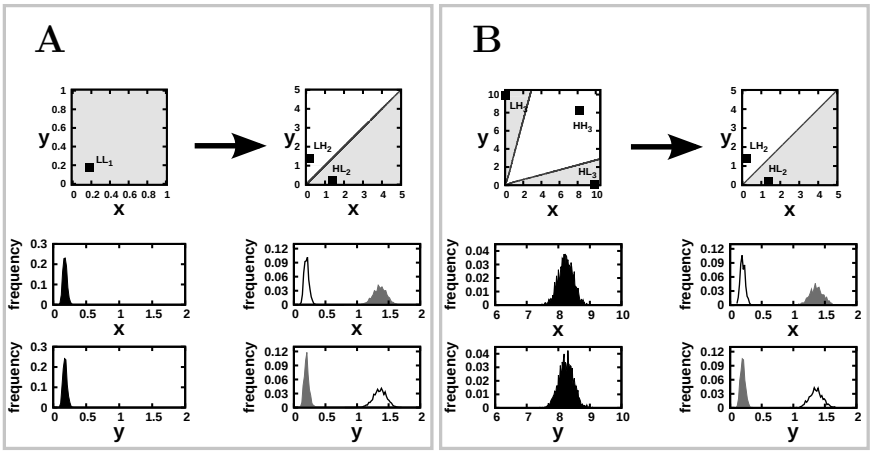

Figure 2.4 Permanent signals that drive two-fate cellular decision making. (A,B; Top) Initial (left) and final (right) phase portrait (top). (A,B; Bottom) Initial (left) and final (right) protein distribution (in dimensionless units) of the cellular population. (A) The signal drives a bifurcation from a monostable regime ($a_x = a_y = 0.14$) to a bistable one ($a_x = a_y = 0.2$). The initial cell population is at the monostable stationary state LL_1. The final cell population is distributed between the two new cell states: LH_2 (black line); HL_2 (grey shade). (B) The signal drives a bifurcation from a tristable regime ($a_x = a_y = 1$) to a bistable one ($a_x = a_y = 0.2$). The initial cell population is at the HH_3 steady state value of the tristable regime. The final cell population is distributed between the two new cell states: LH_2 (black line); HL_2 (grey shade). In A and B, the signal is applied at $t = 20$ and it abruptly (step-function) changes the value of the parameters from the initial ($a_x = a_y = 0.14$ or $a_x = a_y = 1$) to the final values ($a_x = a_y = 0.2$). Other parameters: $t_{final} = 70$, $\sigma = 0.2$, $\rho = 10$, $K = 10^{-5}$, $V = 10$.

This permanent change of the stability regime – driven by a permanent parameter change – makes cells decide between these two new asymmetric states. We reproduce the main idea of their work – adapted to the model of Eqs. (2.15) – in the results of Fig. 2.4. Figure 2.4 shows that a two-state population can arise from a rather homogeneous one if the initial state is destabilized by a parameter change. This occurs either if the initial stability regime is monostable (Fig. 2.4A) or if it is tristable (Fig. 2.4B).

The cellular decision not only depends on the initial and final stability regimes, but also on the intermediate regimes explored by the system. Guantes and Poyatos (2008) explored in their work how different decisions can be driven by different transient signals. They defined two transient signal types: (i) differential duration signals, which modify identically two parameters but with different

duration and (ii) differential strength signals, which modify asymmetrically two parameters during the same time. Their results introduce two cellular decisions controlled by the two type of signals described: decision of changing of state or remaining at the initial one; decision of choosing between two new states (while the initial state is finally unpopulated). They explored the dependency of the final selection on the asymmetry of the signal (either duration or strength). We have reproduced some of their main results in Fig. 2.5A.

The research of Nené et al. (2012) sheds light on how the path on the parameter space favours a certain cell fate selection. They built a parameter change profile whose speed controls the path described by the system until reaching the final stability regime. The speed difference between the two control parameters determines, not only the asymmetry of stability regime transiently explored, but also the time spent by the system there. Nené et al. implemented continuous functions to describe the parameter changes. Herein, we reproduce the basic elements of their conclusion by implementing the stochastic model of Eqs. (2.15) with two discontinuous changes of the parameters such that the asymmetry these changes drive and their duration are decoupled (Fig. 2.5A). We set the system to start at the steady symmetric value of a monostable regime, to transiently explore another monostable regime where the stable state is not perfectly symmetric, and to finally reach a bistable regime. The results of Fig. 2.5A confirm – as the work of Nené et al. showed – that both the asymmetry of the transient state and the transient duration of the intermediate stability regime favour one cell fate over the other. Nené et al. (2012) revealed that the final decision is determined not only by the initial and the final parameter values, but also by the way that the parameters evolve from the initial values to the final ones.

2.7 Discussion

In this Chapter we explored a common network motif underlying cell state changes that involves two auto-activating genes interacting with mutual-inhibition. We used a phenomenological simple stochastic description of these interactions, which can also be understood as an adiabatic limit of a set of potential biochemical reactions. We offered two descriptions of the adiabatic limit and showed they are rather equivalent.

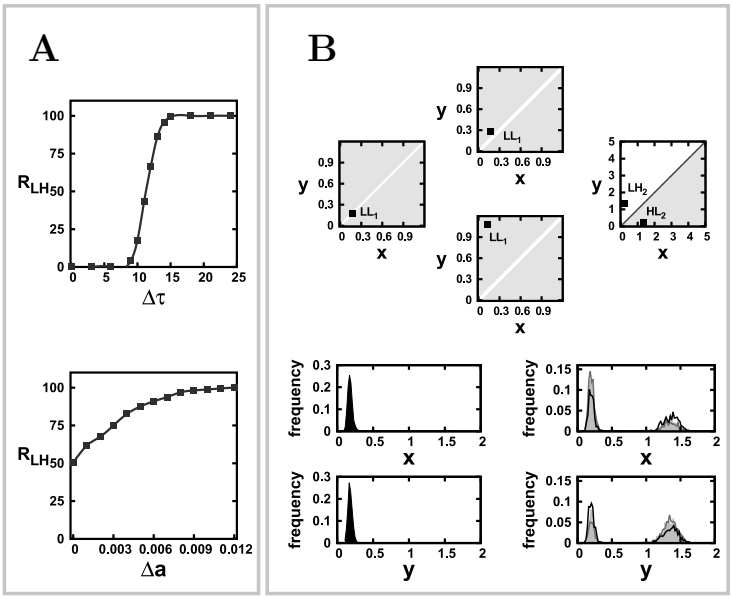

Figure 2.5 The path on the parameter space can favour a certain cell fate selection. (A) Selection rate of the LH state (R_{LH}) after a transient signal that modifies a_x and a_y parameters. The transient signal modifies both parameters with a temporal delay ($\Delta\tau = \tau_y - \tau_x$, $\tau_x = 140$) (top) or with a differential strength ($\Delta a = a_y - a_x$, $a_x = 0.2$) (bottom). Differential duration signals (top) generate a tristable regime when the signal modifies both parameters ($a_x = a_y = 0.8$), and a monostable regime ($a_x = 1$,$a_y = 0.8$) when the signal only affects one parameter. Differential strength signals (bottom) generate transiently ($\tau = 140$) a bistable regime. (B) The signal drives first a change from a symmetric ($a_x = a_y = 0.14$) to an asymmetric monostable regime and afterwards to a bistable regime ($a_x = a_y = 0.2$). (Top) Phase portrait at initial (left), intermediate (middle) and final (right) times. The asymmetric monostable regime lasts a time τ. Two asymmetric monostable regimes: $a_x = 0.14$, $a_y = 0.17$ (top central phase portrait) and $a_x = 0.14$, $a_y = 0.185$ (bottom central phase portrait) are shown. Notice how the difference between a_x and a_y controls the asymmetry of the LL_1 state ($x = y$ line is depicted in white). (Bottom) Initial (left) and final (right) distributions for three transient conditions: $a_x = 0.14$, $a_x = 0.17$, $\tau = 5$ (light grey shade); $a_x = 0.14$, $a_x = 0.17$, $\tau = 0.1$ (black line); $a_x = 0.14$, $a_x = 0.185$, $\tau = 5$ (dark grey line). Other parameters: $t_{final} = 50$, $\sigma = 0.2$, $\rho = 10$, $K = 10^{-5}$, $V = 10$. Simulations of panel A have been computed with 1000 temporal evolutions started at the HH state of the tristable regime ($a_x = a_y = 1$). Simulations of panel B have been performed with 10000 temporal evolutions.

The rich range of stability regimes that this system is able to produce make it a good candidate to study cellular decision making processes. We have reported three cellular decision making studies developed with this network motif (but with different mathematical formulations) in which cellular decision making is induced by a dynamical signal. The features of the signal determine the stability regime during its effect. The main conclusions of relevance for the work in this Thesis are: (1) Cellular decision making requires a multistable regime to drive different responses (Huang et al., 2007; Guantes and Poyatos, 2008; Nené et al., 2012); (2) Not only the initial and the final stability regime determine the final selection, but also the intermediate stability regimes (Guantes and Poyatos, 2008; Nené et al., 2012); (3) The asymmetry of a transient stability regime and the time spent by the system there can favour a certain final cell fate (Guantes and Poyatos, 2008; Nené et al., 2012); (4) A transient change of the stability regime can drive a permanent cell change (Guantes and Poyatos, 2008).

Part II

RESULTS

Chapter 3

Cellular decision making involving two cell types

3.1 Introduction

As reviewed in the previous chapter, cellular decisions can be classified according to the cell states involved before and after the decision, and depend on the action of the inductive signal. In other words, not only the initial and the final attractors of the dynamics are important, but also the attractors – and the phase space – which are transiently available to the system while the signal is taking place. Our study in this Chapter shows which different properties are conferred by each signal, suggesting different scenarios in which each signal may act. Conversely, our study reveals some of the properties to look for in a cellular decision making process in order to unveil which phase space changes is the signal driving and hence learn more about the system dynamics.

Since the dynamics of the biochemical motif toggle switch with auto-activation (3.1A, reviewed in the previous Chapter) underlie many cellular decision making processes, we selected it for the study presented herein. This dynamics drives a variety of stable stationary states (Section 2.4 of Chapter 2, Fig. 2.3). As in the previous Chapter, these states have been termed according to the value of both proteins (X and Y), denoting with "L" a low value and with "H" a high

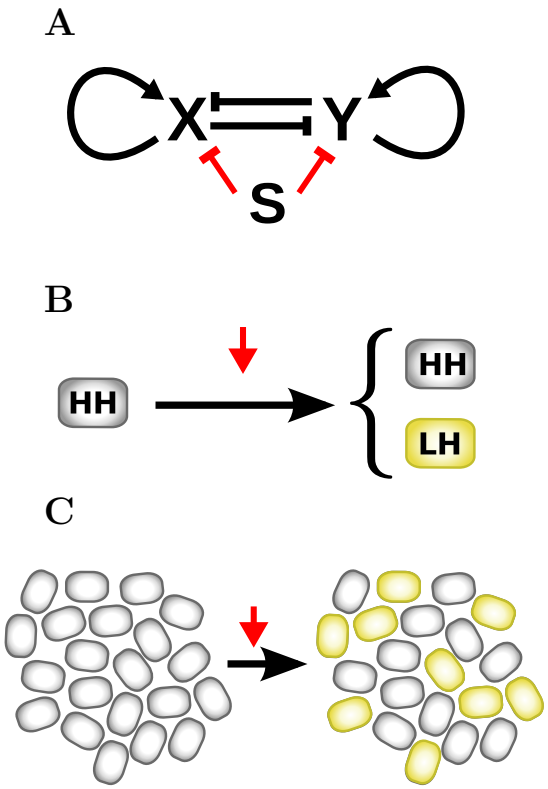

Figure 3.1 Description of the 2-state cellular decision making. (A) Toggle switch with auto-activation motif. The two proteins, X and Y, are being auto-activated (black arrows) and cross-inhibited (blunt black arrows). The signal (S) transiently represses (blunt red arrows) both proteins. (B) The cell is initially at the symmetric cell state HH (grey) and, after a transient signal application (red arrow), decides between two cell states: The former HH state (grey), or the new LH state (yellow). (C) The initial population of cells is homogeneous, with all the cells in the same state (grey). After the signal application (red arrow), the population becomes heterogeneous, with two cell states involved (grey and yellow).

value: LL, LH, HL and HH. Notice that hereafter we use the term "cell" to refer to the system made only of the toggle switch with auto-activation.

We focused on decisions in which a cell decides to either remain as it is or to change of state upon a transient signal (Fig. 3.1B,C). We name it *2-state decision*. As reviewed in the previous Chapter, transient changes in the parameter values of the dynamics driven by transient signals can drive cells to change from

one state to another one when cells are in a multistable scenario. This is so because the transient signal enables them to partially explore the space of possible states. This exploration is partial since it is constrained by the transient signal itself, which enables some explorations but not others. This aspect is constantly present in this Chapter. Specifically, we consider that the parameter values of the cell dynamics in the absence of signal enable three stable states (HH, LH and HL). Yet, one of these states (HL) is never observed during the decision.

We implemented two distinct dynamical mechanisms that drive the *2-state decision*. At the biochemical level, both mechanisms can be thought of being identical, the only difference being their actual quantitative value. Moreover, the probability of the decision to change of state depends on the strength of the signal in a similar manner in both mechanisms. Hence, if this probability is the only measure being done (in terms of ratios of cell populations) both mechanisms may seem identical. However, from the dynamical point of view, the two mechanisms are very distinct since each of them drives very different phase space changes. We analyse which properties confers each process and how these depend on its dynamical characteristics.

3.2 The model and the signals

We studied the cell-autonomous decision in which a cell can either remain in the same state or change to a new state as a result of a transient signal (Fig. 3.1B-C). It was assumed that cell states can be characterized by the stable attractors of the dynamics of two molecules, X and Y. The two proteins were chosen to interact through the well-known toggle switch with auto-activation (Fig. 3.1A) and intrinsic noise in their dynamics was taken into account. Specifically, the stochastic dynamics were modelled according to Eqs. (2.15) in Chapter 2. To unravel how transient (versus non permanent) signals drive cellular decision making, we chose a regime of parameter values in the absence of signal that sustains three stable states (HH, HL, LH) and corresponds to $a_x = a_y = 1$, $\sigma = 0.2$ and $\rho = 10$ for the deterministic dynamics (Fig. 3.2A, Eqs. 2.13). We checked that for the stochastic dynamics with $K = 10^{-5}$ and $V = 10$, no stochastic switching between these states occurs for the long time periods being explored ($t = 10000$).

HH was chosen as the initial cellular state (hereafter precursor state) (Fig. 3.2A). This choice can be justified in some contexts like in stem cell differentiation (Huang et al., 2007; Guantes and Poyatos, 2008). We focused on the decision to remain in this HH state or to change to the LH state (Fig. 3.1A).

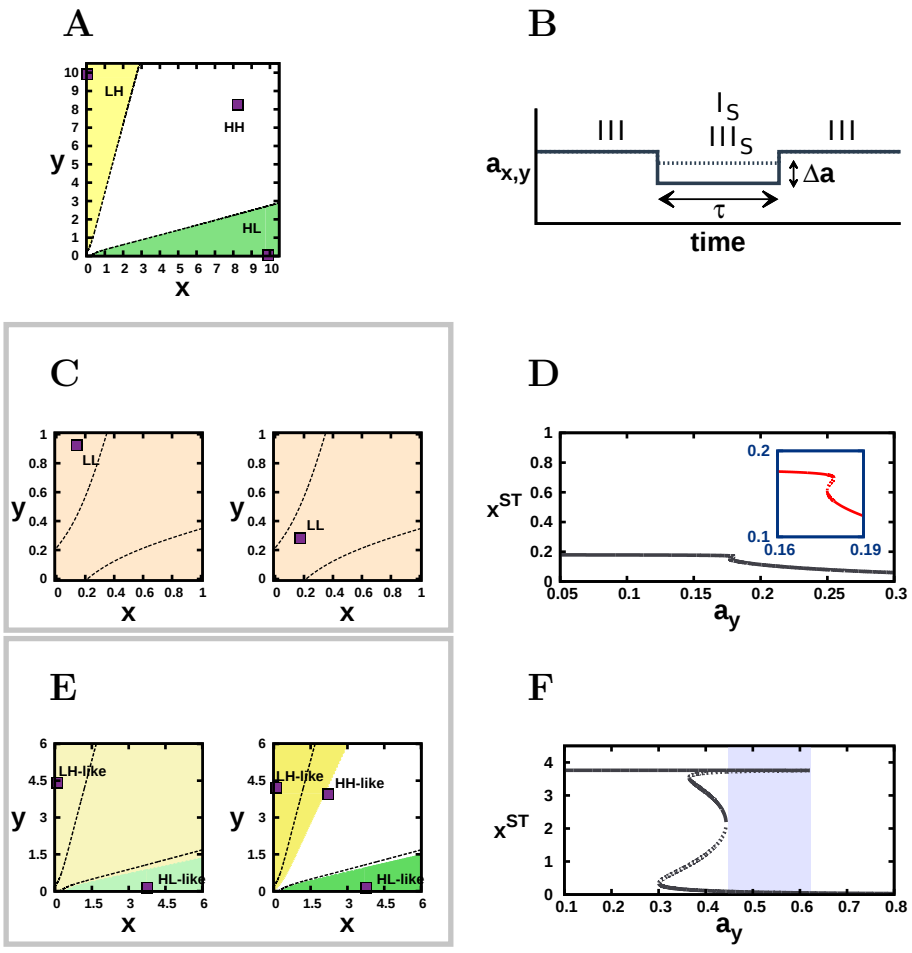

Figure 3.2 Monostable and multistable signals. (A) Phase portrait of x and y variables in the absence of signal ($a_x = a_y = 1$). Three stable states: LH, HH, HL (purple squares), and their basins of attraction (yellow, white and green, respectively) are depicted. (B) The transient signal reduces a_x (dashed line) and a_y (solid line) and places the system either in a transient monostable regime (I_S) or in a new multistable regime (III_S). τ is the signal duration and $\Delta a = a_y - a_x$ is the signal strength. (C, E) Phase portrait driven by the (C) monostable ($a_x = 0.14$) or (E) multistable ($a_x = 0.4$) signal showing the stable stationary states (squares) and their basins of attractions (colours). The manifolds of the tristable regime in the absence of signal are depicted by dashed lines. (C, left) for $\Delta a = 0.0305$ and (C, right) for $\Delta a = 0.04$. The signal strength Δa controls the asymmetry of the LL stable state, such that it is located outside (left) or inside (right) the LH basin of attraction of the tristable regime without signal. (E) The signal strength Δa controls the stability and number of states (left for $\Delta a = 0.043$, and right for $\Delta a = 0.061$). (D, F) Bifurcation diagrams of the steady solutions of x versus the a_y parameter for (D) $a_x = 0.14$ and (F) $a_x = 0.4$. In D, the inset (red) corresponds to an amplification of $a_x \in [0.16, 0.19]$ range, where a bistable regime is found. Despite of this bistable regime, the system behaves as monostable due to the similarities between the two stable states. In F, the shadow denotes a bistable regime, where the missed stable branch acts as a ghost state. In D and F, stable solutions are represented with solid lines, and unstable ones with dashed lines. All these panels correspond to the deterministic dynamics of Eqs. (2.13).

We set the signal to decrease the effective production of the two molecular species, by reducing the value of a_x and a_y (Fig. 3.2B), as previously done (Guantes and Poyatos, 2008). Since we are working with a non dimensional model, this change could arise in several different ways, by increasing the degradation rates of the molecules or by decreasing the transcription or translation rates, for instance (see the definition of $a_{x,y}$ in terms of dimensional parameters given in the previous chapter, below Eqs. (2.15). We simplified the signal dynamics, assuming it is much faster than the dynamics of the system, and modeled it as step-like changes (Fig. 3.2B). The transient signal was then characterized by three parameters: the change the signal drives in a_x, the difference in change it drives between a_x and a_y, what we termed signal strength ($\Delta a = a_y - a_x$) following the nomenclature by Guantes and Poyatos (2008), and the signal duration (τ) (Fig. 3.2B). All situations we considered have Δa small compared to the change of value the signal drives on a_x. Also, in order to induce the transition to the LH state and not to the HL state, we considered only $\Delta a \geq 0$.

As Figure 2.3 shows, the number of stable fixed point attractors depends on a_x and a_y. Specifically, for $a_x = a_y$, the number of stable fixed points decreases to

two and one when a_x decreases (Figure 2.3D). According to this, we designed two types of transient signals which should drive the same decision of whether to remain as an HH cell or to change to a LH cell. The first type of signal designed drives a bifurcation to a monostable regime ($a_x = 0.14$, $a_y \geq 0.14$, Fig. 3.2C-D). We named this signal as *monostable signal*. The second type of signal designed maintains the tristable regime ($a_x = 0.4$, $a_y > 0.4$) but changes the relative stability of the states, stabilizing the LH-like state with respect to an HH-like one (Fig. 3.2E-F). The signal that drives this mechanism is called *multistable signal*.

3.3 Results

3.3.1 Two mechanisms to drive the same decision

We applied the two types of signals on a population of N statistically identical cells each. First, to ensure that initially all cells were statistically identical, albeit they were heterogenenous because of their stochastic dynamics, we let the N initial values of both molecular species X and Y to stochastically evolve (each with a different seed of the random number generation algorithm) until $t = 20$, reaching the stationary initial distribution corresponding to the HH state. The signal was then applied at time $t = 20$ and lasted τ. Once the signal was removed from the system, the cells evolved during 50 units of time with the parameter values of the initial (and final) conditions ($a_x = a_y = 1$). The states of cells at time $t = 20 + \tau + 50$ were evaluated to characterize with which frequency cells permanently change of state by the induction of the signal. Since for stochastic dynamics the stationary states correspond to distributions, whereas for deterministic dynamics they correspond to fixed points of well defined values, in order to automatically identify in which state each cell was at time $t = 20+\tau+50$, we evolved deterministically their dynamics for an additional period of time 100. We identified the state of the cell at time $t = 20 + \tau + 50$ as the corresponding to the fixed point reached through this additional deterministic evolution. The number of cells of the whole population that change of state after the signal has disappeared was named R_{LH}. This ratio is an estimation of the probability each cell has to change of state when the transient signal acts.

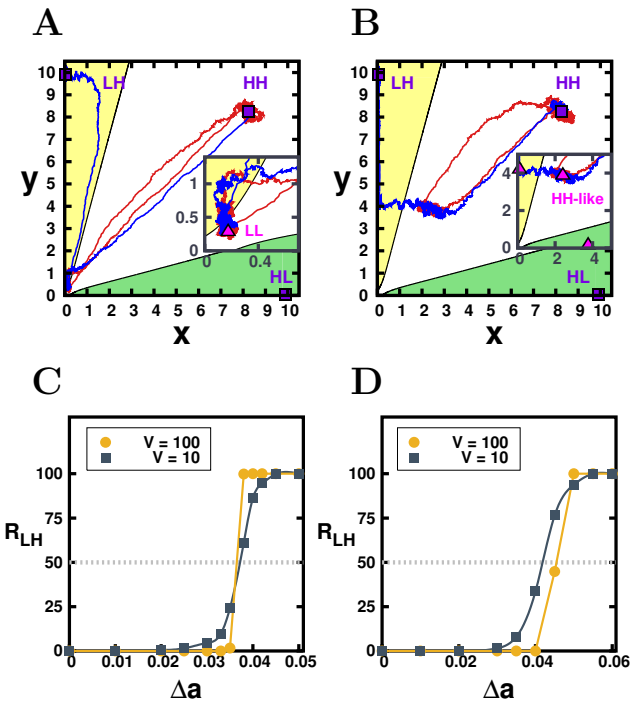

Figure 3.3 Monostable and multistable transient signals drive the same cellular decision making. (A,C) For monostable ($a_x = 0.14$) and (B,D) multistable ($a_x = 0.4$) signals. (A,B) Stochastic trajectories of two cells (red, blue) that initially are in the HH state and end up in different states upon the action of a transient signal ($\tau = 70$, $\Delta a = 0.03$ in A and $\Delta a = 0.04$ in B). Insets: amplification of the trajectories around the states driven by the signal. (C,D) Ratio of cells (in %) that change to the LH state after a signal is applied, for different signal strengths and two volumes (legend). Parameter values are $\tau = 70$ and $N = 600$. Other parameter values as in previous figures.

Figure 3.3A-B shows how, effectively, both signal types (monostable and multistable) can drive the decision to choose (with a certain probability) between remaining at the initial HH attractor or change to the new LH cell state. The probability of choosing a new one cell fate in each mechanism depends on the signal strength (Δa) in a threshold-like manner (Fig. 3.3C-D). Therefore, both signals, from this point of view, seem to drive the same decision making process and thereby seem identical mechanistically. As expected, however, analysis of the dynamics of the system clearly shows that both types of signals drive the decision using different mechanisms. During the monostable signal (Fig. 3.2C), the system relaxes to the unique attractor (Fig. 3.3A). By contrast, when the multistable signal acts (Fig. 3.2E), the dynamics of cells is to evolve first to

the accessible attractor (i.e. the HH-like state). Once there, the dynamics can stochastically switch to the LH-like sate (Fig. 3.3B). Specifically, the change in stability enables stochastic switching from a HH-like to a LH-like and not vice versa for the time periods being studied (Table 3.1). Notice we termed HH-like and LH-like the stable states that exist in the presence of the signal to distinguish them from those in the absence of signal. The HH-like state has only small asymmetries and lies within the basin of attraction of the HH state (Fig. 3.2E). The LH-like state has strong asymmetries as the HL state and lies within its basin of attraction (Fig. 3.2E). Hence, after signal removal, and since the LH-like and HH-like states are respectively each within the basin of attraction of the LH and HH states, cells in the LH-like state will relax towards the LH state, whereas cells in the HH-like state will relax to the HH state (Fig. 3.3B).

	$\mathbf{V = 100}$	$\mathbf{V = 10}$
$\mathbf{\Delta a = 0.042}$	263 ± 83	37 ± 50
$\mathbf{\Delta a = 0.043}$	83 ± 64	21 ± 39

Table 3.1 Switching time beteen HH-like and LH-like states in multistable signals. Mean first passage time (MFPT) values between HH-like and LH-like state during the effect of a tristable signal ($a_x = 0.4$). Two values of signal strength (Δa) and two values of volume (V) have been explored. MFPT in the opposite direction (from LH-like to HH-like), and between the other attractors is > 10000. It has been simulated 500 repetitions to average them up. MFPTs for other parameter values, such as $a_x = a_y = 1$ and $a_x = a_y = 0.4$, are > 10000 between all the attractors involved.

The threshold-like dependence of the probability to change to the LH state as a function of the signal strength can then be understood as follows. For long enough monostable signals, cells reach the transient attractor and will ultimately change to the LH state upon signal removal if this transient attractor lies within the basin of attraction of the LH state. For this to happen, a large enough difference in the degradation rates of X and Y induced by the signal must occur since this difference (Δa) controls the value of the LL state (Fig. 3.2C). For multistable signals, the decision arises from the stochastic switching between the HH-like state and the LH-like state. Accordingly, the more destabilized is the HH-like state and hence the faster is the stochastic switching, the larger the probability for a cell to reach the LH state upon the action of such signal. This larger destabilization occurs for larger values of the signal strength (Fig. 3.3D).

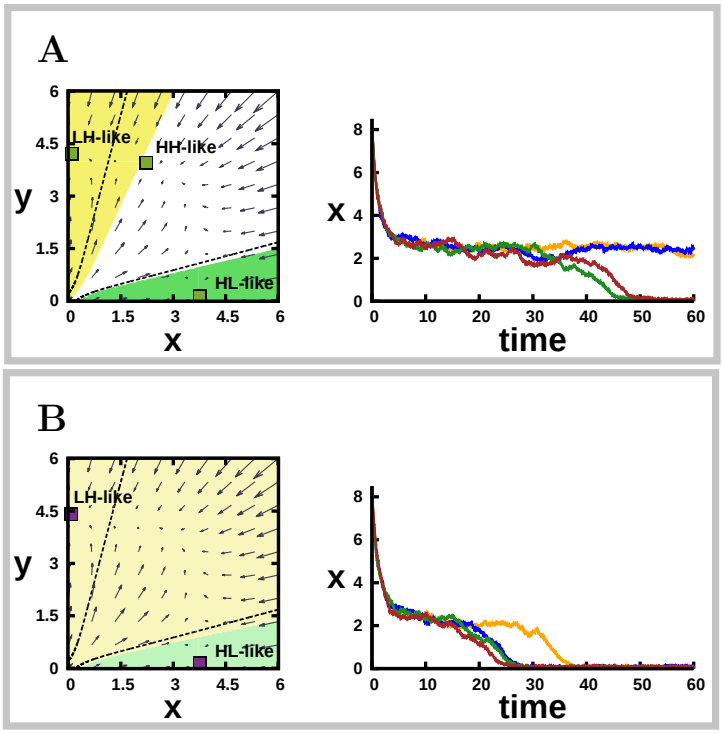

Figure 3.4 The ghost state acts as a steady state in multistable scenarios. (A,B) Phase portrait (left) and different stochastic temporal evolutions of x (right) for a multistable signal with $a_x = 0.4$ and $\Delta a = 0.043$ (A) and $\Delta a = 0.061$ (B). The velocity field (arrows), the linearly stable states (squares), their basins of attraction (colours) and the manifolds in the absence of signal (dashed lines) are depicted in the phase portrait (obtained from the deterministic dynamics). In A, cells are trapped for a while in the HH-like state. In B, the effect of a ghost state around the disappeared HH-like state in phase space B is shown. Other parameter values as in previous figures.

Notice that Figure 3.3D explores signal strength values for which the stability regime generated by the multistable signal does not have three attractors but two (Fig. 3.2E-F). The missed attractor is called a ghost state (Strogatz, 1994) and it slows down the dynamics around it, acting similarly to a metastable HH-like state (Fig. 3.4).

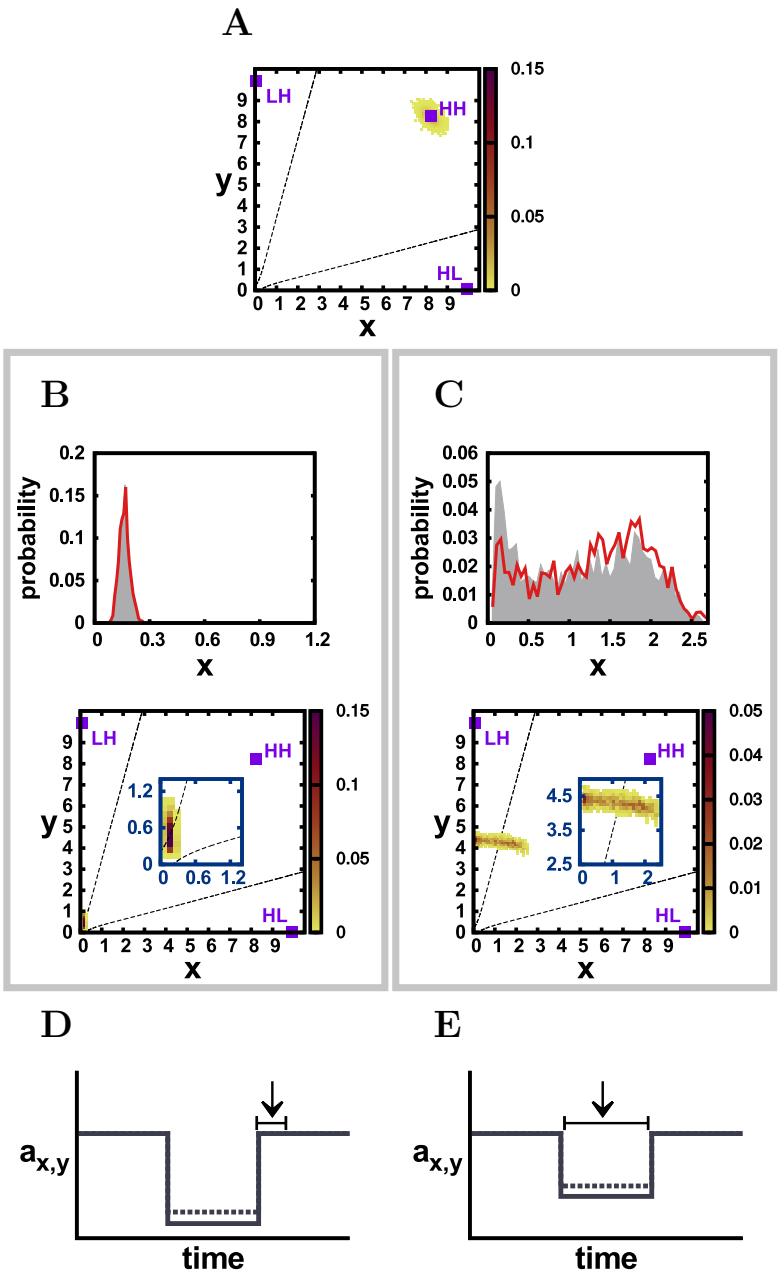
A
LH
HH
HL
x
y
0.15
0.1
0.05
0
B
probability
x
C
probability
x
D
$a_{x,y}$
time
E
$a_{x,y}$
time

Figure 3.5 The cellular decision driven by monostable signals occurs right after the end of the signal while the decisions driven by multistable signals take place while the signal is acting. (A) Deterministic phase portrait with the stochastic initial cell density on top (coluor map) before any signal application ($a_x = a_y = 1$). The three attractors (purple squares) and their basins (dashed lines) are depicted. (B,D) For monostable signals ($a_x = 0.14$, $a_y = 0.1705$). (C,E) For multistable signals ($a_x = 0.4$, $a_y = 0.461$). (B-C, top) Histograms of stochastic x cell values for two different times τ' since the signal started: $\tau' = 19$ (dark grey) and $\tau' = 20$ (grey). (B-C, bottom) Deterministic phase portrait with the stochastic cell density (colour map) at the time of signal removal (for a signal duration $\tau = 20$). The three attractors (purple squares) and their basins (dashed lines) for the deterministic dynamics in the absence of signal are depicted. $N = 10000$ in panels A-C. Other parameter values as in previous figures. (D) Cartoon depicting when the decision takes place (arrow).

Relaxation dynamics, the ones taking place when monostable signals act, are mainly deterministic processes in which fluctuations play a small role. In contrast, for multistable signals, the dynamics of cellular decision making involve stochastic switching, which is an inherently stochastic process that is favoured when fluctuations are larger. Therefore, how the probability of changing of state R_{LH} depends on the amount of fluctuations, controlled by the cell volume, is expected to be different for each of these two mechanisms of cellular decision making (Fig. 3.3C-D). Increasing the amplitude of fluctuations does not change the threshold of signal strength that drives a 50% probability to change to the LH state when the transition is induced by the monostable signal (Fig. 3.3C). In contrast, when the transition is induced by the multistable signal and fluctuations increase through a reduced cell volume, smaller signal strengths are required to achieve a 50% chance of changing of state (Fig. 3.3D).

3.3.2 Different timings for cellular decision making

As indicated above, the dynamics of single cells during the action of the signal is very different for the two types of signals being studied. Indeed, the distribution of the cell population also is. When a monostable signal acts, all cells are in a similar state right after the signal disappears (Fig. 3.5B). The small random differences between cells arising from the stochastic dynamics enable that when the signal disappears, cells may evolve very differently and ultimately reach two distinct fates, either the LH or the HH. Hence, small differences between cells can become strongly amplified. This occurs if right after signal removal some

of the cells lie within the basin of attraction of the HH states whether others, very similar to the first ones, lie within the basin of attraction of the LH state (Fig. 3.5B, bottom).

For the multistable signal, individual cells can show very distinct time-evolutions long before the signal is removed (Figs. 3.5C). Hence, two cell types, which do not change over time, can already be distinguished during the action of the signal. The proportion of cells of each cell type becomes modified over time (Fig. 3.5C). These results hold even for signal strength values that drive bistability instead of tristability, provided a ghost state exists (Fig. 3.5C).

Based on the different behaviour of cells and of the cell population during the action of each type of signal, it can be proposed that the time at which the decision takes place is different between the monostable and multistable scenarios. In the monostable scenario, cells make their decision when the signal is removed (Fig. 3.5D). Oppositely, in the multistable scenario, cells make the decision at stochastically distributed times while the signal is acting (Fig. 3.5E).

3.3.3 Optimal signal duration for cellular decision making

We also expect a dependency between the probability to change of state and the signal duration τ. Since the cell decision to change of cell state is induced by a signal, it is expected that the more time the signal lasts, the more probable it would be to change of state. This is what happens when the signal is the multistable one being proposed. In this case, longer signals let more time for performing stochastic transitions from the HH-like to the LH-like state and hence increase the probability of the decision to change to the LH state (Fig. 3.6A).

However, for monostable signals, we found an optimal duration of the signal for which the probability to change to the LH state becomes maximal (Fig. 3.6B). If the signal lasts longer, the probability to change decreases. This occurs because relaxation towards the unique attractor that exists when the signal acts is not monotonically equivalent for X and Y. Firstly, cells strongly decrease their amount of X and afterwards their amount of Y, as the velocity field shows (Fig. 3.7). This transient asymmetry in the dynamics sets cells in a state similar to the LH state at short times (when just X amount has decreased), and not at

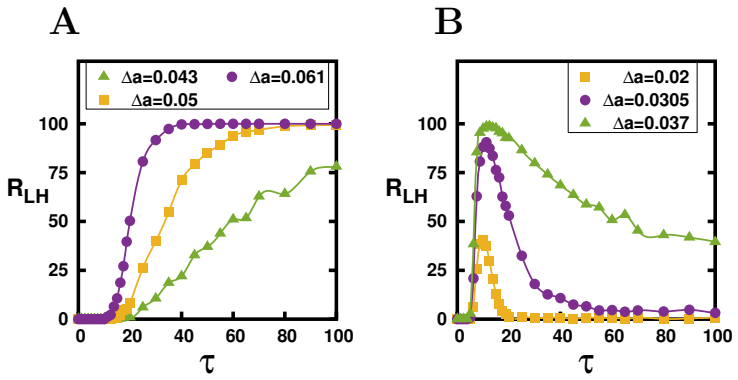

Figure 3.6 The transition to a new cell state exhibits an optimal behaviour with signal duration for the monostable signal, while increases for longer multistable signals. Ratio (in %) of cells that changed to the LH state after the action of a signal as a function of its duration τ, for different signal strength values (see legend). (A) Multistable signal ($a_x = 0.4$). (B) Monostable signal (($a_x = 0.14$). Other parameter values as in previous figures and $N = 900$.

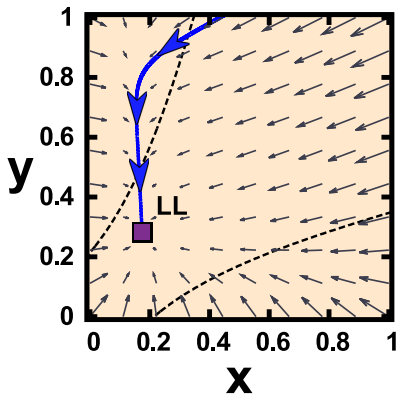

Figure 3.7 The velocity field generated during a monostable signal explains the optimal behaviour as a function of τ. Phase portrait during a monostable signal ($a_x = 0.14$, $\Delta a = 0.0305$). The velocity field (arrows), the unique LL attractor (square), its basin of attraction (light grey), the manifolds separating the basins of attraction of the initial regime without signal (dashed lines) and a deterministic trajectory during the action of the signal (line with arrows) are depicted. The trajectory (in agreement with the velocity field) explores the region of the LH basin of attraction before ending up in the LL state. Other parameter values as in previous figures.

longer times (when both X and Y amounts have decreased). As a result, short signals favour cells to change to the LH state in comparison to longer signals. These non-trivial dynamics would not occur if the cell state is only governed by the dynamics of X, being, for instance, self-activating dynamics.

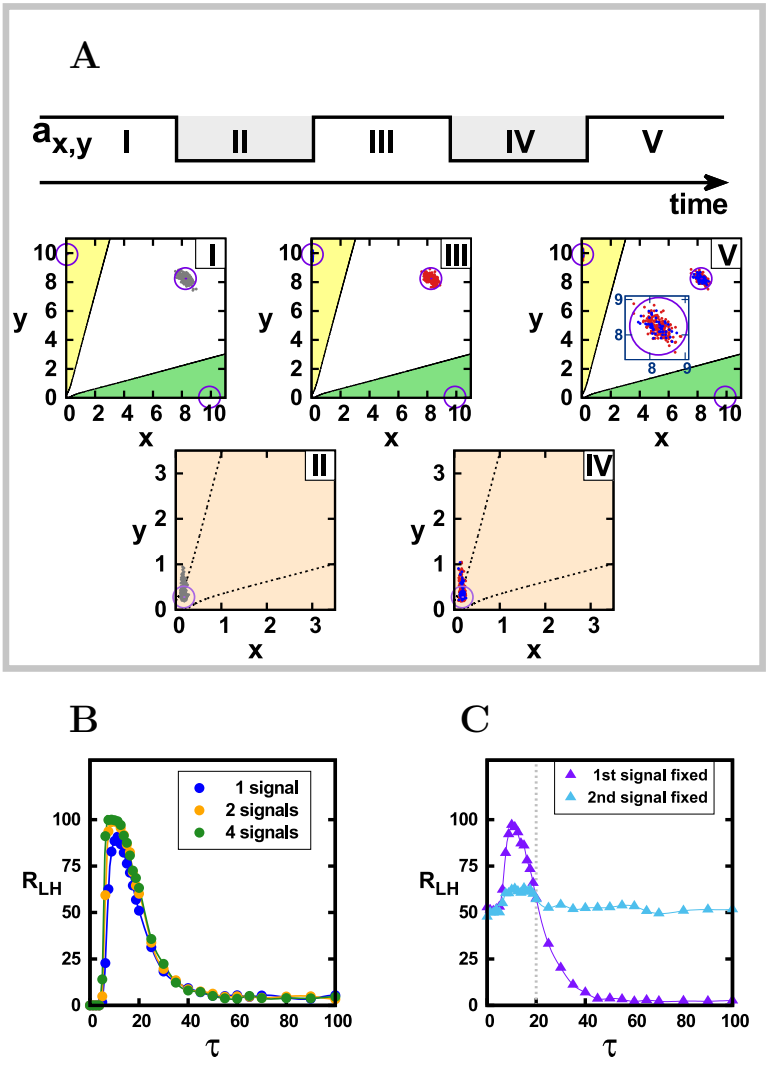

Figure 3.8 The last transient monostable signal determines the final cell fate selection. (A) Evolution of a cell population ($N = 300$) on the deterministic phase portrait when two identical monostable signals act (top cartoon). Cells (dots) initially equivalent (grey), become coloured according to the choice they make after the first signal (red for HH and blue for LH). Phase portraits depict the deterministic attractors (circles) and their basins of attraction (colours). When the signal is acting, the manifolds separating the basins of attraction in the absence of signal are also plotted (dashed lines). Each transient regime is labelled by a roman number. In V (after the two signals), the inset in the middle magnifies the cell population in the HH state, showing it is constituted both by cells that previously decided HH or LH. Parameter values in the absence and in presence of the signal are $a_x = a_y = 1$, and $a_x = 0.14$ with $\Delta a = 0.035$, respectively. Each signal lasts $\tau = 70$. (B, C) Ratio (in %) of cells that changed to the LH state after the action of several monostable signals as a function of their duration τ. (B) For one, two and four identical signals. (C) For two signals of different duration. Two cases are explored: (purple triangles) the first signal lasts $\tau_1 = 20$ and the second signal lasts τ; (cyan triangles) The first signal lasts τ and the second signal $\tau_2 = 20$. Different values of τ are explored (x-axis). The signal duration $\tau = 20$ where the two cases should coincide is denoted by a dashed grey line. Other parameters for the signals in B and C: $a_x = 0.1400$, $\Delta a = 0.0305$ and $N = 900$. Other parameter values as in previous figures.

The results also show that monostable signals enable shorter signals to drive cellular decision making compared to multistable signals. This is because relaxation dynamics are usually faster than the characteristic times for stochastic transitions between attractors of the dynamics.

Another aspect is whether by modulating the duration of the signal a 100% of probability to change to the LH state can be achieved independently of the signal strength value. This happens only for multistable signals, which ensure the choice of the LH state through long enough multistable signals (Fig. 3.6).

3.3.4 Monostable signals erase and restore missing cell types

We evaluated what happens when the signal acts repeatedly over time. We consider the case in which consecutive signals are long enough spaced over time ($\Delta t = 300$ a.u.) such that after each signal removal the dynamics relax to the attractors. From the theoretical point of view, the action of the second and any other subsequent signals differs from the first one in one relevant aspect: the

cell population after the first signal is no longer distributed in a single cell state, but it is distributed among the HH and the HL states.

When several monostable signals act consecutively, all cells, independently of whether they are LH or HH cell types after the first signal, relax to the same monostable attractor (Fig. 3.8A). Hence, all cells tend to become transiently equivalent during the action of each signal. Two consequences arise from this transient behaviour.

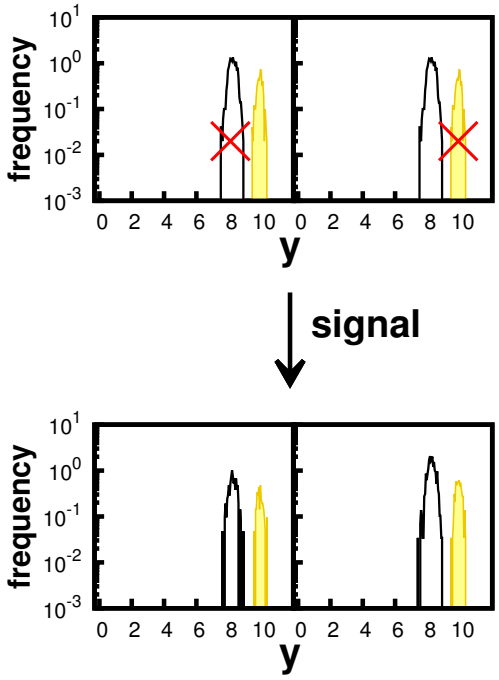

Figure 3.9 A monostable transient signal restores missing cell types. A population of statistically equivalent cells becomes distributed between two states (the initial HH (white), and the new LH state (yellow)) after a monostable signal acts ($a_x = 0.14$, $a_y = 0.175$, $\tau = 70$). If all cells of one of these two cell types are removed (red cross; HH on the right; LH on the left), a second identical transient signal restores the missed cell type and recovers the distribution (normalized). Notice that the normalized distributions are expressed in log scale. $N = 1000$ and other parameter values as in previous figures.

The first consequence is that each signal erases the decisions taken previously by the action of other signals (Fig. 3.8B-C). Cells behave as memoryless: each cell decides *de novo*, independently of which other choices it has done before. Decisions are reversible and cells can switch between states upon the action

of each signal (Fig. 3.8A). Therefore, at any given time, the fraction of cells in the LH state is set only by the last signal and is independent of previous signals (Fig. 3.8C). This occurs when signals are long enough such that all cells, independently of whether they were LH or HH, can reach the attractor (Fig. 3.8A-C). Hence, differences in the characteristic time scale of the relaxation dynamics to the attractor from the HL and the HH states become irrelevant (Fig. 3.8A-C). When signals are too short, these differences provide cells with such a small memory: the probability to choose the LH fate depends slightly on whether it is or not a LH cell (Fig. 3.8B-C).

The second consequence of the transient behaviour of the cells under a second signal is that monostable signals can restore any of the two cell types (LH or HH) if it is lost (Fig. 3.9). Hence, monostable signals provide a mechanism to robustly ensure the existence of two cell types since both cell types can act as the precursor state of the other cell type.

3.3.5 Multistable signals integrate and lock cellular decision making

When a multistable signal acts on a population of two cell types (HH and LH), the HH cells have a probability to change to the LH state by stochastic switching (Fig. 3.10A). However, during the signal effect, LH-like cells can not switch of fate (Fig. 3.10A, Table 3.1). Therefore, the proportion of LH cells in the final population is gradually increased as additional multistable signals act (Fig. 3.10B). Figure 3.10C reveals that the final LH population generated by two consecutive multistable signals does not depend on the order in which these signals are applied. If two signals of different signal duration are applied, the final LH selection is the same, regardless if the first signal is the shorter or the longer one.

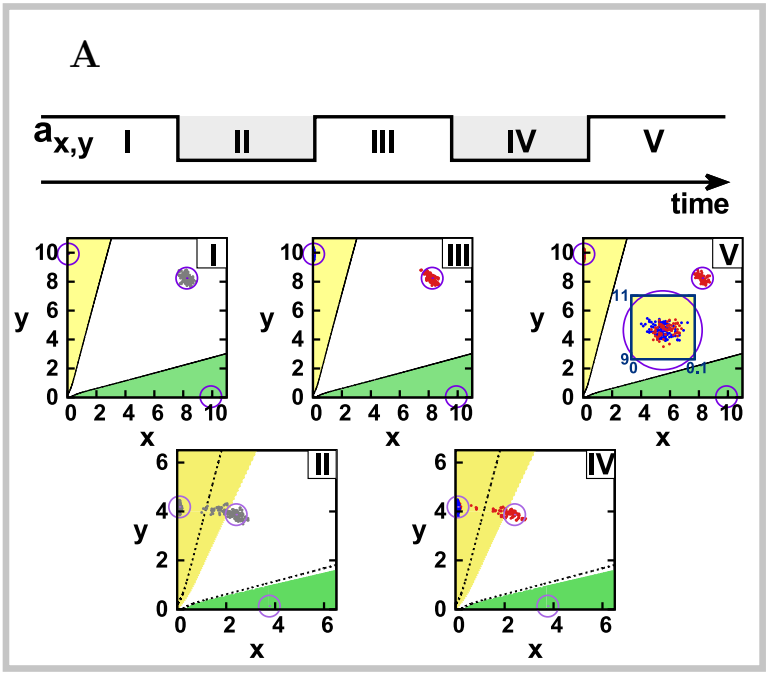
A
$a_{x,y}$
I
II
III
IV
V
time
I
III
V
II
IV
x
y
11
9
0
9.1

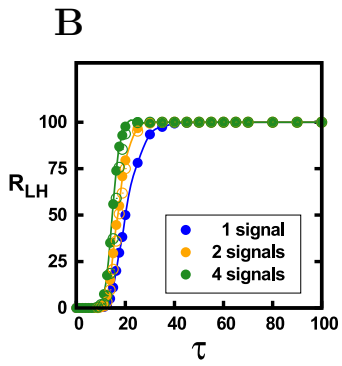
B
R_{LH}
τ
1 signal
2 signals
4 signals

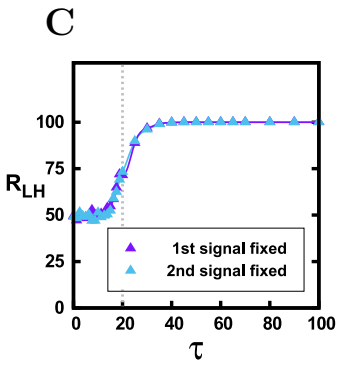
C
R_{LH}
τ
1st signal fixed
2nd signal fixed

Figure 3.10 Multiple multistable transient signals integrate the effect of each signal. (A) Evolution of a cell population ($N = 300$) on the deterministic phase portrait when two identical multistable signals act (top cartoon). Cells (dots) initially equivalent (grey), become coloured according to the choice they make after the first signal (red for HH and blue for LH). Phase portraits depict the deterministic attractors (circles) and their basins of attraction (colours). When the signal is acting, the manifolds separating the basins of attraction in the absence of signal are also plotted (dashed lines). Each transient regime is labelled by a roman number. In V (after the two signals), the inset in the middle magnifies the cell population in the LH state, showing it is constituted by cells that previously decided HH or LH. The population in the HH state is only constituted by cells that previously were HH. Parameter values in the absence and in presence of the signal are $a_x = a_y = 1$, and $a_x = 0.40$ with $\Delta a = 0.04$, respectively. Each signal lasts $\tau = 70$. (B, C) Ratio (in %) of cells that changed to the LH state after the action of several monostable signals as a function of their duration τ. (B) For one, two and four identical signals. (C) For two signals of different duration. Two cases are explored: (purple triangles) the first signal lasts $\tau_1 = 20$ and the second signal lasts τ; (cyan triangles) The first signal lasts τ and the second signal $\tau_2 = 20$. Different values of τ are explored (x-axis). The signal duration $\tau = 20$ where the two cases should coincide is denoted by a dashed grey line. Other parameters of the signals in B and C: $a_x = 0.400$, $\Delta a = 0.061$ and $N = 900$. Other parameter values as in previous figures.

The integration effect of multistable signals can be analytically calculated by knowing the LH selection ratio (R_{LH}) after the first signal. If s identical multistable signals with parameters $\Delta a_i = \Delta a$ and $\tau_i = \tau \ \forall i \in \{1, 2, \ldots, s\}$ are applied to a population of N cells, the HH population after a i-th signal is,

$$N_{HH}(i) = (1 - R_{LH}) \cdot N_{HH}(i-1) = N \cdot \left(1 - R_{LH}\right)^i \tag{3.1}$$

This expression considered that there is no state transition from the LH state to the HH state (as Fig. 3.10A confirms). The signal only drives state transitions between the HH state to the LH state. According to that, the HH population that changes of state by the i-th signal is,

$$N_{LH}(i) = R_{LH} \cdot N_{HH}(i-1) = N \cdot R_{LH} \cdot \left(1 - R_{LH}\right)^{i-1} \tag{3.2}$$

Hence, the total cell population in the LH state after the last signal (s-th signal) is,

$$N_{LH}(\underbrace{\Delta a,\tau;\Delta a,\tau;\ldots;\Delta a,\tau}_{s}) = \sum_{i=1}^{s} N_{LH}(i) = N\Big(1-\big(1-R_{LH}\big)^{s}\Big), \quad (3.3)$$

and the ratio over the whole population corresponds to:

$$R_{LH}(\underbrace{\Delta a,\tau;\Delta a,\tau;\ldots;\Delta a,\tau}_{s}) = 1-\big(1-R_{LH}\big)^{s} \quad (3.4)$$

Through this expression, the total selection ratio after s signals can be calculated by knowing the R_{LH} generated by one single signal (empty symbols of Fig. 3.10B).

The results of Fig. 3.10C, which show that the final fraction of LH selection after two signals of different duration does not depend on which of the two signals is the first one, is explained by the integrating behaviour that gives rise to Eq. (3.4) as follows. The selection ratio driven by two signals ($s = 2$) of different duration (τ_1 and τ_2) is,

$$N_{LH}(\Delta a,\tau_1;\Delta a,\tau_2) = N\,R^1_{LH} + N\,R^2_{LH}\big(1-R^1_{LH}\big), \quad (3.5)$$

where R^1_{LH} and R^2_{LH} are the LH selection ratios driven by signal of $\tau=\tau_1$ and $\tau=\tau_2$, respectively. Notice that,

$$R_{LH}(\Delta a,\tau_1;\Delta a,\tau_2) = R_{LH}(\Delta a,\tau_2;\Delta a,\tau_1) = R^1_{LH} + R^2_{LH} - R^1_{LH}\,R^2_{LH} \quad (3.6)$$

Consequently, the selection rate after two signals of different duration – but identical signal strength – does not depend on which signal acts first.

A multistable signal forces the existence of the LH differentiated state, yet at the expense of the precursor state. If all precursor cells are lost, multistable signals can not recover a new pool of precursor cells (Fig. 3.11). So, due to the asymmetric switching between the LH-like and the HH-like state of the stability regime generated by the multistable signals, the differentiated state (LH state)

is not able to act as a precursor state for future decisions driven by these kind of signals.

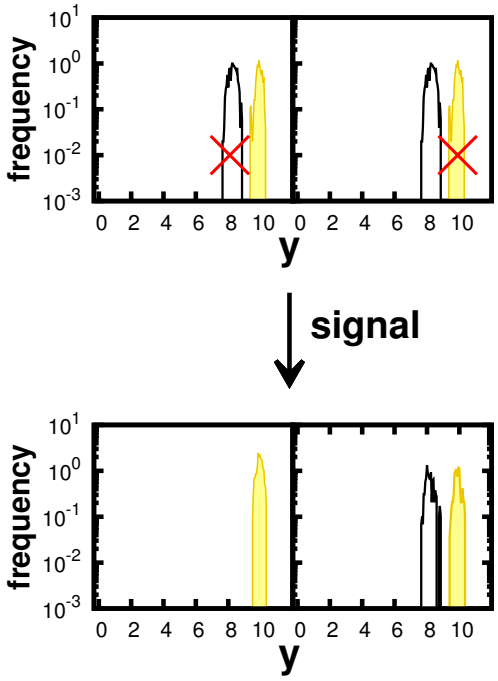

Figure 3.11 A multistable transient signal locks the population in the new cell state. A population of statistically equivalent cells becomes distributed between two states (the initial HH (white), and the new LH state (yellow)) after a multistable signal acts ($a_x = 0.40$, $\Delta a = 0.04$, $\tau = 70$). If all cells of one of these two cell types are removed (red cross; HH on the right; LH on the left), a second identical transient signal restores the missed cell type and recovers the distribution (normalized). Notice that the normalized distributions are expressed in log scale. $N = 1000$ and other parameter values as in previous figures.

3.4 Discussion

We focused our work on a very elemental and simple decision, by which cells decide to change of state or to remain at the initial one. We proposed a transient signal as the inductor that drives the decision with step-like function profiles over time. Smoother signal profiles are not expected to drive differences as long

as the signal is activated and de-activated fast enough such that the stability regimes arising during the turning on/off of the signal play no relevant role.

We described two dynamical mechanisms that are able to drive the same cellular decision. These two mechanisms differ in the stability behaviour that they generate during the signal effect. Despite the fact that both mechanisms are able to drive the same decision, with similar dependency of the probability to change with the signal strength, the decision exhibits different properties according to the signal type that induces it. The work presented in this chapter pretended to connect the decision properties with the dynamical behaviour of the system and suggest which features of the decision are subjected to the dynamical mechanism.

We studied a mechanism that involves a bifurcation to a single stable state (monostable signal). Taking into account that there is only a single basin of attraction during the monostable signal effect, the barrier between the different states involved in the decision disappears and transitions between states can take place.

The other mechanism is based on stochastic switching (multistable signal). The number of states does not change during this signal effect, but the precursor state is stochastically destabilized. Consequently, cells can leave it and reach a new cell state. However, transitions from the differentiated state to the precursor state do not take place during these multistable signals. This asymmetry in the transitions is the main difference, from a dynamical point of view, of this mechanism with the mechanism of the monostable signals.

The mechanism of multistable signals to drive cellular decision making is purely stochastic. So, noise is required to drive the decision under this type of signals. Furthermore, if noise increases, the ratio of differentiated cells in the final population is also increased. Despite its difficulty, noise has been modulated experimentally in some systems by changing the cell volume (Suel et al., 2007). If the cell volumes are reduced, we expect that the probability of changing of state always increases if the decision is induced by a stochastic switching (multistable signals), while if it is a bifurcation mechanism (monostable signals), this probability may increase or decrease depending on which is the signal strength.

For monostable signals, there is only one basin of attraction and so, all the cells behave similarly during the transient signal. As a consequence of this,

the decision takes place once the signal disappears, when the three basins of attractions are restored. By contrast, two differentiated populations of cells are identified during a multistable signal effect. If abundance of cell types are tracked in an experiment (e.g. flow cytometry, microfluidics), we can identify the mechanism that induces the decision according to whether the distribution is unimodal (monostable signals) or bimodal (multistable signals) during the signal effect.

Another experiment to elucidate which mechanism is taking place in the decision is to change the signal duration. According to our results, we expect that a stochastic switching mechanism would increase the differentiation if the signal duration also increases. For long enough multistable signals, we expect that the whole population will choose the new cell state. By contrast, the differentiation ratio driven by a monostable signal can depend on the signal duration in a non trivial way and it may not be able to reach the 100 % of differentiated population even for the longest monostable signal. This non-monotonic behaviour depends strongly on the velocity field and may no arise in other different model dynamics.

Both mechanisms can be also distinguished if the number of signals that induce the decision can be controlled in a experiment. The amount of differentiated cells increases with the number of multistable signals, integrating the effect of each signal. In decisions controlled by monostable signals, the resultant ratio of cells in the new state only depends, mainly, on the last signal. In other words, the amount of change to the new state is not increased by subsequent monostable identical signals.

If an experiment tracks the cell state between two consecutive signals, we would notice that new monostable signals have the capacity of erasing the cell state reached by previous decisions, while multistable signals lock the cells of the differentiated state. Consequently, any attractor of the dynamics can act as a precursor state for decisions driven by monostable signals.

According to the properties of each mechanism, multistable signals fit better in the paradigm of stem–differentiated cell, since differentiated cells are not able to re-program its fate through these signals. Besides, if the precursor cells are removed from the system, this type of signals can not generate new differentiated cells. Monostable signals may have other functions in cellular decision making such as the restoring of any missed cell type.

More sophisticated decisions, where more cell fates are involved, could be also studied with the same approach. In Chapter 4 we are going to characterize a decision where three different cell fates can be reached.

The mechanisms studied in this chapter describe a cell-autonomous decision, where each cell of the initial population makes its decision regardless the choice of the other cells. Non-trivial decision properties can arise if the decision includes some kind of cell-to-cell interaction. In Chapter 5 we are going to explore a system where the system interactions include a cell-to-cell inhibition between first neighbouring cells.

Chapter 4

Cellular decision making involving three cell types

4.1 Introduction

In Chapter 3), we have already introduced an example of cell-autonomous decision making whereby each cell of an homogeneous population chooses between two different responses: remaining unchanged or changing to a new cell state. This change was induced by a transient signal. To this end, we characterized cells by their amounts of two molecules, X and Y. Cells of the same state can differ in these molecular amounts due to the stochastic fluctuations, but not on their statistical properties. This change was induced by a transient signal.

This chapter collects our study of a cellular decision making process which involves the transition to a heterogeneous population of at most three distinct cell types: the initial one and two new ones. Hence, cells are forced to choose between three cell fates. Due to the three cell states required to describe this cellular process, we named this decision as *3-state decision* (Fig. 4.1).

For the sake of simplicity we have studied this *3-state decision* using the network motif of two proteins interacting as a toggle switch with positive auto-regulation reviewed in Chapter 2 and used also in Chapter 3 for the *2-state decision* (Fig. 2.1). As in the previous Chapter, the decision is induced by a transient signal.

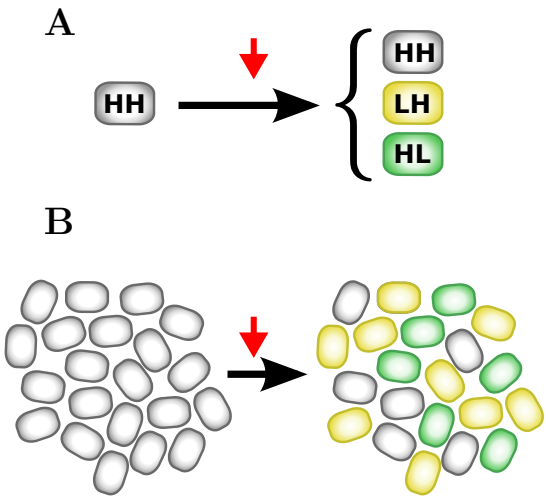

Figure 4.1 Cartoon description of the 3-state cellular decision making. (A) The initial population of cells is all the cells in the same state in statistical terms (grey). After the action of the transient signal (red arrow), the population becomes heterogeneous, with three cell states involved (grey, yellow and green). (B) Decision at the single cell level and nomenclature of states in terms of low (L) or high (H) amounts of molecules X and Y. The cell is initially at the symmetric cell state HH (grey) and, due to the action of a transient signal (red arrow), decides between three cell states: to remain as it was in the former HH state (grey), to change to a new, LH, state (yellow) or to change to another new HL state (green).

In this Chapter we evaluate the properties of this *3-state decision* and how they depend on the parameters of the transient signal applied. Furthermore, we also studied the resultant decision if more than one transient signal is applied and its biological consequences.

4.2 The model, the signal and the phase space transition the signal drives

We implemented the *3-state decision* using the same stochastic model dynamics than in previous Chapters (Chapters 2 and 3). The algorithms and theoretical tools which have been applied to generate the results of this Chapter have been already described in the Sections 2.4, 2.5 and 3.2 of Chapter 2 and Chapter 3 respectively.

Due to the transient nature of the inductive signal, the values of the parameters are the same before and after the signal acts. Hence, to have a *3-state decision* induced by a transient signal, three stable attractors (one for each cell state involved in the decision) have to be present at least when the signal is not acting. To this end, we chose the same value of parameters for the initial condition as in Chapter 3: $a_x = a_y = 1$, $\sigma = 0.2$, $\rho = 10$, $K = 10^{-5}$ and $V = 10$. As shown in Chapter 2, this set of parameter values generates a multistable regime with three stable fixed points, named HH, LH and HL (Figs. 2.3A, 3.2A and 4.1A). Before the signal action, all the cells of the initial population are in the HH state.

As in Chapter 3, the decision is induced by a signal which transiently changes two control parameters of the dynamics to new constant values. These control parameters are the maximal production rates of the molecules X and Y, a_x and a_y (Figs. 2.3D-E). The signal modifies the control parameters (a_x, a_y) as a step-like function profile (Fig. 3.2B).

The signals we studied for this chapter take values of $a_x = 0.2$ and $a_y = a_x + \Delta a$, being $\Delta a << a_x$ and hence $a_y \approx a_x$ (Fig. 4.2A-C). These values drive a phase space with only two stable fixed points, which correspond to LH-like and HL-like states (Figs. 2.3B and 4.2A-B). The signal can then be characterized by only two parameters: the signal duration, τ, and the signal strength, $\Delta a = a_y - a_x$ (Fig. 3.2B).

4.3 Results

4.3.1 The duration of the signal only controls how many cells acquire a new fate, but not which one

We first evaluated the bifurcation driven by the transient signal. During the signal effect, two antisymmetric branches are stable while the HH branch is destabilized according to the bifurcation diagram (Fig. 2.3D). If $a_x = a_y = 0.2$, the two attractors are perfectly antisymmetric and the manifold that divides the phase space in two basins of attraction is the bisecting line (Fig. 4.2A). For $\Delta a = a_y - a_x \neq 0$ with $a_x = 0.2$ there are strong differences between the basins of attraction of the two states, while the states themselves are slightly modified

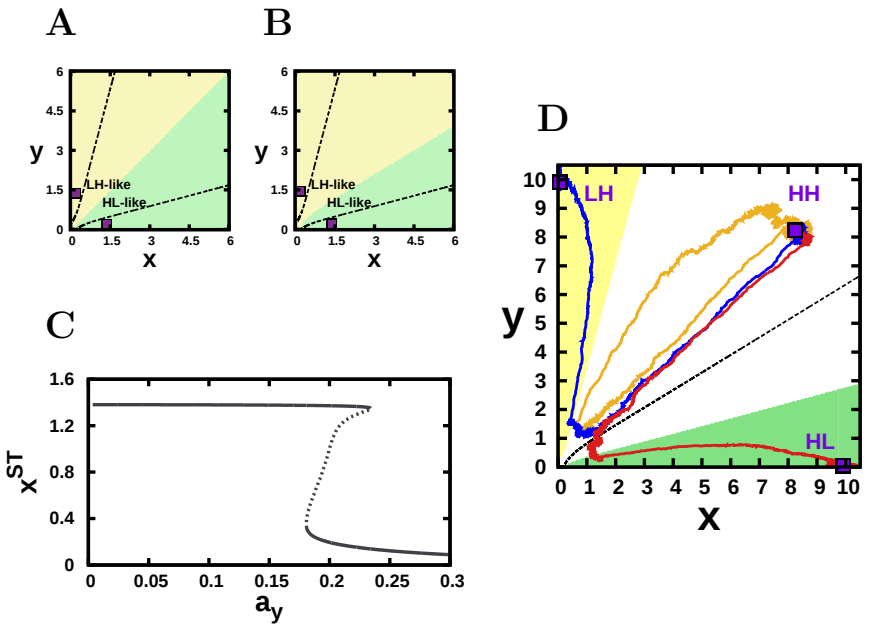

Figure 4.2 The transient signal drives a *3-state decision* through a bifurcation from a tristable regime to a bistable one and backwards. (A, B) Phase portrait for $a_x = 0.2$ and $a_y = a_x + \Delta a$ with (A) $\Delta a = 0$ and (B) $\Delta a = 0.004$. The two stable fixed points (squares), named LH-like and HL-like, and their basins of attraction (yellow and green, respectively) are depicted. Black dashed lines show the manifolds for $a_x = a_y = 1$, which correspond to the absence of signal. (C) Bifurcation diagram of X steady states with a_y as a control parameter for a_x=0.2. Solid and dashed lines are the stable and unstable branches respectively. (D) Phase portrait for $a_x = a_y = 1$ (squares for stable fixed points; white, yellow and green for their basins of attraction) and stochastic trajectories (continuous lines) pursued by three initially equivalent cells (orange, blue, red) in the HH state when a transient signal with $a_x = 0.2$ and $\Delta_a = a_y - a_x = 0.004$ and duration $\tau = 20$ is applied. One cell ended at the same initial state (orange), another one ended in the new LH state (blue) and a third one in the other new HL state (red). The manifold transiently generated during the signal effect that separates the two transient basins of attraction is shown with a black dashed line.

from the $\Delta a = 0$ case (Fig. 4.2B compared to A). Notice also that the two transient fixed points, HL-like and LH-like, lie within the basins of attraction of the HL and LH states, respectively (Fig. 4.2A-B). We then applied this type of signal on a population of N cells. Specifically, at $t = 0$ we started with the concentrations of X,Y for each cell in a gaussian distribution centred in the HH state whose width corresponds to the standard deviation (sd) of the equilibrium distribution – that depends on V ($st = 0.235$ for $V = 10$). These N initial concentrations evolve with a different seed of the algorithm until $t = 20$ without the signal effect, in order to reach the equilibrium distribution. Once the signal is removed from the system, cells evolve during 50 units of time with $a_x = a_y = 1$ (as in Chapter 3).

Trajectories on the phase diagram reveal that three different states can be selected under the same conditions and after an identical bistable signal has acted (Fig. 4.2D).

Despite the stochasticity of the decision, we can describe it according to the ratio of each cell state in the final population. We define the *3-state decision* by two different choices that can be characterized according to two main descriptors of the final population of cells:

- The *Differentiation choice* is the cellular choice of changing of state and is quantified by R_{diff}. R_{diff} is the ratio of the cells which change of state (hereafter named differentiated cells, in analogy to processes taking place in development).
- The *Asymmetric choice* is the cellular choice of selecting the LH state instead of the HL state and is quantified by R_{asym}. R_{asym} is the ratio of the number of cells in the LH state over the total number of cells in the LH and HL states.

Following the same nomenclature than in Section 3.2 (Chapter 3), R_{HH}, R_{LH} and R_{HL} are the selection ratio for each cell state (HH, LH and HL state, respectively). Therefore, $R_{diff} = R_{LH} + R_{HL} = \frac{N_{LH}+N_{HL}}{N}$, where N is the total number of simulated cells and N_{LH} and N_{HL} is the number of cells in the LH and HL state respectively at the end of the simulation, long after the signal has been applied. $R_{asym} = \frac{R_{LH}}{R_{LH}+R_{HL}} = \frac{N_{LH}}{N_{LH}+N_{HL}}$ is the ratio of cells which select the LH cell state among all the cells which select a new cell state.

In the figures of this chapter, we characterize the dependence of the two choices (R_{diff} and R_{asym}) on the two signal parameters: τ (signal duration) and Δa (signal strength). These response curves are named according to the choice and to the signal parameter that is explored.

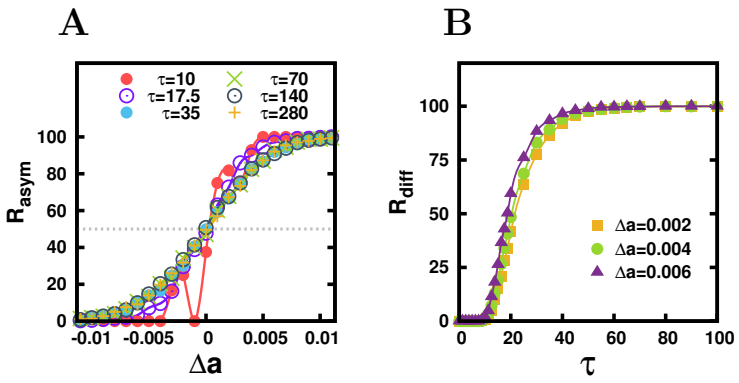

Figure 4.3 Each signal parameter controls only one choice. Response curves when a single signal is applied and all N cells are initially statistically equivalent, being in the HH state. (A) Δa-R_{asym}-response curves for different values of signal duration (τ). $N = 1000$. (B) τ-R_{diff}-response curves for different values of signal strength (Δa). $N = 5000$. R_{asym} and R_{diff} are expressed in percentage (%).

Strong dependence of R_{asym} on Δa was already known from previous studies (Guantes and Poyatos, 2008). Other previous studies explored the dependency of R_{asym} on the signal parameters in a framework of permanent signals where both signal strength and signal duration are controlled by a single signal parameter (Nené et al., 2012). Response curves in Fig. 4.3A reveal that the *Asymmetric choice* of LH over HL (R_{asym}) depends strongly on the signal strength (Δa) while very weakly on the signal duration (τ). R_{asym} describes nearly the same threshold-like function with the 50% ($R_{LH} = R_{HL}$) at $\Delta a = 0$ for different durations of the signal.

Signal duration (τ) has a strong impact in the *Differentiation choice* (R_{diff}), describing a threshold-like function of τ whose threshold position and shape do not significantly depend on the signal strength Δa (Fig. 4.3B). Therefore, our results revealed that each of the two different choices that define the *3-state decision* (*Differentiation choice* and *Asymmetric choice*) are mainly controlled by a single and different parameter (τ and Δa, respectively).

4.3.2 Each choice is made at a different time

According to the results of the previous section (Fig. 4.3), each choice of the decision is mainly controlled by a different signal parameter. The *Asymmetric choice* is determined by the shape of the transient manifold generated by the signal (Fig. 4.2B-C) and the distribution of the initial cell population. So, this choice is made once the signal is applied and this interaction occurs. The *Differentiation choice* also arises from the interaction between manifolds and distributions of cells. In this choice, however, the manifold are those of the tristable regime once the signal is removed (3.2A). These manifolds interact with the distributions at the end of the signal effect and they determine the final attractor reached by each cell of the distribution.

The relationships between each choice and the main parameter that controls each one describe a sigma-like function in both cases (Fig. 4.3). This arises from the equivalent mechanism that drives the choices: manifold-distribution interaction. In the *Asymmetric choice*, Δa value defines the manifold, while the initial distribution does not depend on this parameter. In contrast, the Δa controls the position of the final concentration distributions of cells, but not the manifold shape (determined by the parameter values once the signal is removed) for the *Asymmetric choice*. Consequently, since in both choices the parameter determines the relative position between the manifold and the variable distributions, both relationships behave as a sigma-like function (which is the cumulative probability of a gaussian).

Despite the fact that we can clearly identify which signal parameter, τ or Δa, controls each choice, both choices depend slightly on the other signal parameter (Fig. 4.4A-B). These dependencies are explained by the time at which each choice of the decision takes place.

From the *Differentiation choice* (R_{diff}) dependence on the signal duration, we can define a threshold time at which half of the cells have chosen a new state (Fig. 4.3A). This threshold-time does not depend significantly on Δa, since the values of the LH-like and HL-like attractors generated by the signal effect remain roughly constant with Δa (Fig. 4.2C). Despite of this, notice how the different τ-R_{diff} response curves of Fig. 4.3A exhibit different values of R_{diff} for τ values around the threshold time. This weak dependency of the threshold value on Δa is shown in the Δa-R_{diff} response curves of Fig. 4.4A. Although the

LH-like and HL-like attractors generated by the bistable signal do not depend significantly on Δa, this signal parameter changes the velocity field and thereby the dynamics to reach the new states. Figure 4.4C shows that Δa reduces the time required to reach the favoured attractor (LH-like for $\Delta a > 0$), which is the differentiated state that contributes more to R_{diff}.

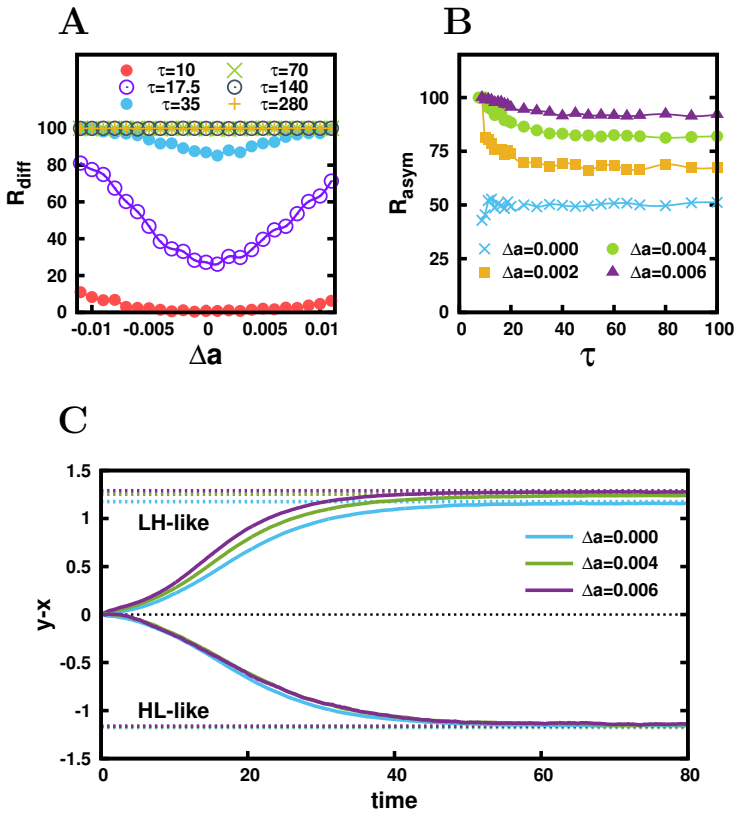

Figure 4.4 The signal strength (Δa) affects the value of both decision descriptors (R_{diff} and R_{asym}) by changing the velocity of the dynamics. Response curves when a single signal is applied and all N cells are initially statistically equivalent, being in the HH state. (A) Δa-R_{diff}-response curves for different values of signal duration (τ). $N = 1000$. (B) τ-R_{asym}-response curves for different values of signal strength (Δa). $N = 5000$. R_{asym} and R_{diff} are expressed in percentage (%). (C) Average time evolution $(y - x)$ for $N = 10000$ cells. All cells started at the HH state. $(y - x)$ values of the LH-like and HL-like attractors are depicted in dashed coloured lines. The trajectories have been divided according to the final attractor reached.

Signal strength (Δa) controls the *Asymmetric choice* by changing the transient the manifold shape (Fig. 4.2B-C). Although the manifold shape does not depend

on the signal duration, R_{asym} exhibits slightly higher values for very low values of τ (Fig. 4.4B). This behaviour comes from the asymmetry in the time required to reach each attractor: LH-like or HL-like. Figure 4.4C reveals that cells require less time to reach the favoured attractor (LH-like for $\Delta a > 0$).

4.3.3 Stochastic effects on the choices involved in the decision

The effective volume of the system (V) is a parameter that controls the fluctuation amplitude of the dynamics. Noise intensity increases as the volume decreases. Figure 4.5 shows how the response curves change if the volume is modified.

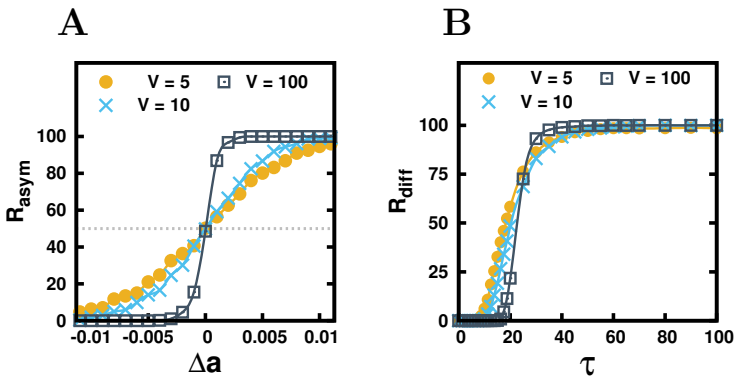

Figure 4.5 Effect of fluctuations on the choices (R_{diff} and R_{asym}). (A) Δa-R_{asym}-response curves for three different values of the volume (V). $\tau = 35$, $N = 1000$. (B) τ-R_{diff}-response curves for three different values of volume (V). $\Delta a = 0.004$, $N = 5000$. R_{asym} and R_{diff} are expressed in percentage (%).

The noise tends to make the choice between the two differentiated states (LH and HL) more symmetric (Fig. 4.5A). This result is reflected in the smoothening of the sigma-like shape of Δa-R_{asym}-response curves of Fig. 4.5A. The threshold position of these curves does not vary with the volume. The key ingredients to understand the noise effect on this *Asymmetric choice* lie in the stochastic basins of attraction and in the cell population distribution amplitude (Fig. 4.6). According to Fig. 4.6, the volume has two main effects on the dynamics during the signal effect: the noise reduces the barrier between the two basins of

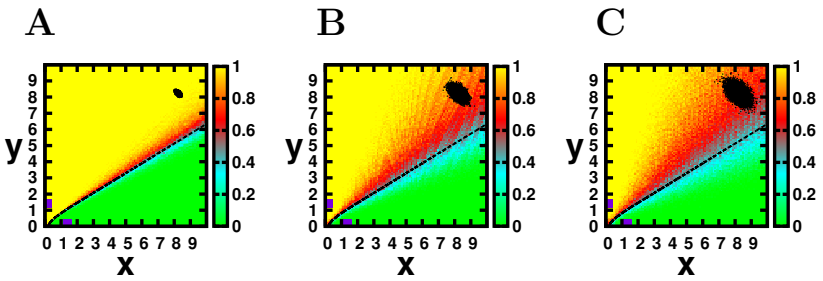

Figure 4.6 Stochastic basins of attraction during the signal effect. Phase portraits for different volume values. The color map expresses the probability of reaching the LH-like state at long times, when $a_x = 0.2$ and $a_x = 0.204$. In the phase portrait, attractors (purple squares) and the deterministic manifold (black dashed line) have been also depicted. Volume values explored: (A) $V = 100$, (B) $V = 10$ and (C) $V = 5$. Stochastic basins of attraction have been computed simulating 100 stochastic trajectories from each point of a 100×100 grid. Black points (10000) are the steady distribution around the HH state, corresponding to $a_x = a_y = 1$.

attraction; and it increases the size of the phase space occupied by the initial population of cells.

The *Differentiation choice*, mainly controlled by τ, exhibits a non trivial dependence on the noise intensity (i.e. volume) (Fig. 4.5B). Despite the fact that noise increases the R_{diff} value for low values of τ, this tendency is inverted as τ increases. This behaviour is not found in symmetric signals ($\Delta a = 0$), where R_{diff} is clearly promoted by fluctuations (Fig. 4.7A). Figure 4.7B reveals that this differentiation increase for symmetric signals ($\Delta a = 0$) is caused by the destabilization of the unstable state of the bistable signal (see the trajectories of Fig. 4.2 D). Under a symmetric bistable signal, cells first evolve to the unstable state following the manifold (bisecting line). As this unstable state is a saddle node, cells eventually leave it and reach the transient attractors of the dynamics. Fluctuations favour the escape from the unstable state and thereby promote differentiation. The situation is slightly different when the signal is not symmetric. Figure 4.7C shows the dynamics of cell contrations over time for asymmetric signals ($\Delta a \neq 0$). Notice how, although the noise-promoted escape of the unstable state also takes place here, noise reduces the velocity of the dynamics once the cells escape from it. The trade off between these two noise effects drives the non trivial behaviour observed in Fig. 4.5B.

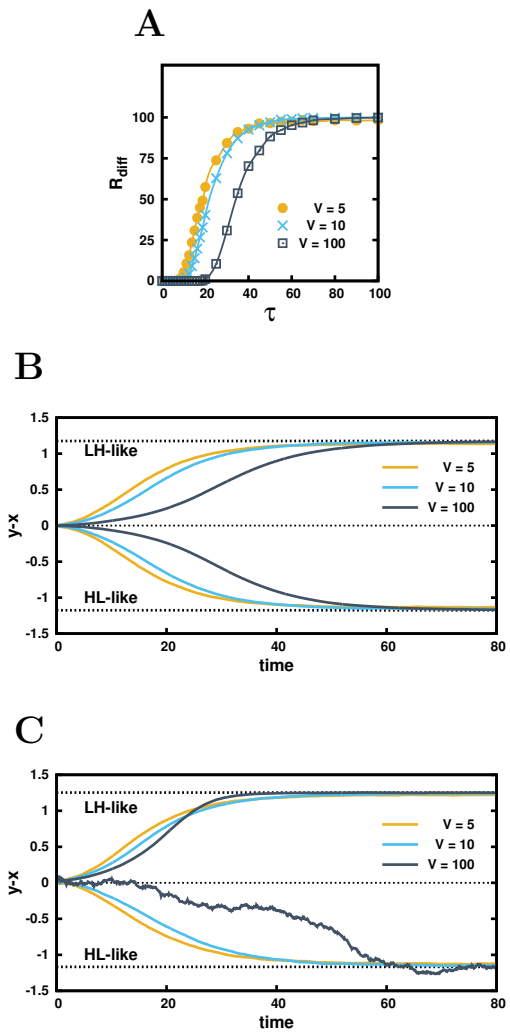

Figure 4.7 Dependence of the cell dynamics on the system volume. (A) τ-R_{diff}-response curves for three different values of volume (V) for a symmetric signal $\Delta a = 0$. $N = 5000$. R_{diff} is expressed in percentage (%). (B,C) Average of $(y - x)$ over $N = 10000$ cells that evolve along time under the effect of (B) a symmetric ($\Delta a = 0$) or (C) an asymmetric ($\Delta a = 0.004$) bistable signal, for three different volumes V (legend). All cells started at the HH state. $(y - x)$ values of the LH-like and HL-like deterministic attractors are depicted in dashed coloured lines. Notice that the trajectories have been divided according to the final attractor reached. For this reason, the curve that reaches the HL-like state for $V = 100$ in panel C averages over few number of cell trajectories (12 trajectories).

The noise intensity, controlled by the system volume, affects both choices of the decision. However, its effect is more significant in the *Asymmetric choice*, where it reduces the capability of discrimination between the two new states.

4.3.4 The initial cell type can not be restored by the differentiated population

The LH-like and the HL-like attractors generated by the bistable signals lie in the LH and HL basins of attraction of the inistial and final tristable regime respectively. Hence, during the bistable effect, the HH state disappears (and so does its basin of attraction) while the other LH, HL states remain although their values slightly change. Because of this, the only cell transitions that can be driven by a bistable signal is from the HH state to the other two (HL and HL).

Figure 4.8 shows the effect of a bistable signal over a cell population generated by a previous bistable signal. Before this second signal application, the cell population of one of the three cell types (HH, LH or HL state) is removed from the initial population. Results of Fig. 4.8 reveal that, if the cell population of either HL or LH state is removed, a second signal can restore it. By contrast, the HH population can not be generated by the cell population in the HL or LH state. Consequently, we can identify the HH state as the precursor state, able to produce the other states.

This conclusion is relevant from the biological point of view to restore a damaged tissue or population, where a cell type is removed from the population. Once a signal is applied on a population of HH cells, a resultant heterogeneous population with three cell types would be generated: HH, LH and HL cell types. If all cells of one of these cell types are removed from the final population, a second signal can restore the missed cell type unless the removed cell type is the HH state (Fig. 4.8).

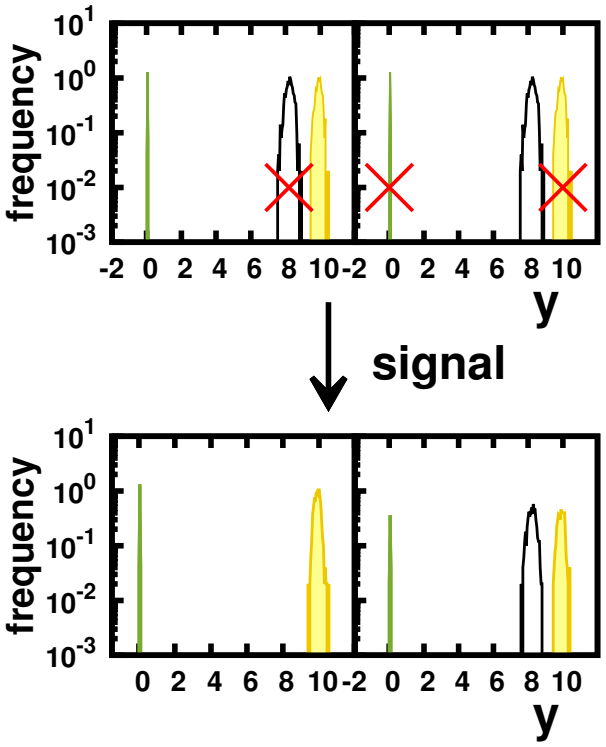

Figure 4.8 Population restoring after a second signal. The final population after a multistable signal applied ($a_x = 0.2$, $a_y = 0.204$, $\tau = 20$) to an initial population on the HH state is distributed between three states: the initial HH one (white), and the differentiated LH state (yellow) and the differentiated HL state (green) (top). (left) A second identical signal can not restore the HH population if it is missed. (right) However, if cells of these differentiated cell types, LH or HL, are removed, a second identical transient signal restores the missed cell type and recovers the initial distribution (normalized). A population of 1000 cells has been simulated to generate the histograms. Notice that the probability is expressed in log scale.

4.3.5 Multiple identical signals drive more differentiated cells with fixed proportions of new fates

From the results of the previous section we can infer the behaviour of a cell population under several bistable signals. The *Differentiation choice*, since it increases with the signal duration, integrates the effect of each bistable signal when several signals are applied. In contrast, the *Asymmetric choice* is mainly

controlled by the basins of attractions generated by the bistable signals. Considering that the shape of these basins of attraction depends mostly on the signal strength (and not on the signal duration), we expect that multiple identical signals would not significantly affect this choice.

In the Section 3.3.5 of the Chapter 3 we calculated the probability of selecting a new state driven by s multiple identical multistable signals (Eq. (3.4)). This probability of selection of a new state studied in Chapter 3 is given by R_{LH}, which is the only new state that is populated in that decision (since the HL state remains unpopulated). The assumption that gave rise to the expression (3.4) is that the transition from the new LH state to the initial HH state is not driven by subsequent signals. Figure 4.8 revealed this same behaviour for bistable signals, with two differentiated states, LH and HL states, instead of a single one. Accordingly, we can analytically calculate the differentiation choice after a number s of identical signals ($R_{diff}(\tau_1, \tau_2, ;\tau_S)$ for $\Delta a_i = \Delta a$ and $\tau_i = \tau$ $\forall i \in \{1, 2, \ldots, s\}$) as it was done in Chapter 3 according to Eq. (3.4):

$$R_{diff}(\underbrace{\Delta a, \tau; \Delta a, \tau; \ldots; \Delta a, \tau}_{s}) = 1 - \left(1 - R_{diff}\right)^s, \tag{4.1}$$

where s is the number of signals, and R_{diff} is the differentiation ratio generated by one single signal.

Figure 4.9 shows the response curves long after multiple identical signals are applied. Time interval Δt between each signal is long enough to enable cells to reach the fixed points of the dynamics and corresponds to $\Delta t = 300$ a.u. The results are evaluated a time interval of 50 a.u. after the last signal ended. These results reveal that the resultant *Differentiation choice* (R_{diff}) driven by multiple signals include the effect that each signal would individually have in this choice- until it saturates at 100% (Fig. 4.9A,C) according to expression (4.1).

The final effect on the differentiation choice of multiple (s) signals of identical duration τ can be understood as the effect of a single longer signal of duration τ_{eff}. The effective duration τ_{eff} that a single signal requires to last to drive the same differentiation as multiple s signals of duration τ (i.e. τ_{eff} such that $R_{diff}(\Delta a_1, \tau_1; \Delta a_2, \tau_2; \ldots; \Delta a_s, \tau_s) = R_{diff}(\Delta a, \tau_{eff})$ for $\Delta a_i = \Delta a$ and $\tau_i = \tau$ $\forall i \in \{1, 2, \ldots, s\}$) is shorter than the addition of all signal durations,

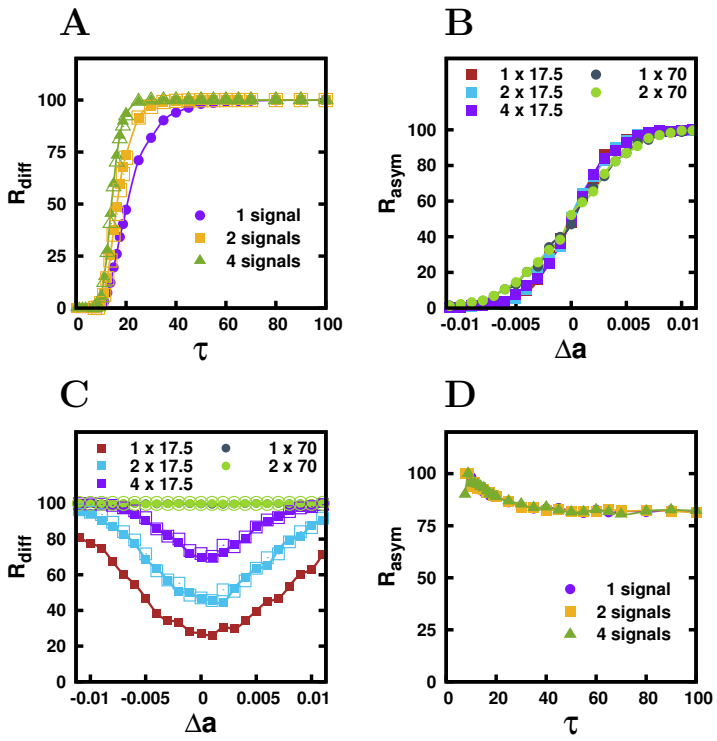

Figure 4.9 Response curves after multiple identical signals. (A) τ-R_{diff}-response curves ($\Delta a = 0.004$) for different identical signals. (B) Δa-R_{asym}-response curves ($\tau = 140$) for different identical signals. (C) Δa-R_{diff}-response curves ($\tau = 140$) for different identical signals. (D) τ-R_{asym}-response curves ($\Delta a = 0.004$) for different identical signals. Simulation details: $N = 1000$ (A,B) and $N = 5000$ (C,D). The empty symbols of panels A and C are the theoretical prediction calculated through the R_{diff} of the first signal (Eq. (4.1)).

$\tau_{eff} < s \cdot \tau$. In other words, the differentiation after a single signal of $\tau_{eff} = 70$ is higher than the differentiation generated by four identical signals of $\tau = 17.5$ ($R_{diff}(\Delta a, \tau = 70) > R_{diff}(\Delta a, 17.5; \Delta a, 17.5; \Delta a, 17.5; \Delta a, 17.5)$, Fig. 4.9A). This is because R_{diff} depends non-linearly with the duration of the signal, increasing according to a sigmoidal function.

We can also calculate the behaviour of the *Asymmetric choice* when s identical signals are applied:

$$R_{asym}(\underbrace{\Delta a,\tau;\Delta a,\tau;\ldots;\Delta a,\tau}_{s}) = \frac{R_{LH}(\underbrace{\Delta a,\tau;\Delta a,\tau;\ldots;\Delta a,\tau}_{s})}{R_{diff}(\underbrace{\Delta a,\tau;\Delta a,\tau;\ldots;\Delta a,\tau}_{s})} \tag{4.2}$$

Since we already know the expression of $R_{diff}(\Delta a,\tau;\Delta a,\tau;\ldots;\Delta a,\tau)$ (Eq. (4.1)), we have to evaluate $R_{LH}(\Delta a,\tau;\Delta a,\tau;\ldots;\Delta a,\tau)$ (see Section 3.3.5 for further details),

$$R_{LH}(\underbrace{\Delta a,\tau;\Delta a,\tau;\ldots;\Delta a,\tau}_{s}) = \sum_{i=1}^{s} R_{LH}\cdot(1-R_{diff})^{i-1}, \tag{4.3}$$

where R_{LH} and R_{diff} are the ratio of LH-selection and the ratio of differentiation after a single signal respectively. Evaluating the summation,

$$R_{LH}(\underbrace{\Delta a,\tau;\Delta a,\tau;\ldots;\Delta a,\tau}_{s}) = R_{LH}\frac{1-\left(1-R_{diff}\right)^{s}}{R_{diff}} \tag{4.4}$$

Substituting Eqs. (4.1) and (4.4) in expression (4.2) results into,

$$R_{asym}(\underbrace{\Delta a,\tau;\Delta a,\tau;\ldots;\Delta a,\tau}_{s}) = \frac{R_{LH}}{R_{diff}} = R_{asym} \tag{4.5}$$

According to this expression (4.5), the ratio between the cells in LH and HL state (R_{asym}) does not depend on the number of signals and this is confirmed by the stochastic simulations (Fig. 4.9B,D).

4.3.6 Decision after two different signals

In the previous section we saw how that choices depend on the number of signals when s identical signals are applied. Herein, we focus on the action of two signals with different parameter values.

The differentiation ratio driven by two signals ($s=2$) of different strength (Δa_1 and Δa_2) and duration (τ_1 and τ_2) is,

$$R_{diff}(\Delta a_1, \tau_1; \Delta a_2, \tau_2) = R^1_{diff} + R^2_{diff}\big(1 - R^1_{diff}\big), \tag{4.6}$$

where R^1_{diff} and R^2_{diff} are the differentiation ratios driven by a signal characterized by $(\Delta a_1, \tau_1)$ and $(\Delta a_2, \tau_2)$, respectively. This expression is independent on the signal order.

The *Asymmetric choices* depends on the signal order. Notice that this choice is mainly controlled by the signal strength and it is not relevantly affected by the signal duration (Fig. 4.3A). So, the asymmetric ratio driven by multiple signals of different duration but identical signal strength would be the same, regardless the signal order. The asymmetric ratio that results from the application of two bistable signals ($s = 2$) of different strength (Δa_1 and Δa_2) is,

$$R_{asym}(\Delta a_1; \Delta a_2) = \frac{R_{LH}(\Delta a_1; \Delta a_2)}{R_{diff}(\Delta a_1; \Delta a_2)} \tag{4.7}$$

Notice that signal duration has not been explicitly introduced in the expression for simplicity. Besides, $R_{diff}(\Delta a_1; \Delta a_2) = R_{diff}(\Delta a_2; \Delta a_1)$. This identity is not satisfied by the LH selection ratio:

$$R_{LH}(\Delta a_1; \Delta a_2) = R^1_{LH} + R^2_{HL}\,(1 - R^1_{diff}) = R^1_{LH} + R^2_{LH} - R^2_{LH}\,R^1_{diff} \tag{4.8}$$

And so,

$$R_{asym}(\Delta a_1; \Delta a_2) = \frac{R^1_{LH} + R^2_{LH} - R^2_{LH}\,R^1_{diff}}{R^1_{diff} + R^2_{diff} - R^1_{diff}\,R^2_{diff}} \tag{4.9}$$

According to the expression (4.9), $R_{asym}(\Delta a_1; \Delta a_2) \neq R_{asym}(\Delta a_2; \Delta a_1)$ unless the asymmetric ratios generated by both signals are identical ($R^1_{asym} = R^2_{asym}$).

Herein, we show the results after two signals of identical signal strength ($\Delta a_1 = \Delta a_2 = \Delta a$) but different duration ($\tau_1 \neq \tau_2$).

We evaluated the τ-R_{diff}-response curves under two conditions: A first signal of a fixed signal duration value (τ) followed by a second transient signal which

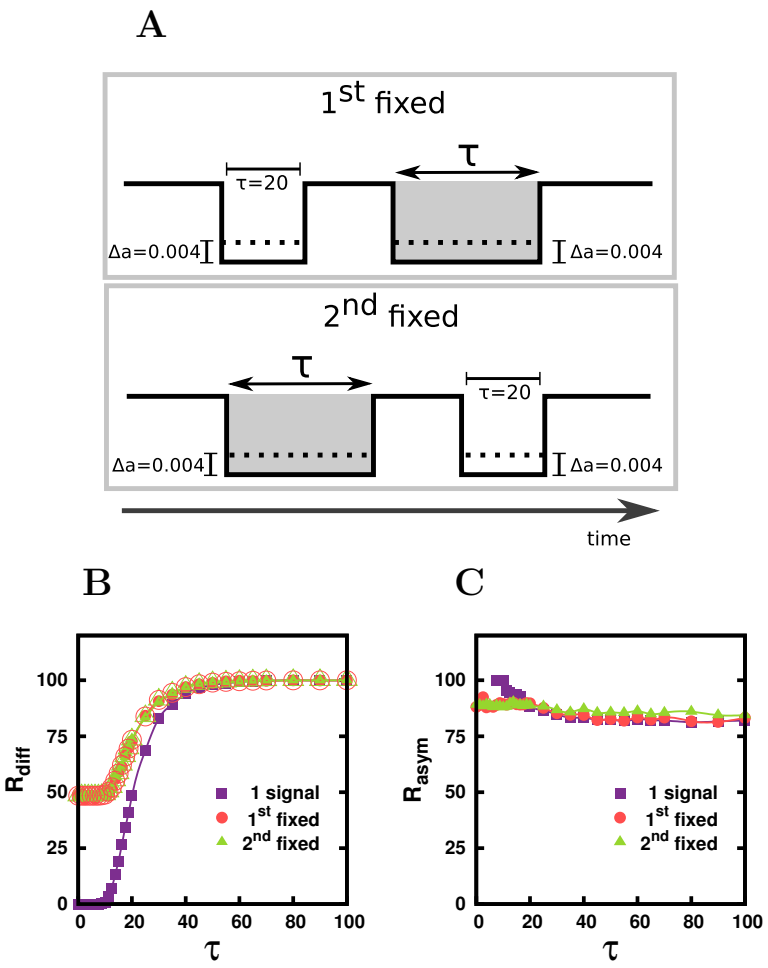

Figure 4.10 Two signals of different signal duration. (A) Schematic representation of the two cases explored. One signal of duration $\tau = 20$ is followed (1^{st} fixed, top) or preceded (2^{nd} fixed, bottom) by a signal which explores values of signal of duration τ ranged between 0 and 100. Both signals have the same signal strength ($\Delta a = 0.004$). (B) τ-R_{diff}-response curves for a single signal ($\Delta a = 0.004$) and for two different signals as described in panel A. The empty symbols correspond to the theoretical prediction calculated through R_{diff} (Eq. (4.6)). (C) τ-R_{asym}-response curves for a single signal ($\Delta a = 0.004$) and for two different signals as described in panel A. Simulation details: $N = 5000$, time between signals is 300.

explores different values of τ (1^{st} fixed); a first signal which explores different values of signal duration (τ) followed by a second fixed signal duration value (2^{nd} fixed) (Fig. 4.10A). We compare the decision after these two pairs of signals with the τ-R_{diff}-response curves generated by a single signal. These results are collected in Fig. 4.10B-C and they agree with those calculated by Eqs. (4.9) and (4.6).

Figure 4.10B shows that the *Differentiation choice* does not depend on which signal (the first or the second) has the fixed duration value. The resulting *Differentiation choice* integrates both signals. Furthermore, the *Asymmetric choice* is not affected by the number of signals applied (what has been already seen in Fig. 4.9D), but by the signal strength of these signals.

We also studied the behaviour of the decision when the two signals that take place differ in their signal strengths ($\Delta a_1 \neq \Delta a_2$) while their duration is identical ($\tau_1 = \tau_2 = \tau$). We evaluated the *Differentiation choice* for different strength values of the first signal (with $\Delta a_2 = 0.004$), and for different strength values of the second signal (with $\Delta a_1 = 0.004$) (Fig. 4.11A). We compared these results with the Δa-R_{diff}-response curve generated by a single signal of strength Δa. These results are collected in Fig. 4.11B-C and they agree with those predicted by Eqs. (4.9) and (4.6).

Because one of the signals has $\Delta a = 0.004 > 0$, the Δa-R_{asym}-response curve after the two signals have acted shows a bias to select the LH state for Δa values below 0.004 (Fig. 4.11C). The bias is stronger when the first signal is more asymmetric than the second one. This is because before the first signal, there are more cells undifferentiated than after the first one.

According to these results of two signals of different strength shown in Fig. 4.11, the two main conclusions are: (1) there is an integration behaviour of the two signals involved in the *Differentiation choice*; and (2) the first signal has more effect on the final *Asymmetric choice* (R_{asym}).

4.4 Discussion

In this chapter we characterized a cellular decision making which involves three cell states and is driven by a transient signal: a cell chooses between remaining

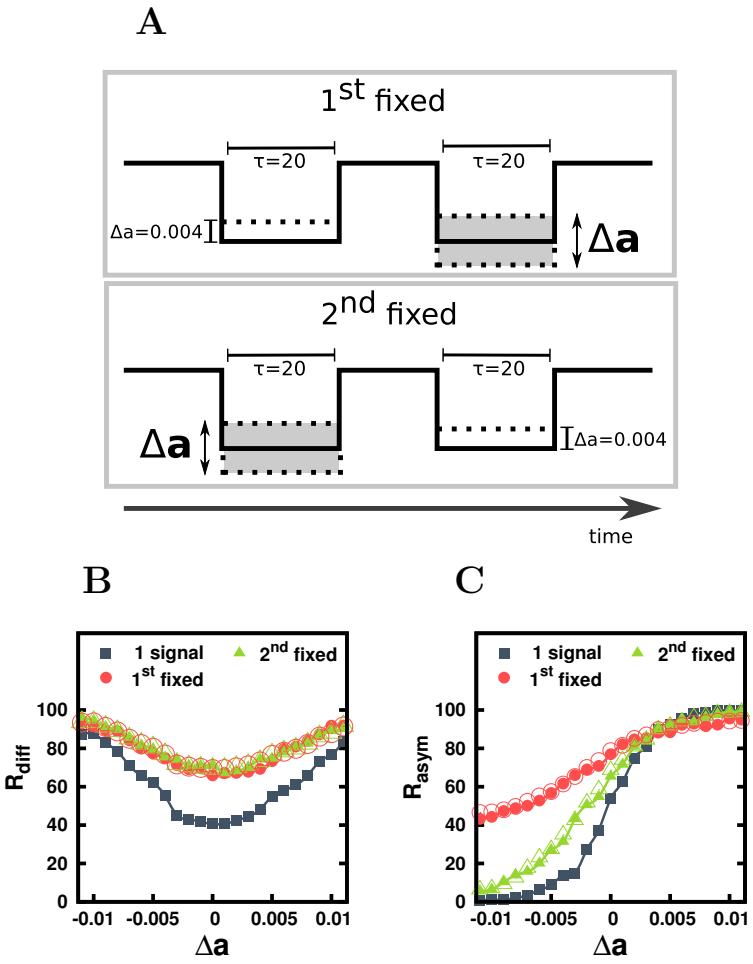

Figure 4.11 Two signals of different signal strength but identical time duration. (A) Schematic representation of the two cases explored. (1^{st} fixed, top) One signal of strength $\Delta a_1 = 0.04$ is followed by a signal of strength $\Delta a_2 = \Delta a$. (2^{nd} fixed, bottom) One signal of strength $\Delta a_2 = 0.004$ is preceded by a signal of strength $\Delta a_1 = \Delta a$. Values of Δa ranged between -0.01 and 0.01 have been explored. Both signals have the same duration ($\tau = 20$). (B) Δa-R_{diff}-response curves for a single signal ($\tau = 20$) and for two different signals as described in panel A. The empty symbols correspond to the theoretical prediction calculated through R_{diff} (Eq. (4.6)). (C) Δa-R_{asym}-response curves for a single signal ($\tau = 20$) and for two different signals as described in panel A. The empty symbols correspond to the theoretical prediction calculated through R_{asym} (Eq. (4.9)). Simulation details: $N = 5000$, time between signals is 300.

as it was or to change to either one of two new states. The decision is induced by a transient signal that transiently destabilizes the initial state, driving a change in the phase space from a tristable regime to a bistable one and back, when the signal disappears, to a tristable regime.

For the sake of clarity, we divided the comprehension of this decision in two elemental choices: the choice of leaving the initial state (*Differentiation choice*) and the choice of selecting one new state over the other new one (*Asymmetric choice*). According to our results, the *Asymmetric choice* is made first, mostly when the signal starts to act, by the interaction between the initial concentrations of cells and the basins of attractions generated by the signal. In contrast, the *Differentiation choice* is made when the signal is removed, when the basins of attraction of the tristable regime are restored. These two choices are controlled by distinct parameter values of the signal: the *Differentiation choice* depends mostly on the duration of the signal, while the *Asymmetric choice* depends on the signal strength.

The *Differentiation choice* has an integrative behaviour. Both longer and multiple signals favour the differentiation, being better to drive differentiation a long signal than multiple identical short signals that overall last the same as the long signal. In contrast, the *Asymmetric choice* depends strongly on the first signal when multiple signals of different strength are applied. This arises from the fact that the pool of cells that remain undifferentiated is reduced after each signal application. If these cells were able to proliferate – e.g. by divisions – the contribution of each signal on the final *Asymmetric choice* could be more similar.

Comparing the mechanism of the bistable signals of this Chapter with the mechanisms already studied in the previous Chapter, we see some similarities between the bistable signals and the multistable ones. The integrative behaviour is the main one. Furthermore, while in the multistable signals the precursor state is destabilized by stochastic effects, in bistable signals this is produced by a bifurcation (deterministic effect).

If the initial conditions of all the cells of the initial population were identical, deterministic dynamics could not explain how the cells reach different cell states after the signal. Besides, the noise – characterized by the effective volume of the system – has the effect to make the decision become more symmetric: less

differences between the number of cells that choose one new cell state or the other new one.

The dynamical properties of the decision reported by all these results has biological implications. While a population of three cell types can be generated through this kind of signal, the initial symmetric state – which is destabilized during the signal effect – is key to this decision. If there are no cells in this cell state, this state can not be recovered by subsequent signals. Hence, we can interpret the cells of the initial state as a precursor cell type of the other two states involved.

Chapter 5

Pattern selection by dynamical biochemical signals

5.1 Introduction

This Chapter extends the study of the previous Chapters (Chapter 3 and 4) on cellular decision making in single cells to a system of interacting cells. Most of it has been published in Biophysical Journal (Palau-Ortin et al., 2015). Due to the spatial pattern solutions that arise from cell-to-cell communication, instead of cell states, the decisions characterized in this chapter are defined by different patterns selected by a tissue of cells, i.e., we are interested in the decision of the whole tissue.

There is experimental evidence pointing out at multistability and selection of patterns in developing embryos, for instance for patterning processes driven by Notch signalling (Artavanis-Tsakonas et al., 1999). Since Notch signalling was already introduced in Chapter 1, herein we describe only those selection processes of patterning. These processes do not show the characteristic stochastic behaviour of cellular decision making. In the *Drosophila*'s eye, photoreceptor

neuron precursors adopt distinct cell fates (R1/R6 or R7) in a cell–to–cell coordinated manner upon the spatially sequential activation of the protein ligand. Changes only in the spatio–temporal sequence of this signal (i.e. ligand activation) alters the pattern that is formed (Miller et al., 2009), suggesting that under the same final conditions, different patterns can exist (i.e. those of the wild-type conditions and those driven by the manipulated temporal sequence of the biochemical signal). Another example arises from ommatidial photoreceptor patterning in the fly. It has been shown that different patterns of R8 photoreceptors (salt-and-pepper and stripes patterns) can arise in genetically identical tissues through Notch signalling pathway (Lubensky et al., 2011). In addition to this experimental evidence, computational studies of pattern formation by Notch signaling have shown that different patterns can be stable solutions for the same set of parameter values (Formosa-Jordan et al., 2012; Lubensky et al., 2011; Formosa-Jordan and Ibañes, 2014). Therefore, in this Chapter we explain how a pattern is chosen and not another one when the choice is induced by a dynamical signal. In other words, we look for features of the signal that can bias the selection to one pattern and not another one.

It is known that initial conditions can determine the selection of a pattern (Wearing and Sherratt, 2001; Shoji et al., 2003; Lubensky et al., 2011; Corson and Siggia, 2012). However, little is known on how selection of different patterns occurs from the same initial pattern and conditions, upon the action of a signal that changes the parameter values since current studies on pattern formation and selection usually deal with parameters that are constant both in time and space.

We perform a computational study to provide key elements for pattern selection upon the action of a signal. In contrast with previous Chapters, we make use of continuous time-varying parameters (i.e. non-autonomous) in stochastic dynamical systems with spatial interactions. As in previous Chapters, we consider stochastic dynamics. Herein specifically, we deal with stochastic ordinary differential equations.

5.2 The model and signal dynamics

5.2.1 A model for cis inhibition mediated by notch signalling

Because of the theoretical knowledge on multiple pattern solutions for Notch signalling dynamics (Lubensky et al., 2011; Formosa-Jordan et al., 2012; Formosa-Jordan and Ibañes, 2014), we focused on them. We used a stochastic version of the deterministic model presented in (Formosa-Jordan and Ibañes, 2014) as detailed as follows. The model establishes a minimal description of the dynamics of the activities of the Notch pathway (s_i) and of the ligand (l_i) in each cell i, as first described in (Collier et al., 1996). It phenomenologically includes the process of Notch signal activation, according to which a fragment of the Notch receptor translocates into the nucleus of a cell upon binding to a ligand at the membrane of an adjacent cell (Artavanis-Tsakonas et al., 1999). This signal in turn represses the transcription of the gene encoding the protein ligand. Thus, a ligand expressing cell drives lateral inhibition to its neighbours, i.e., it inhibits the expression of the ligand in its adjacent cells. The model also takes into account that the protein ligand can impede Notch signaling by binding to the Notch receptor within the same cell, what is known as cis-inhibition (Heitzler and Simpson, 1993; Jacobsen et al., 1998; Sakamoto et al., 2002; Álamo and Schweisguth, 2009; Miller et al., 2009; Fiuza et al., 2010; Sprinzak et al., 2010; Fleming et al., 2013). We recall that, as explained in Chapter 1, lateral inhibition mediated by Notch signalling has been shown to drive spontaneous pattern formation from linear unstabilization of the homogeneous state (Collier et al., 1996).

We extended the dimensionless model proposed in (Formosa-Jordan and Ibañes, 2014) for cis-inhibition to phenomenologically include stochastic dynamics arising from intrinsic noise, such that the stochastic differential equation for each species in the Itô interpretation (Gillespie, 2000; Adalsteinsson et al., 2004) is as follows:

$$\begin{cases} \dfrac{ds_i}{dt} &= P_s(\langle l_i \rangle, l_i, t) - s_i + \sqrt{P_s(\langle l_i \rangle, l_i, t) + s_i}\ \xi_i(t) \\ \dfrac{dl_i}{dt} &= v\left(P_l(s_i) - l_i + \sqrt{P_l(s_i) + l_i}\ \chi_i(t)\right) . \end{cases} \tag{5.1}$$

The deterministic part is formed by the production terms, $P_s(\langle l_i \rangle, l_i, t)$ and $P_l(s_i)$, minus the degradation terms. v accounts for the ratio between the time scale of the dynamics of the ligand and the signal activities and is set to $v = 1$. The stochastic multiplicative terms are proportional to the square root of the corresponding production plus the degradation terms. $\langle l_i \rangle \equiv \sum_{j \in nn(i)} l_j/z$ is the average ligand activity of the z nearest neighbour ($nn(i)$) cells of cell i. ξ_i and χ_i are independent Gaussian random numbers of zero mean and uncorrelated in space and time: $\langle \xi_i(t) \cdot \xi_j(t') \rangle = \frac{1}{V}\,\delta_{ij}\,\delta(t-t')$ and $\langle \chi_i(t) \cdot \chi_j(t') \rangle = \frac{1}{V}\,\delta_{ij}\,\delta(t-t')$, with V being a characteristic volume. We used a white noise according the standard procedures from Master to Langevin equations (Gillespie, 2000; Adalsteinsson et al., 2004).

The productions of Notch and ligand activities are:

$$\begin{aligned} P_s(\langle l_i \rangle, l_i, t) &= \frac{r_t^i(t)\ \langle l_i \rangle}{1 + r_t^i(t)\ \langle l_i \rangle + r_c^i(t)\, l_i} \\ P_l(s_i) &= \frac{1}{1 + b\, s_i^n}\,, \end{aligned} \tag{5.2}$$

where n is an exponent representing the degree of nonlinearity of ligand inhibition by the signal and b indicates the strength of such ligand inhibition. $r_t^i(t) \equiv r_{trans}^i(t)$ and $r_c^i(t) \equiv r_{cis}^i(t)$ are the strengths of trans-interactions and cis-interactions of cell i, respectively (See the of trans and cis interaction in Chapter 1, Section 1.1.3) and they are proportional to the rate of maximal ligand production, which is not explicitly seen in the equations due to the nondimensionalization of variables being used. Herein we considered that $r_t^i(t)$ and $r_c^i(t)$ can change over time and be different between cells, as described in the Path definition and characterization subsection.

Note that the dynamical model is an example of a regulatory circuit involving mutual inhibition and self-activation seen in Chapter 4 (Fig. 5.1). In this case, the toggle switch is between adjacent cells. r_t^i favours mutual inhibition while r_c^i, promotes self-activation. In the absence of cis–inhibition and fluctuations, Eqs. (5.1-5.2) recover the model proposed by Collier et al. (1996). As expected from the multistability exhibited by the toggle switch dynamics with auto-activation (Fig. 2.1) (Guantes and Poyatos, 2008), this model exhibits multiple stable spatially extended solutions (Formosa-Jordan and Ibañes, 2014).

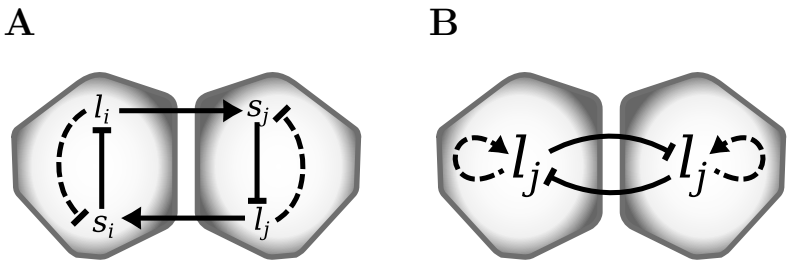

Figure 5.1 Scheme of the model interactions between two adjacent cells. (A) Ligand activity in cell i (l_i) induces (sold arrow) Notch activity in the adjacent cell j (s_j) and inhibits (solid blunt arrow) Notch activity in cell i (s_i). In turn, s_i inhibits (dashed blunt arrow) l_i which is called cis-inhibition. The reciprocal interactions in cell j are also depicted. (B) Simplified model where the there are only depicted the interactions from the ligand point of view (l_i and l_j). This simplified version illustrates the toggle switch (solid arrows) with self-activation (dashed blunt arrows) architecture which underlies the model.

5.2.2 The scenarios and their dynamical paths

We aimed at evaluating how a pattern and not another one is selected when there are multiple patterns that are stable. We focused on three different patterns, defined only by their symmetries: the homogeneous one (H), the fine-grained lateral inhibition pattern (P) and the stripe pattern (S) (Fig. 5.2). We considered selections of these patterns induced by biochemical signals (Fig. 5.2).

We considered three scenarios: (1) the signals act on all the tissue at the same time, (2) they act on a group of cells and (3) they act sequentially over all cells of the tissue (Fig. 5.3). In the three scenarios, all cells had equivalent dynamics (i.e. all cells had the same parameter values) before the signals act (initial time) and at the final time. To study selection processes, parameter values at the final time were such that multiple patterns were stable. In scenario 1, we analysed whether and how the selection of a pattern depends on the path, and it extends cell-autonomous decision making to spatially interacting systems. Therefore, we focused only on the selection of those patterns that do not require any spatial cue to be formed. These correspond to patterns that either do not involve a periodicity (H) or are periodic but have the spatial symmetries that grow the fastest from linear instabilities (P). In scenario 2, we propose an intrinsically spatially based mechanism for the selection of patterns that can spontaneously

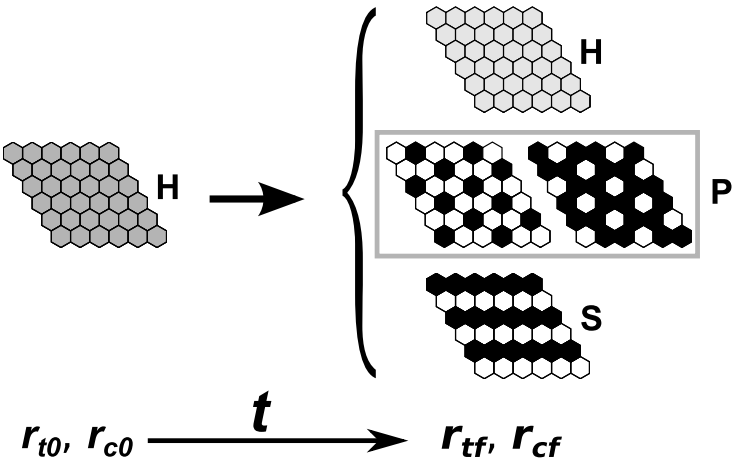

Figure 5.2 Cartoon exemplifying the problem of pattern selection. Initially, the system is in a stable homogeneous (H) pattern determined by the initial value of the control parameters (r_{t0}, r_{c0}). These parameters evolve over time (t) to final values (r_{tf}, r_{cf}) due to the action of biochemical signals. At these new values of the parameters, there are multiple patterns which are all stable: the homogeneous (H), a periodic salt-and-pepper (P) and a stripped (S) pattern, among others. The problem tackled here is how to select one of these patterns. We considered three different scenarios according to how the parameters change over time and across the tissue. The figure exemplifies the selection from an initial monostable H pattern. Other initial conditions involving multistability are explored too.

invade another pattern. Finally, in scenario 3 we propose another spatially-based mechanism that enables the selection of a pattern with a more singular symmetry given the isotropy of the dynamics like the stripes pattern (S).

5.2.3 The signal defines the path

We modelled the action of biochemical signals as spatio–temporal changes of the trans r_t^i and cis r_c^i interaction strengths. We chose these interactions to be modulated over time and space (among cells) since there are context-dependent proteins that can modulate them, like the glycosyltransferase Fringe (Panin et al., 1997; Sakamoto et al., 2002; Lebon et al., 2014) or the ubiquitin ligase Neuralized (Barad et al., 2011). Moreover, changes in the activation of the ligand, which are known to drive transitions from one pattern to another one (e.g. in vertebrate inner ear development and in the differentiation of photoreceptors in the *Drosophila*'s eye) impinge also on these parameters. The spatio–temporal

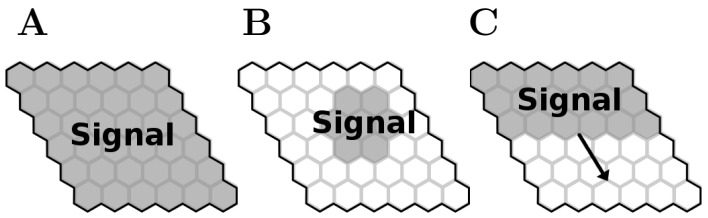

Figure 5.3 Schematic representation of the signal effect in the three scenarios. (A) Scenario 1. The signal (paramer change) affects the whole tissue at the same time. (B) Scenario 2. The signal (parameter change) only affects a group of cells of the tissue. (C) Scenario 3. The signal (parameter change) propagates along the tissue (starting at the first cell row). The size of the tissue and the relative size of the domain in grey in B depicted here are not representative of the sizes of the tissue and the domain of the simulations.

sequence of the changes in the values of r_t^i and r_c^i defines what herein we named dynamical paths. The temporal changes of the parameters of a cell can be depicted as a trajectory across the $r_t - r_c$ parameter space. For simplicity, we devised trajectories which, for each cell, involved changing either r_t^i or r_c^i, or one after the other. Accordingly, these trajectories were constituted by vertical and/or horizontal lines along the r_t–r_c parameter space. In this chapter, we focused on two regions of the parameter space: $n = 2$ (Fig. 5.4A) and $n = 4$ (Fig. 5.4B). In Figure 5.4, there are depicted the points of the parameter space that describes the different paths explored in the Results.

We analysed several paths driven by signals and numbered them according to the scenario (1, 2 or 3) they belong to.

Changes of r_t^i and r_c^i over time from value r_{a0} to value r_{af} and from cell to cell were phenomenologically modelled by time-dependent continuous hyperbolic tangent functions as:

$$r_a^i(t) \equiv r_a^{(j,k)}(t) = \frac{1}{2}\left((r_{af} - r_{a0})\tanh\left(\frac{t - t_a - t_{prop}\,k}{\alpha}\right) + r_{a0} + r_{af}\right)\delta_{j,k\in D}\,, \tag{5.3}$$

where a stands for t (*trans*) or c (*cis*) and two indexes, j, k, were used to label the cell i (denoting the row, j, and the column, k) (see Eqs. (5.1-5.2)). Parameter α sets the time scale of the parameter change, t_a is the time at which the parameter has reached the value $(r_{a0} + r_{af})/2$ and t_{prop} sets the spatio–temporal scale of propagation of the parameter change across the tissue.

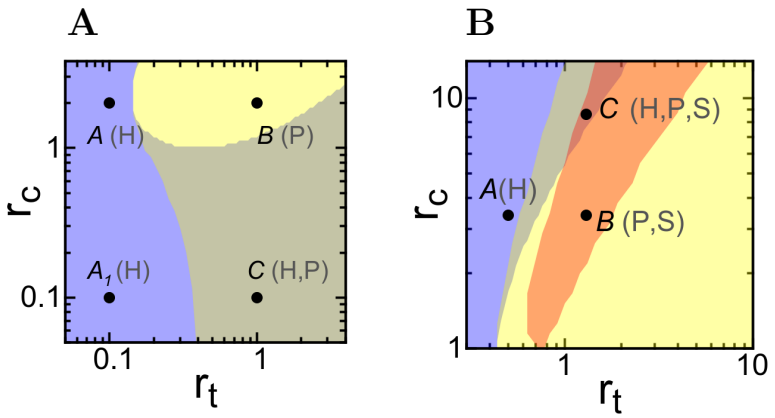

Figure 5.4 Parameter space ($r_t - r_c$). Parameter space of trans r_t and cis r_c interaction strengths. There are different domains defined by the pattern solutions which are stable there: the homogeneous (H), the salt-and-pepper (P) or the stripes (S). These regions are coloured according to which of these patterns are stable: H (blue), P (yellow), H and P (grey), S and P (orange), or H, P and S (red). There are depicted four values of the parameters (solid points). The stable solutions stable at these points are indicated within parentheses. Parameter values: (A) $n = 2$, (B) $n = 4$. These figures have been created from data in (Formosa-Jordan and Ibañes, 2014).

For $t_{prop} = 0$ (scenarios 1 and 2), all cells within the spatial domain D change simultaneously the value of the parameter, and D stands either for all the tissue (scenario 1, Fig. 5.3A) or for a small fraction of it (scenario 2, Fig. 5.3B). For $t_{prop} > 0$ (scenario 3, Fig. 5.3C), the change of parameter value occurs as a propagating planar front across the tissue (i.e., simultaneously in all cells of row j and propagating along rows). To ensure that initially the parameter is at value $r_a(t = 0) \approx r_{a0}$, we set $t_a = -\alpha \tanh(-0.995)$. For sequential changes of parameters r_t^i and r_c^i or vice versa, we defined $t_d \equiv |t_c - t_t|$ as the delay between these changes. To ensure that changes of r_t^i followed changes of r_c^i (or vice versa) and did not overlap, we set $t_d >> \alpha$.

We also considered transient changes of r_t^i and r_c^i from r_{a0} to r_{af} and back to r_{a0}. These were modelled through Eq. 5.3 for each change, from r_{a0} to r_{af} and backwards, with $t_a = t_{a1}$ for the first change from r_{a0} to r_{af} and $t_a = t_{a1}+t_{up}+\phi$ for the change from r_{af} to r_{a0}, where ϕ measured the time period during which the parameter is at value r_{af}. The same value of α was used for both changes.

We defined the following time scales to characterize the path across the $r_t - r_c$

parameter space: $t_{up} \equiv t_a + \alpha \operatorname{arctanh}(2P-1)$ for $P = 0.9933$ measured the time spent from the departure from a vertex point to the arrival at the subsequent vertex point of the path in the parameter space; τ measured the time spent on an intermediate (not the initial nor the final) vertex. When the path is constituted by a single intermediate vertex point, τ is computed as $\tau = t_d - t_{up}$. When there are several intermediate vertex points, we used a subindex with the name of the vertex to denote the time spent at each vertex point. Herein we exemplify the case of three vertex points and denote each of them by a number which is the order with which they are visited: $\tau_1 = t_d - t_{up}$, $\tau_2 = \phi_1 - t_d$ and $\tau_3 = t_d - t_{up} + \phi_2 - \phi_1$. For paths involving $t_{prop} > 0$ (scenario 3), we defined $N_{rows} = \tau / t_{prop}$ as the number of cell rows with the parameter values of an intermediate vertex point.

5.2.4 Stability of multiple solutions and numerical integration of the dynamics

The model of Eqs. (5.1-5.2), in the absence of fluctuations (deterministic dynamics) and for homogeneous and constant parameter values ($r_t^i(t) = r_t$ and $r_c^i(t) = r_c$ for $\forall i, t$) in perfect hexagonal lattices with toroidal periodic boundary conditions, has been analysed in (Formosa-Jordan and Ibañes, 2014). It has been shown to exhibit different stationary stable patterns for the same set of parameter values. Some of these patterns are: homogeneous (H), periodic salt-and-pepper (P) and stripe (S) patterns (Fig. 5.2). We defined different patterns by their spatial symmetries and not by the exact values of the variables s and l (Fig. 5.2). This implies that the solutions classified as P and I in (Formosa-Jordan and Ibañes, 2014) are herein considered as being the same, P (Fig. 5.2).

Linear stability analysis indicates that the fastest growing mode that destabilizes the H solution corresponds to the periodicity of the P pattern (Formosa-Jordan and Ibañes, 2014). Therefore, the P pattern is expected to arise spontaneously from the H pattern through small random variability between the values of the signal and/or ligand for this model dynamics. Accordingly, formation and thereby selection of the S or other patterns is expected to require

mechanisms that impose properly the specific spatial symmetries of these patterns, in contrast with selection of the P or H patterns. We only focused on the selection of the S pattern, besides selection of the P and H patterns.

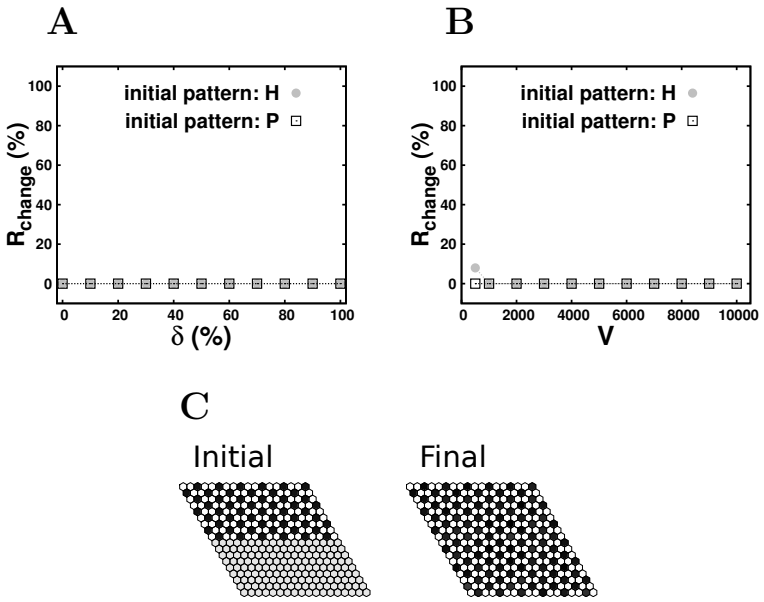

Figure 5.5 Numerical stability analysis of the H and P patterns at point *C* in the parameter space of Fig. 5.4A. (A,B) Percentage of simulations that reach a steady pattern at $t = 200$ that is distinct from the initial pattern in the absence of any biochemical signal for (A) deterministic dynamics and (B) stochastic dynamics. (A) Both the H (orange circles) and P (blue squares) patterns are deterministically stable for a large range of amplitudes δ of random initial perturbations. Initial conditions are $s_i(t=0) = s_{0i}\,(1+\delta\ \ (2\,r-1))$ and $l_i(t=0) = l_{0i}\,(1+\delta\ \ (2\,r-1))$, where r is a uniformly distributed random number within $[0,1]$, and s_{0i} and l_{0i} are the theoretical predicted values of s_i and l_i, respectively of the pattern being analysed. (B) Both the H (orange circles) and P (blue squares) patterns are stochastically stable. Initial conditions as in panel A with $\delta = 0$. The initial pattern remains at the end of the simulation for a wide range of V values (except for the H pattern for very large fluctuations with $V = 500$). The percentages in panels A and B ($R_{change} = (100 - R_{initial})$) have been obtained with 1000 simulations for each δ and V value. (C) Relative spatial stability of the H and P patterns. (Left) Initial condition with the top half of the tissue in the P pattern (with the theoretical predicted values) and the other bottom half in the H pattern (with the theoretical predicted values). (Right) Steady state reached after numerical integration of the stochastic dynamics for $V = 1000$ with the initial condition shown in left panel. The P solution invades all the tissue.

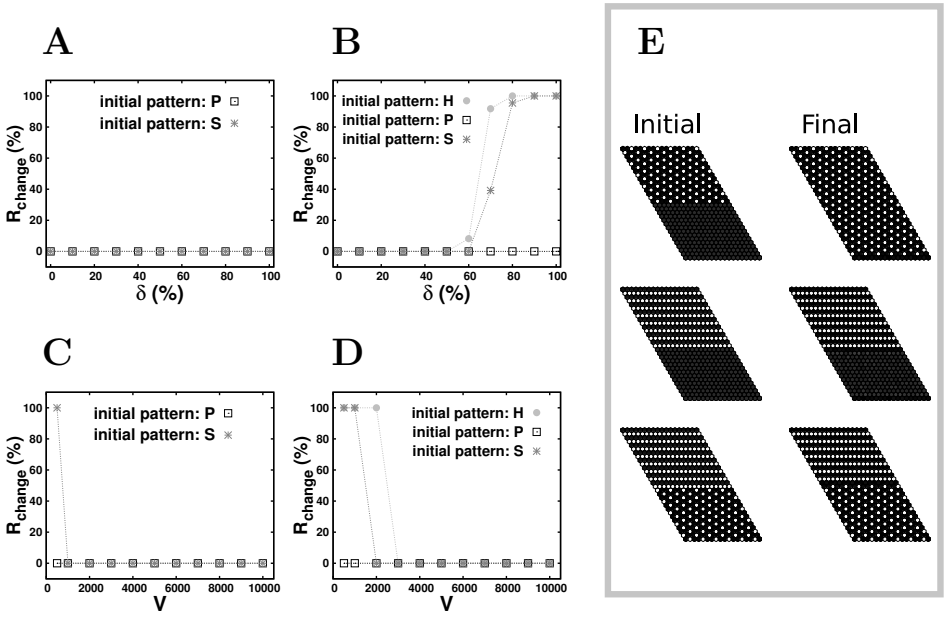

Figure 5.6 Numerical stability analysis of the H, P and S patterns at points *B* and *C* in the parameter space of Fig. 5.4B. (A-D) Percentage of simulations that reach a steady pattern at $t = 200$ that is distinct from the initial pattern in the absence of any biochemical signal for (A,B) deterministic dynamics and (B,C) stochastic dynamics for the parameter values of point (A,C) B and (B,D) C of the parameter space of Fig. 5.4B. (A,B) Stability for deterministic dynamics for different amplitudes of initial random perturbations of the theoretical predicted patterns. The initial conditions are $s_i(t=0) = s_{0i}\,(1+\delta\ \ (2\,r-1))$ and $l_i(t=0) = l_{0i}\,(1+\delta\ \ (2\,r-1))$, where r is a uniformly distributed random number within $[0,1]$, and s_{0i} and l_{0i} are the theoretical predicted values of s_i and l_i, respectively of the pattern being analysed. (C,D) Stability for stochastic dynamics with different V values for initial conditions being the theoretical predicted patterns ($\delta = 0$). Notice that for the value of V used in the simulations of scenario 3 ($V = 10000$) all the pattern solutions are stochastically stable. The percentages shown in panels A-D ($R_{change} = (100 - R_{initial})$) have been obtained with 1000 simulations for each δ and V value. (E) Relative spatial stability of the H, P and S patterns at point C in the parameter space of Fig. 5.4B. (Left) Initial tissue with: (top) half of the cells in the P pattern and the other half in the H pattern; (middle) half of the cells in the stripped S pattern and the other half in the P pattern; (bottom) half of the cells in the P pattern and the other half in the S pattern (bottom). Theoretical predicted values for the H, P and S solutions were used. (Right) Steady state reached after numerical integration of the stochastic dynamics for $V = 10000$ with the initial condition shown in left panel. If the initial condition is the P and S patterns in contact through a black stripe, this stripe is invaded by the P pattern (data not shown). These simulations have been performed considering fixed boundary conditions at bottom and top rows ($s = 0$ and $l = 0$ for neighbours on top of the first row and below the last row) and periodic conditions between left and right sides.

The domains where the H, P or S patterns are deterministically stable are depicted in Fig. 5.4 according to the information in (Formosa-Jordan and Ibañes, 2014) for two set of parameter values: $b = 1000$, $n = 2$ (Fig. 5.4A); and $b = 1000$, $n = 4$ (Fig. 5.4B). Other pattern solutions can be stable too in these domains (Formosa-Jordan and Ibañes, 2014). Stability of the H, P and S patterns for the stochastic dynamics of the model and its comparison with the deterministic dynamics was verified at these specific sets of parameter values (Figs. 5.5 and 5.6). This was done numerically by simulating the dynamics

The dynamics of Eqs. (5.1-5.2) were numerically integrated on a two-dimensional array of 12×12 regular hexagonal cells with toroidal periodic boundary conditions, unless otherwise stated. The algorithm presented in (Carrillo et al., 2003) extended to time-dependent parameter values was used for integration with time step $dt = 0.1$ (robustness of the results was checked for $dt = 0.01$, Fig. 5.7). Equations (5.1-5.2) can drive negative values because of the stochastic fluctuations. To avoid them, a not crossing boundary to negative values was used, such that negative values are converted to zero (Fig. 5.7). To confirm the correctness of our results, we checked that the states reached by cells correspond to distributions of values centred on the exact deterministic solutions of the Eqs. (5.1-5.2) (Fig. 5.7), which can be theoretically computed as described in (Formosa-Jordan and Ibañes, 2014).

Deterministic stability of each pattern solution to increasing amplitudes of random-perturbations was also evaluated. The deterministic dynamics was implemented through the fourth order Runge-Kutta algorithm.

Snapshots of the tissue state depicted in all figures of this chapter correspond to a linear greyscale of ligand activity values with white for $l = 0$ and black for $l = 1$.

In addition, we evaluated whether a stable pattern can spontaneously invade and propagate over another stable one. To this end, we set as initial condition for one half of the tissue a pattern solution that is stable and for the other half another stable pattern solution. We numerically integrated the stochastic dynamics until a stationary situation was reached (until a final time, $t = 500$). For the parameter values being evaluated, the P pattern was able to invade the

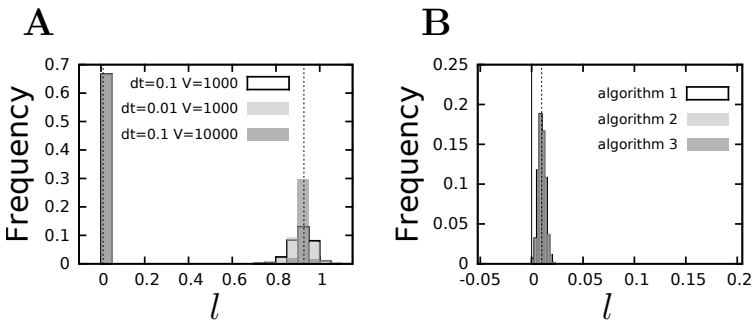

Figure 5.7 The stochastic implemented algorithm is consistent with the theoretical deterministic predicted values. Histograms of the ligand activity values (l_i) in a lattice of $N = 48 \times 48$ cells with periodic boundary conditions at the steady state ($t = 10000$). Initially ($t = 0$) the lattice starts with the perfect pattern solution theoretically predicted for the deterministic dynamics (values denoted by dashed vertical lines) for $r_t = 1.0$ and $r_c = 0.1$, $b = 1000$ and $n = 2$. (A) Histograms for different values of V and time integration step dt. In the model, the intensity of fluctuations depends on $1/V$. The mean values are in agreement with the theoretical predictions. (B) Due to the multiplicative noise, the variables might reach negative values. The algorithm implemented in the simulations presented in all figures corrects it by fixing the variable to zero when it is going to become negative (*algorithm 1*, in open red boxes). We compared the results obtained by this algorithm with those arising from two different algorithms: with a reflective barrier in zero (i.e., the negative values are converted into their positive counterpart; *algorithm 2*, in cyan boxes) or without any correction (i.e. negative values exist; *algorithm 3*, in magenta boxes). The three distributions are very similar. The solid line is depicted to denote the zero value. The simulations of the three algorithms have been generated with $V = 1000$.

H solution and not vice versa. Accordingly, we termed the P pattern to be spatially more stable than the H pattern.

5.2.5 Criterion for pattern selection

Due to the stochasticity of the dynamics, we measured the normalized frequencies R_H, R_P and R_S of cases that selected the H, P and S patterns for a given path. To measure $R_{H,P,S}$ we discriminated systematically which pattern was selected for each stochastic temporal evolution (i.e. numerical integration of the dynamics) of the path. To this end, we defined the following three-component order parameters (for $x = s, l$) which take distinct values for each pattern:

$$\eta_x^\theta = \frac{1}{N}\sum_{i=1}^{N} |x_i - \langle x_i \rangle_\theta| \ , \tag{5.4}$$

where N is the total number of cells in the tissue and brackets stand for averages over the two nearest neighbouring cells along each spatial direction with $\theta = 0, -, +$ which denote the directions that form an angle $0°$, $-60°$ and $+60°$ respectively with the horizontal. The characteristic values of these order parameters for each pattern for deterministic dynamics and perfect periodicity are: $\eta_x^\theta = 0 \ \forall\theta$ for the H pattern; $\eta_x^\theta = \bar{\eta}_x > 0 \ \forall\theta$ with $\bar{\eta}_x = \frac{\eta_x^0+\eta_x^-+\eta_x^+}{3}$ for the P pattern; For the perfectly aligned S pattern, the order parameter has only one null component, which corresponds to the component in the direction parallel to the stripes.

Points	$\mathbf{r_t}$	$\mathbf{r_c}$	**Patt**	$\boldsymbol{s^{st}}$ (Δs^{st})	$\boldsymbol{l^{st}}$ (Δl^{st})	$\boldsymbol{\bar{\eta}_s^{th}}$	$\boldsymbol{\bar{\eta}_l^{th}}$
A	0.1	2.0	H	0.027 ($\pm$0.007)	0.6 ($\pm$0.1)	0.00	0.00
A_1	0.1	0.1	H	0.038 ($\pm$0.007)	0.41 ($\pm$0.07)	0.00	0.00
B	1.0	2.0	P	0.32 ($\pm$0.02), 0.003 ($\pm$0.002)	0.009 ($\pm$0.003), 0.99 ($\pm$0.03)	0.22	0.65
C	1.0	0.1	H	0.09 ($\pm$0.01)	0.10 ($\pm$0.02)	0.00	0.00
			P	0.32 ($\pm$0.02), 0.009 ($\pm$0.003)	0.010 ($\pm$0.003), 0.93 ($\pm$0.05)	0.21	0.61

Table 5.1 Order parameter values for different points of the parameter space shown in Fig. 5.4A, with $n = 2$. The fourth column (*Patt*) shows the pattern solutions which are stable for the parameter values (Points, first column) of r_t, r_c (second and third columns; see them depicted in the parameter space in Fig. 1, 5.4A). s^{st} and l^{st} are the theoretical stationary deterministic values of each cell type for each pattern. Δs^{st} and Δl^{st} are the fluctuation amplitude. These amplitudes have been obtained by computing the standard deviation of the final states of the cells in a tissue of 48×48 cells, when the stochastic dynamics of Equations 1-2 are considered with $V = 1000$. $\bar{\eta}_s^{th} = \frac{\eta_s^0+\eta_s^-+\eta_s^+}{3}$ and $\bar{\eta}_l^{th} = \frac{\eta_l^0+\eta_l^-+\eta_l^+}{3}$ are the theoretical deterministic values of the order parameters as defined in Section 5.2.5 for the different stable solutions. Other parameters: $b = 1000$ and $n = 2$; and final time $t = 100$ for the numerical simulations.

For each stochastic temporal evolution of the dynamics, we computed numerically the order parameters η_x^θ at the final time $t_{max} = 10000$. We decided whether the system exhibited at t_{max} the H, P or S pattern according to the following criteria: (i) The system exhibited the H pattern if $\bar{\eta}_x < 0.2$ for $x = s, l$. The values of the order parameters extracted for the steady H pattern of the stochastic dynamics were not null, yet very small, because of the stochasticity. The threshold value 0.2 was chosen by taking into account this stochasticity and the specific values of the order parameters for the P and S patterns at the relevant parameter values; (ii) The system exhibited the P pattern if $|\bar{\eta_x} - \bar{\eta}_x^{th}| < 0.2$ and $\bar{\eta}_x > 0.2$ for $x = s, l$ being $\bar{\eta}_x^{th}$ the theoretical expected value of $\bar{\eta}_x$ for the

perfect P pattern of deterministic dynamics (see its values in Tables 5.1 and 5.2), which can be evaluated theoretically without numerical integration of the dynamics (Formosa-Jordan and Ibañes, 2009, 2014). The 20% difference between $\bar{\eta}_x$ and $\bar{\eta}_x^{th}$ was chosen to take into account that the final pattern may not be perfectly periodic; (iii) The system exhibited the S pattern if $\bar{\eta}_x > 0.2$ and $\sigma_x > 0.8$ being $\sigma_x = 1 - \eta_x^{min}/\eta_x^{max}$, where η_x^{min} and η_x^{max} are the maximum and the minimum components of $\left(\eta_x^0\,,\,\eta_x^-\,,\,\eta_x^+\right)$ respectively. Parameter σ_x described the degree of stripes formation.

Path points	$\mathbf{r_t}$	$\mathbf{r_c}$	**Patterns**	$\bar{\eta}_s^{th}$	$\bar{\eta}_l^{th}$	$\left(\eta_s^0, \eta_s^-, \eta_s^+\right)^{th}$	$\left(\eta_l^0, \eta_l^-, \eta_l^+\right)^{th}$
A	0.5	3.4	H	0.00	0.00	(0.00, 0.00, 0.00)	(0.00, 0.00, 0.00)
B	1.3	3.4	P	0.23	0.63	(0.00, 0.00, 0.00)	(0.00, 0.00, 0.00)
			S	0.22	0.60	(0.00, 0.33, 0.33)	(0.00, 0.90, 0.90)
C	1.3	8.6	H	0.00	0.00	(0.00, 0.00, 0.00)	(0.00, 0.00, 0.00)
			P	0.32	0.65	(0.32, 0.32, 0.32)	(0.65, 0.65, 0.65)
			S	0.23	0.64	(0.00, 0.35, 0.35)	(0.00, 0.96, 0.96)

Table 5.2 Order parameter values for different points of the parameter space shown in Fig. 5.4B, with $n = 4$. The "Patterns" column shows the pattern solutions which are stable for the parameter values r_t, r_c (see them in the parameter space in Fig. 5.4B). $\bar{\eta}_s^{th} = \frac{\eta_s^0+\eta_s^-+\eta_s^+}{3}$ and $\bar{\eta}_l^{th} = \frac{\eta_l^0+\eta_l^-+\eta_l^+}{3}$ are the theoretical deterministic values of the order parameters for the different stable solutions. $\left(\eta_s^0, \eta_s^-, \eta_s^+\right)$ and $\left(\eta_l^0, \eta_l^-, \eta_l^+\right)$ are the theoretical three-component order parameters for the different solutions (see Section 5.2.5). Notice that we have shown a certain direction (among three possible directions in the cell lattice) for the stripes.

5.3 Results

5.3.1 Scenario 1: Patterns are selected by specific global paths

In this first scenario, we evaluated how selection between the H and P patterns can occur when a biochemical signal acts in all the tissue at the same time. To test the relevance of the path for the selection process, we constructed two different paths that connect in different manners the initial and the final conditions. In the initial condition, only the H pattern is stable (point A in the $r_t - r_c$ parameter space of Fig. 5.8A). In the final condition, both the H and the P patterns are stable (point C in Fig. 5.8A). Thus, the two paths could be visualized as two different trajectories across the $r_t - r_c$ parameter space

that connect the initial and final points. For simplicity, these two paths were constructed as sequential changes in $r_t^i = r_t$ and $r_c^i = r_c$ parameters, and the two paths differ in the order of these changes (Fig. 5.8A). According to which parameter changes first (r_t or r_c), the path transiently explores a domain where the P pattern is stable and the H pattern is not (path 1a) or it only traverses domains where the H pattern is stable (path 1b) (Fig. 5.8A).

Figure 5.9A shows some frames of the tissue state along time for each path. At the end of the paths, selection of a different pattern becomes evident: through path 1a the P pattern is selected, while path 1b selects the H pattern. The results show that selection of a new pattern that is distinct form the initial one (P from H) occurs through a path that drives the transient destabilization of the initial pattern.

We then envisaged two paths that drive the destabilization of all the initially stable patterns. These paths start and end at the same point of the parameter space, where both the H and P patterns are stable (Fig. 5.8B). In addition, the two paths trace exactly the same cyclic trajectory over the parameter space, but evolve in opposite sequential order (clockwise, and counter-clockwise): path 1a' and path 1b' (Fig. 5.8B). Our results show that selection of a pattern that is distinct from the initial one becomes possible for the two paths (Figs. 5.9B), since both paths transiently destabilize the initial pattern. In addition, the results show that each path selects a different pattern independently of the initial one (Figs. 5.9B). The pattern that is selected corresponds to the one that is stable at the last intermediate point of the path: the P pattern is selected through path 1a', while the H pattern is selected through path 1b' (Figs. 5.9B). These results show that identical trajectories across the phase diagram but evolved in opposite sequential order can drive distinct pattern selections, which are independent of the initial pattern.

We next evaluated whether these selection processes are robust and reasoned that the time scales of the path could be relevant. To this end, we looked at the selection process as a function of the time τ_X spent at the intermediate X parameter space point (being X the point A_1, B or A, depending on the path, as shown in Fig. 5.8, Eq. 5.3). When the initial state is never destabilized, this time is irrelevant, as expected (Fig. 5.10). In contrast, a minimal time at the parameter space region driving the selection is required for robust selection of a new pattern to happen (Figs. 5.10A-B). To ensure that the final distinct

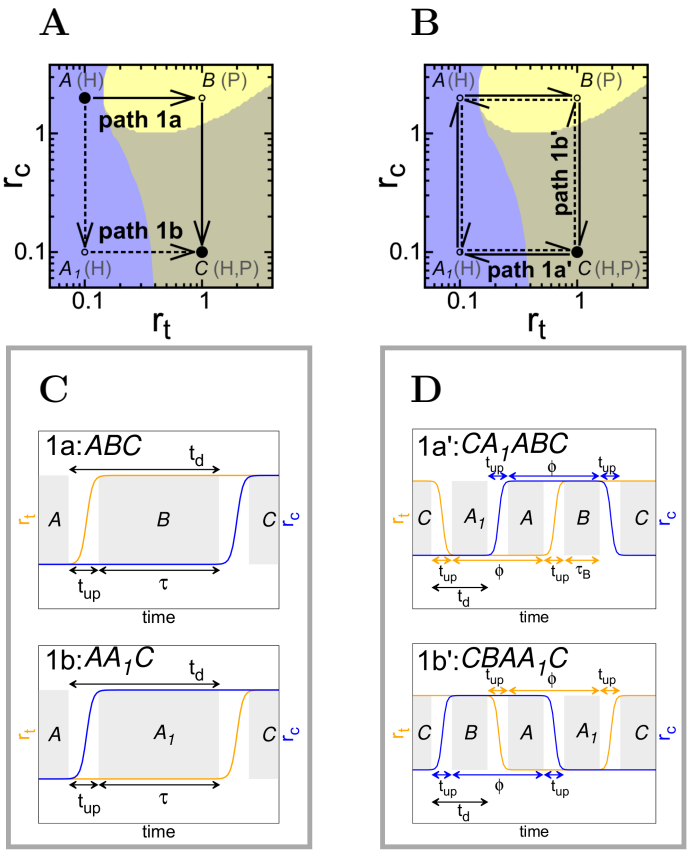

Figure 5.8 Global paths of scenario 1. (A,B) Paths (arrows) across the parameter space of trans (r_t) and cis (r_c) interaction strengths. Solid circles stand for the initial and final points of the paths, while the intermediate vertex points are represented by open circles. It is indicated within parentheses at relevant points of the path (denoted by letters A, B, A1 and C) whether the homogeneous (H) and/or the salt-and-pepper (P) patterns are stable. The paths cross different domains (colours) each defined by which of these patterns are stable: H (blue), P (yellow), or H and P (grey). (A) Paths 1a (continuos line) and 1b (dashed line) start at point A and end at point C. (B) Paths 1a' and 1b' start and finish at the same point C. Path 1a' (continuous line) is clockwise whereas path 1b' (dashed line) is counter clockwise. (C) Temporal profile of parameter change that defines the paths 1a (top) and 1b (bottom). Paths 1a and 1b share the same initial and final parameter space points, but they differ in the parameter space points visited along time. In path 1a, r_t changes first and then r_c. The opposite order happens in path 1b. (D) Temporal profile of parameter change that defines the paths 1a' (top) and 1b' (bottom). Paths 1a' and 1b' are cyclic (the end coincides with the start) and share the same parameter space points visited. Paths 1a' and 1b' only differ in the temporal sequence. In path 1a', r_t changes first and then r_c changes. The reverse order happens in path 1b'. The time period spent by the system in each of these points is shadowed in grey (e.g., τ_B for B). Parameters defining the time scale dynamics (t_{up}, τ, t_d and ϕ) of the parameter changes are also depicted. Notice that the examples shown correspond to changes which involve the same values of ϕ and t_{up} for r_c and r_t.

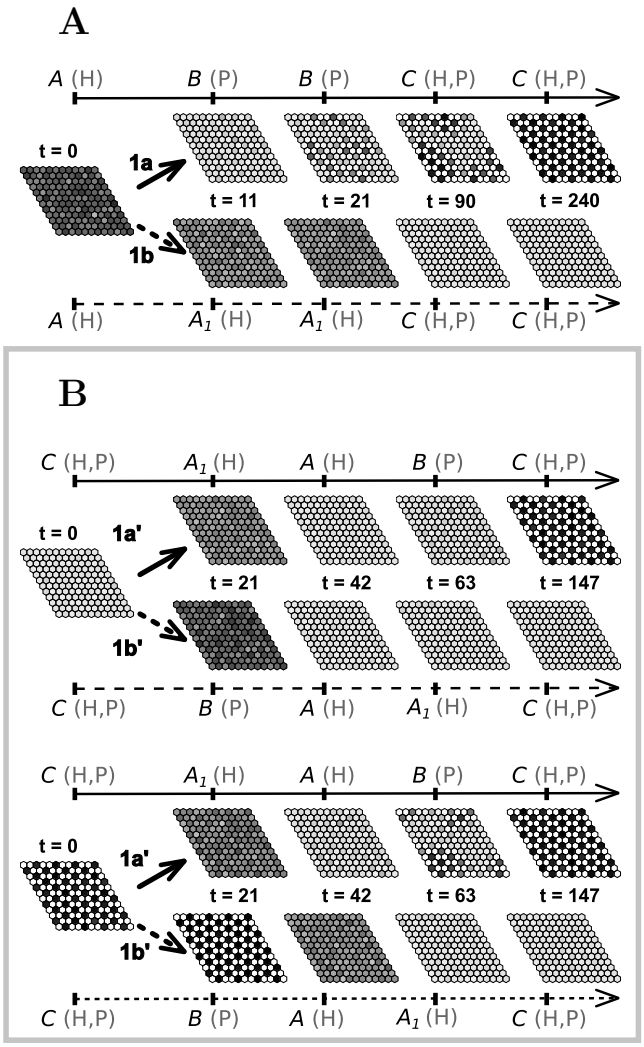

Figure 5.9 Pattern selection achieved through a specific global path. Snapshots of the tissue state over time (t) when the same signal acts in all cells of the tissue at the same time (scenario 1) and changes the values of the parameters (A) permanently according to paths 1a or 1b, or (B) transiently according to paths 1a' and 1b'. The parameter space points and whether the H or P patterns are stable for these parameter values are indicated at each depicted time. (A) The tissue that evolves according to the paths 1a or 1b starts ($t = 0$) at an homogeneous state (H). (B) The tissue that evolves according to the paths1a' and 1b' starts ($t = 0$) at either an homogeneous state (H, top) or P pattern solution (P, bottom). Additional parameter values are $\tau = 10$, $t_{up} = 11$, $t_{prop} = 0$, $b = 1000$, $n = 2$, $V = 1000$ and those detailed in Table 5.1.

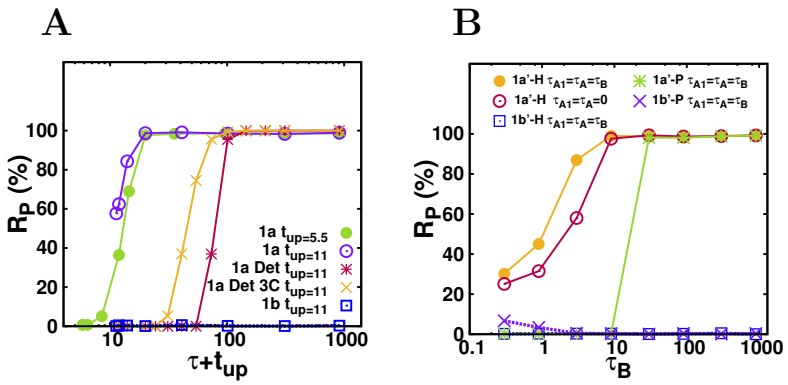

Figure 5.10 Pattern selection through a specific global path is robust and requires a minimal yet short time. Frequency of selection of the P pattern (R_P in percentage) versus a characteristic time of the signal. The same signal acts in all cells of the tissue at the same time (scenario 1) and changes the values of their parameters (A) permanently or (B) transiently, according to the paths in Fig. 5.8, A and B, respectively. (A) Results for path 1a are shown by circles for stochastic dynamics and by stars in the absence of fluctuations (*Det*), while squares denote the results for path 1b. Blue stars correspond to a low-dimensional system of three-cells interacting in pairs (*3C*). (B) Circles for path 1a' (solid for $\tau_{A1} = \tau_A = \tau_B$ and open for $\tau_{A_1} = \tau_A = 0$) and squares for path 1b' started at the homogeneous H solution. Stars for both paths (1a' and 2a') started at the pattern P solution. $\phi = 191$ for all curves. Other parameter values as in Fig. 5.9, with $t_{up} = 11$ and 12×12 cells unless otherwise specified. The deterministic curves (*Det* in the legend) use a 10% uniform random variability in the initial condition. In all cases, each point corresponds to 1000 repetitions of the selection process.

domain visited during the path is the one that sets the selection, we analysed path 1a' (Fig. 5.8B) for different time intervals τ_B spent at the final intermediate point B with unchanged time intervals spent at the previous vertex points ($\tau_A = \tau_{A1} = 0$, Fig. 5.10B,D). The similarity of this selection curve with the one with all τ variable ($\tau_B = \tau_{A1} = \tau_A$) indicates that the last intermediate distinct domain is the relevant one to decide which pattern is selected.

The frequency of selection follows a sharp threshold-like response curve as a function of the time during which destabilization occurs (Figs. 5.10). For instance, in the case of path 1a (Fig. 5.9A), the characteristic time spent at the region where the H pattern is not stable is approximately $t_{up} + \tau$, as shown by analysing different τ and t_{up} values (Fig. 5.10A). t_{up} is the time spent since the departure from the A or B parameter space point until the arrival to the subsequent one along the path whereas τ is the time spent at the intermediate

A

V	Size	T
100	12×12	38 ± 6
1000	6×6	58 ± 18
1000	12×12	54 ± 5
1000	24×24	54 ± 2
10000	12×12	73 ± 7

B

Size	T
12×12	103 ± 16
3 cells	73 ± 14

Table 5.3 Characteristic time, T, for pattern formation in point B of Fig. 5.4A. Tables showing the average characteristic time T of pattern formation and its standard deviation for (A) stochastic dynamics and (B) deterministic dynamics for the parameter values of point B of Table 5.1 (Fig. 5.4A.). The initial condition is the H pattern solution at parameter space point A. T is defined as the time at which the order parameters $\bar{\eta}_s$ and $\bar{\eta}_l$ reach 90% of their stationary values each. The stationary values of the order parameters (for $x = s, l$) were computed as the time-averaged values of $\bar{\eta}_x(t)$ over a period $\Delta t = 10$ during which the standard deviation of $\bar{\eta}_x(t)$ is less than 0.01 times the time-average value. In table B, the initial condition is the H pattern of parameter space point A of Fig. 5.4, with a random perturbation of amplitude $\delta = 10\%$

vertex point B. For small $t_{up} + \tau$ values, selection of the P pattern is not robust but probabilistic and the process is more evidently a tissue decision making. Our results show that stochasticity in the dynamics enables robust selections at times shorter than in the absence of fluctuations (Fig. 5.10A). In contrast, the high-dimensionality of many interacting cells increases the threshold characteristic time for robust pattern selection (Fig. 5.10A).

To have a sense of whether the time required for robust selection in all these cases is long or short, we compared it with the corresponding characteristic time scale T of the full formation of the P pattern from an unstable homogeneous pattern (Fig. 5.11, Table 5.3). This time T is shortened by fluctuations and in low-dimensional systems (Table 5.3). In all cases being shown, T is longer than the time $t_{up} + \tau$ required for robust selection (Fig. 5.10A, Table 5.3).

It is worth mentioning that the P pattern is not always perfectly formed for the B values of the parameter space of Fig. 5.4A (Fig. 5.11). Despite of this, once the system arrives at the parameter space point C, the P pattern is perfectly formed (Fig. 5.9). This is because in point B, there is another pattern (not shown in the Fig. 5.4A) whose symmetry causes these deffects in the tissue

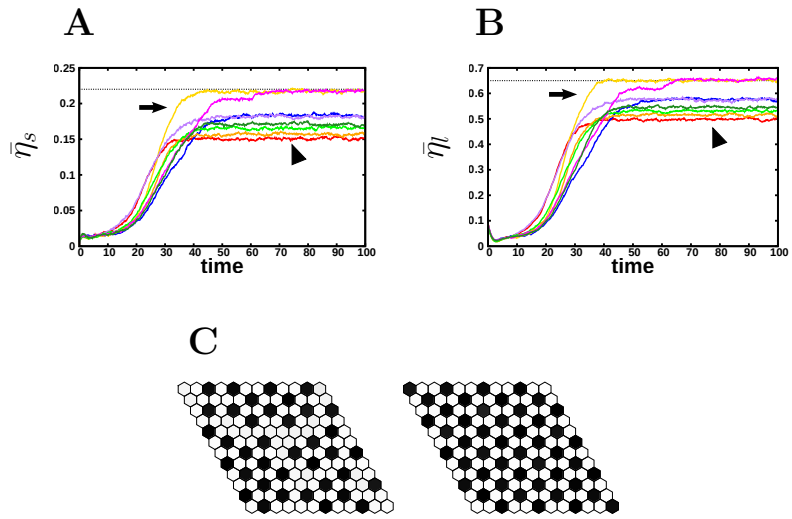

Figure 5.11 Stochastic time evolution of order parameters during pattern P formation. (A, B) Eight different stochastic time evolutions of order parameters $\bar{\eta}_s$ (A) and $\bar{\eta}_l$ (B), for the parameter values of parameter space point B of Fig. 5.4A ($r_t = 1.0$, $r_c = 0.1$). The initial condition is the H pattern with the theoretical predicted values of s and l of the homogeneous stable state of point A in the parameter space ($r_t = 0.1$,$r_c = 2.0$). The dashed line stands for the predicted theoretical value of the order parameter for a perfect periodic deterministic stationary pattern (see the value in Table 5.1). (C) Pattern at time $t = 100$ for those trajectories of panes A and B that are shown with an arrow (left) and an arrowhead (right). These patterns are stationary. According to panels A and B, the characteristic time to form the P pattern in point B of parameter space is $T \sim 40 - 50$ (see Table 5.3 for the average values of T, with more volumes and tissue sizes explored). Moreover, the final stationary states are different because the final pattern is not perfectly periodic in all the tissue. Other parameters of the simulation are: $V = 1000$, $b = 1000$, $n = 2$.

(Formosa-Jordan and Ibañes, 2014). By contrast, this pattern solution is not stable in point C (data not shown).

Taken together, the results show that the dynamical path defined by the biochemical signal or signals, and not only the initial and final conditions, is a critical element for pattern selection. Selection of a new pattern involves the transient destabilization of the initial state and the subsequent exploration of a new pattern that will finally end in the desired selection. This is accomplished through a proper path which has to evolve dynamically slow enough to enable first destabilization and afterwards emergence of a new state. The pattern selected corresponds to the latest different pattern explored during the path. If

the path evolves too fast, selection might not be robust and become probabilistic. However, our results show that robust selection can involve short time scales compared to those required for full pattern formation. Accordingly, this robust selection can become visible at late times (i.e. at the end of the path) and not when the selection is actually taking place or when the signal is acting (Fig. 5.9C).

5.3.2 Scenario 2: Pattern selection by local paths

In scenario 1, the selection is driven by the transient destabilization of the initial stable solution. The destabilization depends on two factors: the path –and the domains of the parameter space explored by it –, and the time spent by the system in the intermediate vertex points of the path. We explored two types of path: those generated by two concatenated permanent changes on two parameter values (Fig. 5.8A,C), and those generated by transient concatenated changes of two parameter values (Fig. 5.8B,D). However, a change of a single parameter value can be enough to destabilize the initial solution in order to select a new one.

In this new scenario we explored the pattern selection driven by local paths that act only in a few cells. These paths implement trajectories on the parameter space that involve only one parameter modification, r_t or r_c (Fig. 5.12). If these parameter changes are applied to the whole tissue (global path) the conclusions are the same than in scenario 1 (Fig. 5.13). However, if the signal does not affect to all the cells of the lattice, non trivial behaviours arise in the selection.

We wondered whether selection of the P pattern in all the tissue could occur from biochemical signals that act locally only in a small subset of cells. We reasoned that such selection can occur if the P pattern is spatially more stable than the H pattern and thus can spontaneously propagate over the H solution. This spontaneous propagation occurs for the parameter values of point C of the parameter space of Fig. 5.4A where both the H and P patterns are stable. We then envisaged a path that acts only and transiently in a cluster of cells (path 2a in Fig. 5.12A). Hence, all cells have the same equivalent dynamics (i.e. those characterized by the parameter values of point C) at initial and final times. The path drives the cells within the cluster to evolve from the parameter space point C to a point where the H pattern is unstable (B) and

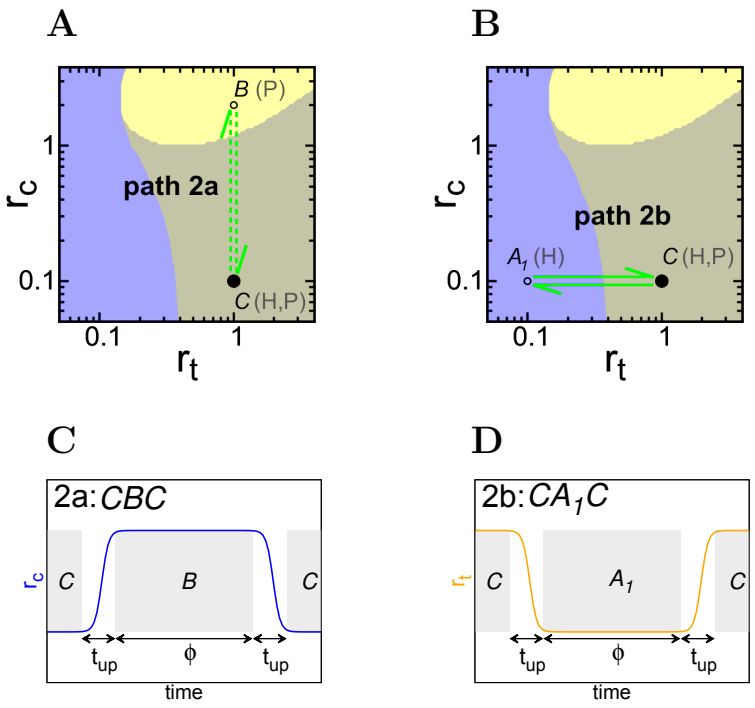

Figure 5.12 Local paths of scenario 2. (A,B) Paths (arrows) 2a (A) and 2b (B) in the parameter space of Fig. 5.4A. These paths involve transient temporal changes of a single parameter value acting in a cluster of cells. Solid circles stand for the initial and final points of the paths, while the intermediate vertex points are represented by open circles. (B,C) Changes of r_t (orange) and r_c (blue) along time for the different paths in scenario 2: (B) path 2a, (C) path 2b. The parameter space points that characterize each path are depicted. The time period spent by the system in each of these points is shadowed in grey (e.g., τ_B for B). Parameters defining the time scale dynamics (t_{up} and $\phi = \tau$) of the parameter changes are also depicted. Paths 2a and 2b differ in the parameter that is changed along the path (r_c in path 2a, and r_t in path 2b) while the other one remains constant. Hence, these paths differ in the parameter space point transiently visited (B in path 2a, and A_1 in path 2b).

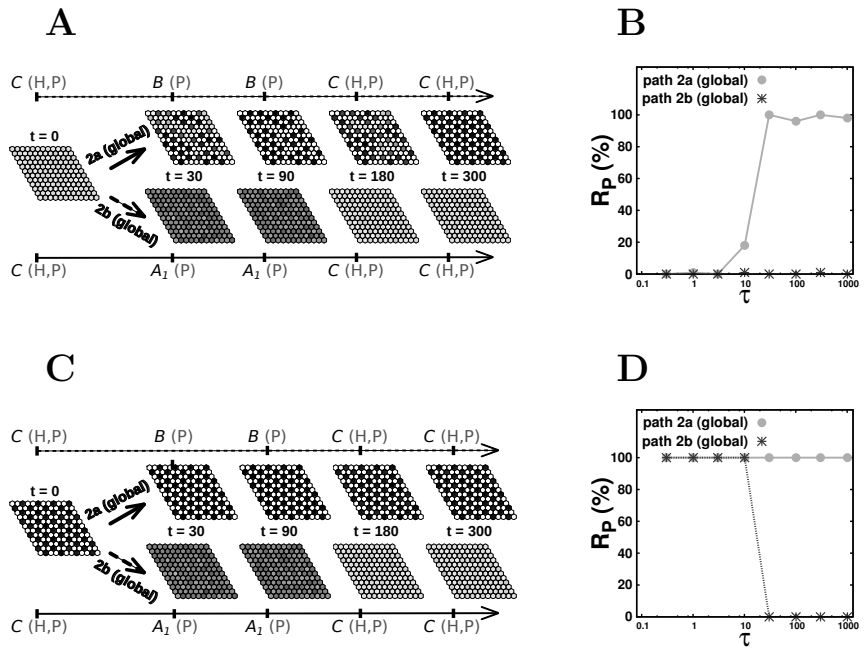

Figure 5.13 Pattern selection through transient global path. Pattern selection through the 2a path (A-B) and 2b path (C-D) acting as a global path (Fig. 5.12A-B). (A,C) Snapshots of the state of the system over time for each path and for initial condition being the (A) H or (C) P pattern, for $\tau = 90$. The initial, intermediate path vertex and final points of each path and the time t of each snapshot are indicated. The results show that the selection of a pattern different from the initial one only occurs when the path involves a transient destabilization of the initial pattern. (B,D) Percentage of selection of P pattern (R_P) versus τ when the initial state is H (B) and when the initial state is P (C). Different colours and symbols are used to distinguish selections from each path (global path 2a in orange circles, and global path 2b in blue stars), as indicated. Notice that selection of a new pattern requires a minimal time (τ). Other parameter values as in Fig. 5.9 and in Table 5.1.

backwards (Fig. 5.12A). When this path acts, the P pattern is selected (Fig. 5.14A). The P pattern forms within the cluster and propagates all through the tissue. Therefore, selection of a more spatially stable pattern can be driven by transient signals acting locally within the tissue. The transient local signal drives the selection of the new pattern within the cluster. Then, because the new pattern is spatially more stable, it spontaneously (without the action of any signal) invades the remaining tissue. Notice that path 2a is such that if the signal acted in all cells and not only within a cluster, the P pattern would be selected as well, as expected from the global paths of Fig. 5.13.

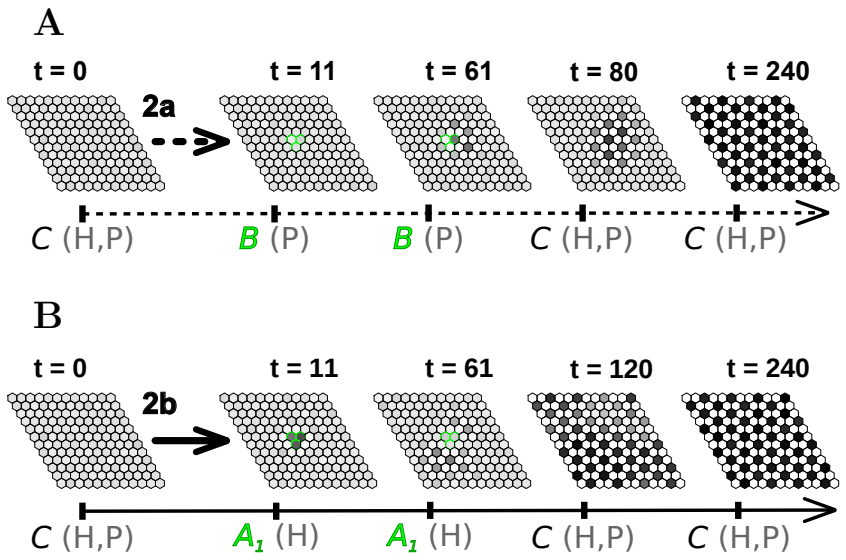

Figure 5.14 Pattern selection achieved through a spatially localized signal. Snapshots of the tissue state over time (t) when the system initially ($t = 0$) exhibits the H pattern and the signal acts only in three cells (green cell borders) which change their control parameter values transiently according to paths 2a (A) and 2b (B), while the remaining cells of the tissue have constant parameter values corresponding to those of parameter space point C. Parameter values are $\tau = 50$ and $t_{up} = 11$ and those in Fig. 5.9.

In scenario 1 we found that selection of a new pattern involved the transient destabilization of the initial pattern. Specifically if the path described the trajectory from point C to A_1, where only the H pattern is stable, and backwards (Fig. 5.12B), the P pattern was not selected from the H one (Fig. 5.13). We devised this same change to occur only within a subset of clustered cells (path 2b in Fig. 5.12B). Our results show that in this case the P pattern can be selected in the whole tissue (Fig. 5.14B). Snapshots of the dynamical evolution of the state of cells reveals that the P pattern starts to emerge at the boundary outside the clustered cells, i.e. where the signal is not acting (Fig. 5.14D). This initial nucleation of the pattern then spreads to all the tissue. Thus, this signal drives selection of the P pattern only if it acts on a subset of cells and not in all the tissue. In this case, the destabilization of the H pattern arises from the spatial inhomogeneities the signal drives on the tissue through the large differences between the average values of the ligand and receptor activities of the H pattern at points A_1 and C (Table 5.1). Thus, the P pattern can only arise at

the boundary where the signal acts.

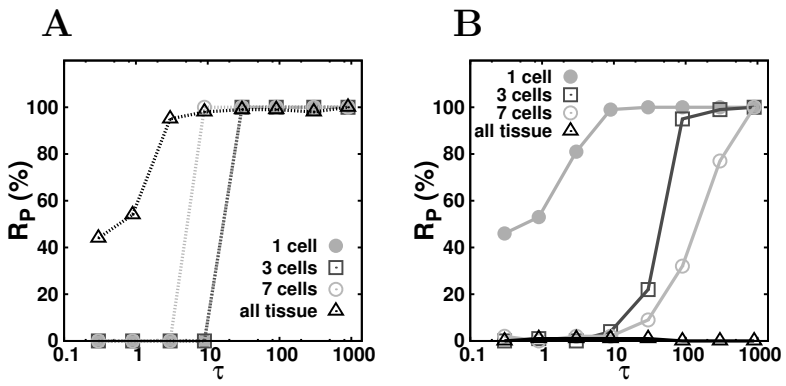

Figure 5.15 The robustness of the selection process depends on the amount of cells that sense the signal (Cluster size). requency of selection of the P pattern (R_P in percentage) for 100 repetitions versus the time τ spent at the intermediate parameter space vertex point of the path. The signal drives the change of the control parameters only in the number of cells detailed in the legend, located at the centre of the tissue, according to (A) path 2a and (B) path 2b of Fig. 5.14, respectively. All parameter values as in Fig. 5.14.

We explored the robustness of these selection processes as a function of the time τ spent at the intermediate point (B for path 2a and A_1 for path 2b) and of the number of cells on which the signal acts. In all cases, the selection process shows a threshold-like response requiring a minimal time to be robust (Fig. 5.15). For path 2a (Fig. 5.14A), this minimal time is larger than when the signal acts in all the tissue (Fig. 5.15A). The minimal time decreases as the number of cells responding to the signal is larger (Fig. 5.15A). For path 2b (Fig. 5.14B), the selection process required much more longer time scales (Fig. 5.15B). This is to be expected since the pattern does not form from a linear, small, instability, but from a nonlinear one. In addition, the minimal time increases with the size of the cluster of cells (Fig. 5.15B). It is also worth to be stressed that the selection becomes less robust, becoming less sharp.

The distinct behaviour paths 2a and 2b show for the time required for robust selection as a function of the size of the cluster of cells indicates that we may expect non-monotonic functionalities on the size of the cluster for more complex paths. Figure 5.16 shows the system behaviour for a local path such as the 1a path' but only affecting to a subset of cells (cluster size).

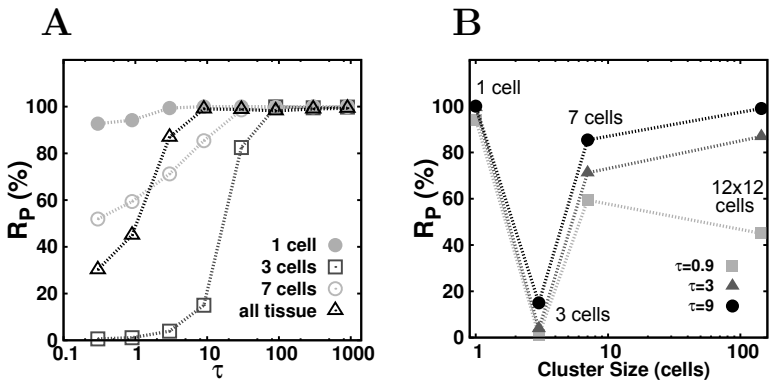

Figure 5.16 Selection by a local path such as the path 1a' that acts only on a cluster of cells (cluster size). The cyclic path used herein involves transient changes of the parameter values as those depicted for path 1a' in Fig. 5.8A,C. The path starts and ends at point C of the parameter space. The changes of the parameter values only occur on a subset of cells, while the rest of the cells of the tissue remain at all time with the parameter values of point C. This is in contrast with path 1a' which acts upon all cells of the tissue. (A) Frequency of selection of the P pattern (R_P in percentage) for 1000 repetitions versus the time spent at each intermediate parameter space vertex point of the path τ ($\tau = \tau_B = \tau_{A1} = \tau_A$). The signal drives the change of the control parameters only in the number of cells detailed in the legend, located at the centre of the tissue. (B) The same results as in panel A but depicted as a function the number of cells that change their parameter values. Different curves correspond to different τ values (see the legend). Notice the non monotonous dependency of the pattern selection with the cluster size for this path. Other parameter values as in Fig. 5.10B. The total size of the tissue is 12×12.

Together, these results show that selection of a pattern that is more stable than another stable one and can spatially invade it can be triggered by a signal acting locally in a cluster of cells and propagate across the tissue spontaneously, without requiring the signal anymore. The signal can destabilize the initial pattern either dynamically inside the cluster of cells or in a spatial manner by setting borders. Therefore, the instability can arise either within the region where the signal acts or outside this domain, at its border.

5.3.3 Scenario 3: Spatio–temporal paths can select the stripe pattern

It is quite common to have patterns that although they are stable, they can not arise spontaneously from an H pattern unless specific spatial symmetries are broken. In our model, the stripe S pattern is such a case whereas the dynamics are completely isotropic, the S pattern is not. To ensure stochastic stability of this pattern, we focused on the phase diagram for $n = 4$ (Fig. 5.4B and 5.17A). We evaluated whether selection of the S pattern can arise when the system is initially at the H pattern. According to the phase diagram (Fig. 5.17A), transient destabilization of the initial H pattern can occur but it does not drive an univocal selection. Although H becomes now unstable, both the S and P patterns are stable and able to be selected (e.g., at point B).

To drive the selection from the H pattern to the S one, we envisaged that signals could act in domains of the tissue, which could break the spatial symmetry appropriately. It is worth to mention that for deterministic dynamics, the S pattern does invade the H pattern and it can be induced by local non-propagating signals (data not shown). However, evaluation of the relative stability of the S pattern for stochastic dynamics indicated that the S pattern can not propagate over the H pattern (Fig. 5.6), discarding a mechanism like scenario 2. Therefore, if the S pattern was to arise in a small spatial domain of the tissue, it would not propagate spontaneously over the whole tissue. This prompted us to consider spatio–temporal signals and paths that sweep rows of cells along time (Fig. 5.17B, Eq. 5.3). These kind of spatio–temporal paths could be driven, for instance, by diffusing morphogens.

We designed that changes of parameter values within a cell over time trace the trajectory shown in Fig. 5.17A, which traverses a region where the H pattern becomes unstable. These changes evolved progressively from row to row (path 3) (Fig. 5.17B). Figure 5.18 shows that the S pattern can be selected through this path.

We evaluated how the selection of the S pattern depends on the time t_{prop} the path takes to evolve from row to row and on how many rows (N_{rows}) are at point B of the path where the H pattern is unstable (Fig. 5.17A-B). For short t_{prop} (i.e. fast propagation of the signal over the tissue) the S pattern is not selected but the P pattern is (Figs. 5.19). Specifically, $t_{prop} = 0$ corresponds

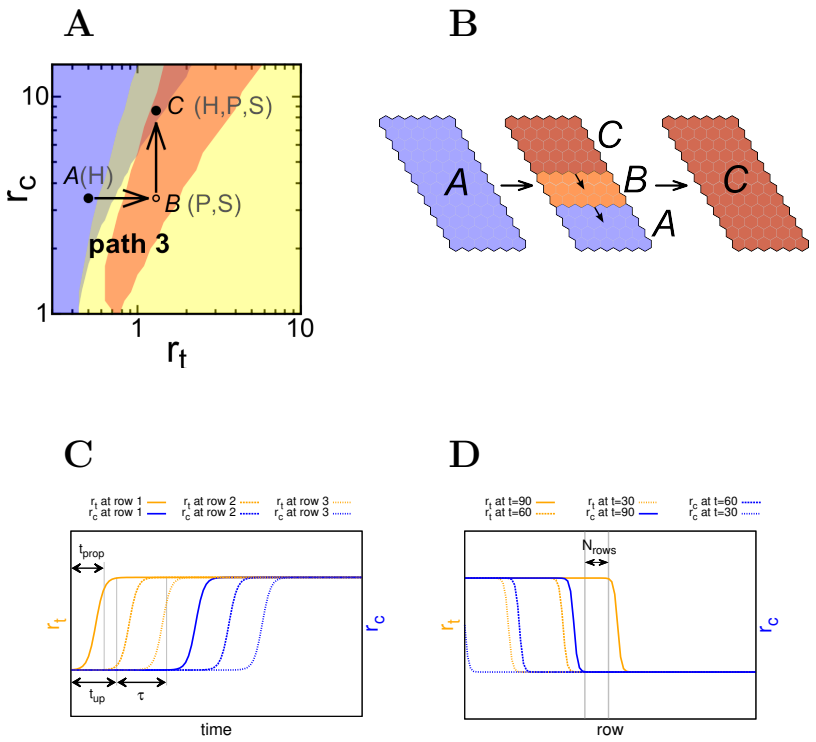

Figure 5.17 Spatio–temporal path of scenario 3. (A) Path depicted as arrows across the parameter space of trans (r_t) and cis (r_c) interaction strengths. Solid circles stand for the initial and final points of the path, while the intermediate vertex points are represented by open circles. It is indicated within parentheses at relevant points of the path (denoted by letters A, B, A_1 and C) whether the homogeneous (H), the salt-and-pepper (P) and/or stripes (S) patterns are stable. The path crosses different domains (colours) each defined by which of these patterns are stable: H (blue), P (yellow), H and P (grey), S and P (orange), or H, P and S (red). Stability of these patterns for stochastic dynamics and fixed boundary conditions at bottom and top rows is found in Fig. 5.6. (B) Representation of path 3 across the tissue (denoted by the black border) at the initial (left), an intermediate (middle), and the final (right) times. Small arrows within the tissue denote the spatial direction of change of the parameter values: from top to bottom rows. Colours and letters, as in panel A, denote the parameter values of cells. (C) Temporal evolution of the r_t (orange) and r_c (blue) parameters for different rows of the tissue, as indicated. τ stands for the time period during which a row is at the intermediate vertex point, B, of the path. t_{prop} is the time required for the parameter to change from one row to the adjacent one. (D) Spatial distribution of the r_t (orange) and r_c (blue) parameters at different times, as indicated. N_{rows} is the number of rows that are at the same intermediate vertex point of the path 3.

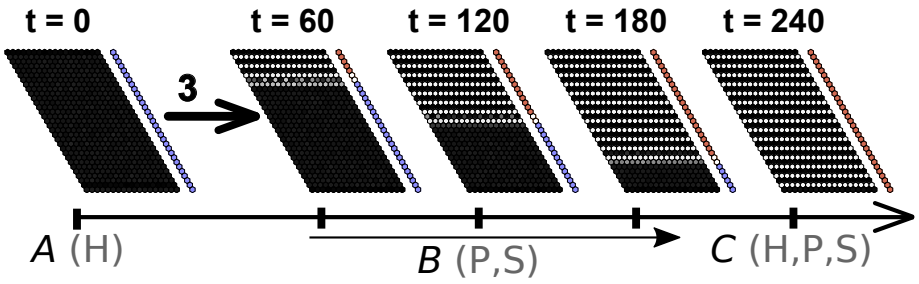

Figure 5.18 Stripes selection achieved through a propagating signal. Snapshots of the tissue state over time (t) when the system starts ($t = 0$) with the homogeneous H pattern and parameters change over time according to path 3 (i.e. propagating from top to bottom cell rows). The column of coloured cells at the right of each panel shows the point of the parameter space at which each cell row is (blue for point A, white for B and red for C). Parameter values are $t_{prop} = 7$, $N_{rows} = 2$, $b = 1000$, $n = 4$, $V = 10000$, and r_c and r_t values can be found in Table 5.2. A lattice of $N = 18 \times 31$ cells with fixed boundary conditions at bottom and top rows ($s = 0$ and $l = 0$ for neighbours on top of the first row and below the last row) and periodic conditions between left and right sides were used. These results are also found if toroidal periodic boundary conditions are considered (data not shown).

to the signal acting in all cells at the same time, and not propagating (scenario 1). Therefore, non-propagating signals can not select the S pattern as expected (Fig. 5.20). For higher values of t_{prop} (i.e. slower propagation of the signal), the S pattern is robustly selected, with the stripes arising sequentially as the signal propagates, and finally all the tissue exhibits the S pattern (Figs. 5.19). If the signal propagates too slowly (large t_{prop}), the stripes become destabilized and the P pattern is selected again (Figs. 5.19). These two limits give an optimal selection of the S pattern within a range of t_{prop}. Increasing the value of N_{rows}, enlarged the maximal t_{prop} for optimal selection of the S pattern, albeit up to a maximal range (Figs. 5.19). The range of t_{prop} values for which the selection of the S pattern occurs is of the same order as the time for the formation of stripes in few rows surrounded by the H pattern (data not shown). We also found that short t_{prop} values, below the optimal range, drove stripes to be formed consistently only partially within the tissue (Figs. 5.19B-C). In contrast, for t_{prop} values above the optimal range, in some stochastic circumstances all the tissue could form the S pattern, while only partially in other cases (Figs. 5.19B-C).

We checked that the selection of stripes can also occur through spatio–temporal

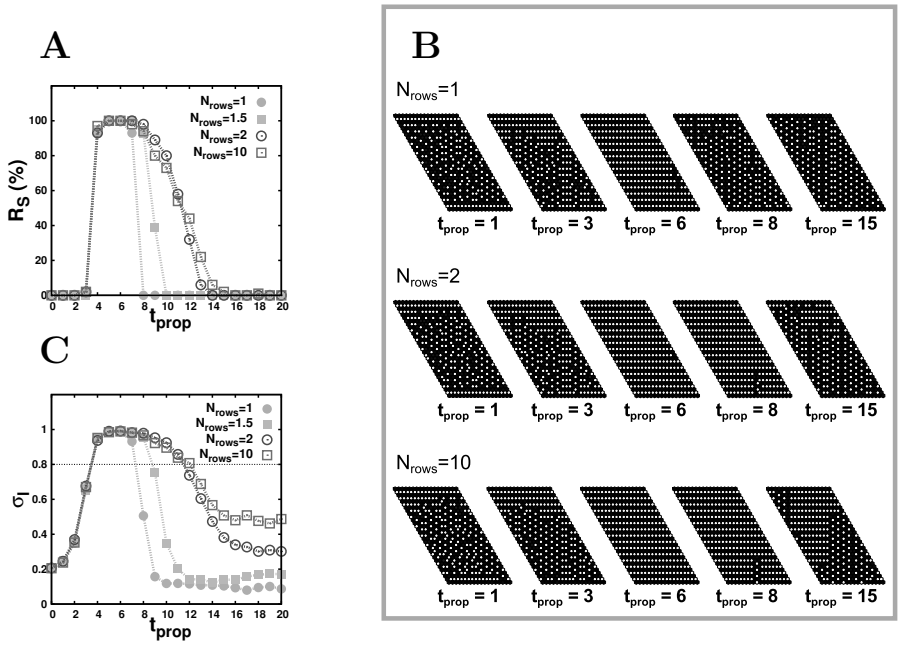

Figure 5.19 Robust selection of stripes occurs for an optimal signal propagation time along the tissue. (A) Frequency of selection of the S pattern (R_s in percentage) for path 3 (Fig.5.17A) versus t_{prop} (propagating time) for 100 repetitions. Results for different number of cell rows being simultaneously at point B of the path (N_{rows}, see legend) are shown. (B) Snapshots of the stationary state reached through path 3 (Fig.5.17A), for different spatio–temporal dynamics of the path, i.e., different values of t_{prop} and N_{rows}. (C) Values of σ_l (average of 100 repetitions) for path 3 versus t_{prop} (propagating time). Results for different number of cell rows being simultaneously at point B of the path (N_{rows}, see legend) are shown. The dashed line points out the value of 0.8, which has been considered as a threshold for stripes selection (R_S). See the definition of σ_l in Section 5.2.5. All other parameter values and boundary conditions as in Fig. 5.18.

paths that start and end up at the same multistable point of the phase diagram, exhibiting similar features as those described above (Fig. 5.21).

These results show that selection of the S pattern, which can not arise through random variability from the H pattern, requires a spatio–temporal path that favours its spatial symmetry. Yet, and in contrast with the other selection processes being analysed, there is an optimal time scale for the signals to select the S pattern.

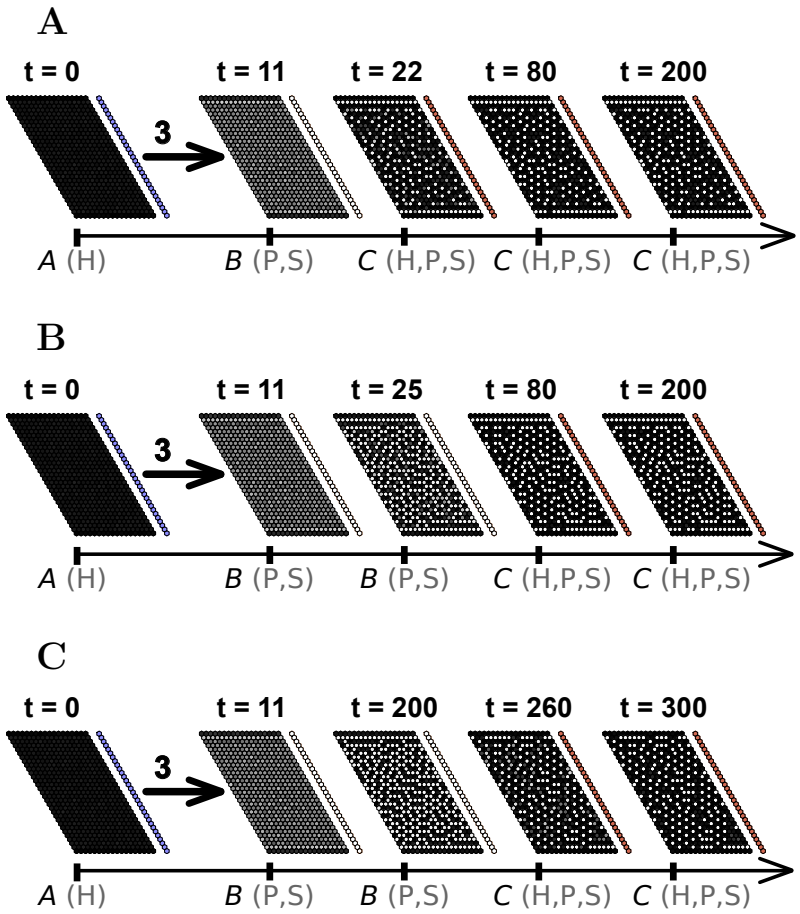

Figure 5.20 Pattern selection achieved through path 3 with $t_{prop} = 0$. Snapshots of the tissue state over time (t) when the system starts ($t = 0$) with the homogeneous H pattern and parameters change over time according to path 3 in Fig. 5.18 but with $t_{prop} = 0$. Therefore, all cells change their parameter values at the same time. In these cases, path 3 (with $t_{prop} = 0$) is of the scenario 1-like type. The column of coloured cells at the right of each panel shows the point of the parameter space (Fig. 5.17A) at which each cell row is (blue for point A, white for B and red for C). Three values of τ have been explored. (A) The tissue spends no time in B parameter space point, so $\tau = 0$. (B) Each cell of tissue spends as much time in B as a cell does in the path studied in Fig. 5.18. It uses $\tau = 14$. (C) The whole tissue spends as much time in B ($\tau = 231$) as the tissue in Fig. 5.18 remains with at least one row of cells in B. Other parameter values and boundary conditions as in Fig. 5.18.

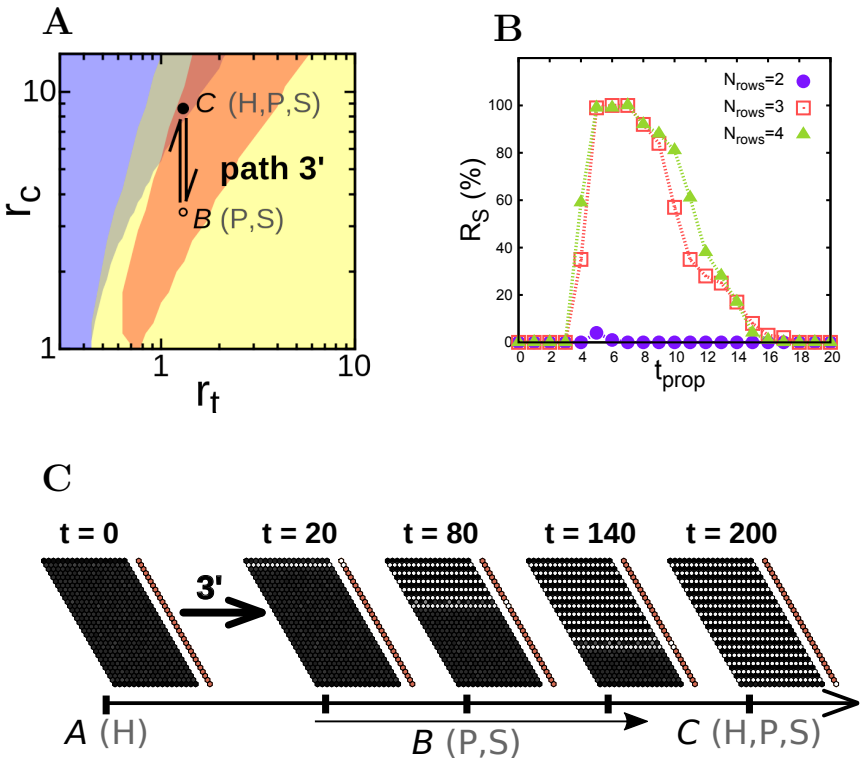

Figure 5.21 Selection of the S pattern through a transient spatio–temporal change of a parameter value. (A) Path 3' depicted as arrows in the parameter space of Fig. 5.4B. The path starts at point C and transiently visits the point B. (B) Snapshots of the tissue state over time (t) when the system starts ($t = 0$) with the homogeneous H pattern (of C point) and parameters change over time according to this path 3'. The column of colored cells at the right of each panel shows the point of the parameter space at which each cell row is (white for B and red for C). Parameter values are $t_{prop} = 6$, $N_{rows} = 4$. (C) Frequency of selection of the S pattern (R_S in percentage) for the path described in panel A versus t_{prop} for 100 repetitions. Results for different number of cell rows being simultaneously at point B of the path (N_{rows}, see legend) are shown. Parameter values and boundary conditions as in Fig. 5.18.

5.4 Discussion

Previous works have addressed the question of how different cellular patterns can be established in a tissue, e.g., how a system can select between spots and stripes (Ermentrout, 1991; Shoji et al., 2003; Lin et al., 2009; Lubensky et al., 2011; Simakov and Pismen, 2013). These works focused on the univocal correspondence between the parameter and initial conditions values with the selected pattern. Our work sheds light to new mechanisms for the selection among multiple stable patterns based on time-dependent parameter variation. Our results showed that the selection of a specific pattern does not depend only on the initial and the final values of the control parameters. The main factor in our approach was the specific path followed by parameter changes and the spatio–temporal characteristics of these changes such that the path drives the selection. Herein, changes of the parameter values are understood as the result of biochemical signals. We expect these mechanisms to help to understand some of the pattern formation processes occurring in the context of development. Despite the fact that the signals that induce the decision in this chapter follows a continuous profile, this study could be also performed by implementing step-like functions, as in previous chapters.

We presented different dynamical paths that select patterns which are all stable for the same value of the parameters. To this end, we made use of a model of tissue differentiation based on cell–to–cell communication through the Notch signalling pathway. We showed that patterns that can spontaneously break the spatial symmetry can be robustly selected through paths which only involve temporal, and not spatial, dynamics. The time scales of the path (i.e., of the parameter changes) can be shorter than the time required for the full pattern to emerge. Therefore, the selection can become evident after the path has finished, i.e., at the final set of parameter values. In this sense, the tissue has a memory of the conditions (the path) into which it has been. Even for fast paths, the selection can be robust. Indeed, the selection exhibits a threshold-like behaviour as a function of the characteristic time scale of the path. This conclusion on the relevance of the sepeed of the parameter change for selecting a certain system state connects with general ideas of cellular decision making: the decision does not only depend on the bifurcation involved, but also on how fast the system changes this bifurcation parameter (Nené et al., 2012; Ashwin and Zaikin, 2015).

We showed that when several patterns are stable and one is able to spatially invade another one, the invading pattern can be selected through signals acting in a small subset or cluster of cells. Such selection spontaneously propagates through all the tissue, without requiring further the action of the signal. Moreover, our results showned that selection can arise among cells that are not within the cluster of cells where the biochemical signal acts. In this case, the initial pattern becomes destabilized by the spatial inhomogeneities the signal drives at the boundary of its acting domain. In all these cases, selection exhibits as well a sharp threshold response with time. The robustness of the selection process depends as well on the size of the cluster of cells, and this dependence can be antagonistic for different paths.

Finally, our results showed that patterns which can not arise spontaneously because of their symmetries, they require spatio–temporal signals that set appropriate symmetries. This is the case of the S pattern. A propagating front can drive its selection, yet robust selection only occurs for a range of optimal propagation times.

Summarizing, the most relevant aspects involved in the selection of a pattern among multiple stable ones through dynamical paths are: (i) The destabilization of the initial pattern either by dynamical (scenario 1) or spatial (scenario 2) mechanisms. (ii) The different stable patterns that the path visits during its evolution, being the last explored pattern the most relevant one for the final selection when all are explored for long enough times. Therefore, the order that signals acting sequentially have is relevant. (iii) The interplay between two relevant time scales: the characteristic time of the parameter changes, which sets the time spent in the exploration of a pattern, and the characteristic time to form the pattern. (iv) Selection can be triggered at localized clustered regions and spontaneously extend to all the tissue, when the selected pattern can propagate over the initial one. (v) For more singular pattern selections, time–specific symmetries of the spatio–temporal parameter changes.

Recently, it has been shown that dynamic filopodia in *Drosophila* enables the creation of sparser salt-and-pepper patterns mediated by Notch signalling (Cohen et al., 2010, 2011). This is an example of a stochastic spatial and time-dependent trans-interactions strength (r_t) extended to longer range interactions. A more recent study suggests that growing cell projections in certain

cells in zebrafish embryos would drive stripes formation through Notch signalling (Hamada et al., 2014), what could probably be understood as a pattern selection phenomenon through a dynamical path. Hence, an extension of our framework to more complicated dynamical paths in the parameter space might be helpful for studying these and other phenomena that exhibit more complicated spatio–temporal patterning.

Notch signalling is just an example of a pathway that is orchestrated and modulated by different agents along time and space. Therefore, the patterning selection mechanism characterized here can also be applied to other signalling pathways acting during development. In addition, in this work we explored what happens if trans and cis interaction strengths in Notch pathway are modulated in time, but other parameters could also be explored, like the signalling intensity elicited by a ligand when interacting with the receptor. Indeed, recently it has been shown that there is spatio-mechanical regulation for signal activation, what could probably drive time-dependent signalling efficiency for the Notch receptor (Narui and Salaita, 2013).

Chapter 6

Stochastic decision making in the malaria parasite

6.1 Introduction

In this chapter we deal with a decision making process taking place in a real system: the decision to become sexual in malaria parasite. This study has been done in collaboration with Prof. Alfred Cortés from the Barcelona Institute of Global Health. Instead of focusing on the mechanism inducing the decision, we evaluate the consequences of the probability of each choice on the parasite functionality. In this section, an introduction to the biological context of this decision and previous works on this topic are presented.

Malaria is an infectious disease that affects humans, among other vertebrates, and it is caused by parasitic protozoans (unicellular eukaryotic organisms) belonging to the genus *Plasmodium* (Bousema and Drakeley, 2011). The disease is transmitted between humans through bites of mosquitoes (of the *Anopheles* genus). It is endemic in tropical and subtropical regions, where it is still a relevant cause of disease and death. In these warm regions, mosquitos have longer lifes enabling and facilitating the transmission. There were 219 million documented cases of malaria in humans in 2010, according to the World Health Organization (WHO).

Several species of *Plasmodium* cause malaria infections in humans. Because of the specificities each specie drive on the infection, a single common strategy for malaria eradication is not envisaged. According to the number of people at risk of their transmission, the most relevant *Plasmodium* species are *P. falciparum* and *P. vivax* (Bousema and Drakeley, 2011; Guerra et al., 2010; Mueller et al., 2009). But, *P. falciparum* is responsible for the vast majority of mortality cases (Bousema and Drakeley, 2011; Guerra et al., 2010; Mueller et al., 2009).

We focus our study on malaria caused by *P. falciparum*. Typically, malaria becomes symptomatic 8 to 25 days after infection. The infected human experiences then cyclic episodes of fever every 36-48 hours. These fever episodes are caused by the high proliferation of asexual parasites. The density of these parasites in blood is known as the level of parasitemia. Yet, the asexual form of the parasite is not transmitted to the mosquito when it bites a human. Instead, the transmissible form of the parasite, which becomes allocated in the peripherial blood that is accessible to the mosquito, is the sexual one (i.e. *gametocytes*). These gametocytes arise from asexual precursors within the human (Fig. 6.1). Our study focuses on the decision that parasites take inside a human to either remain asexual or to become gametocytes. It is well accepted that, despite its variability, the sexual conversion rates are typically very small, below 5% (Eichner et al., 2001). In addition, results of our collaborator Prof. Alfred Cortés and colloeagues show that this decision is stochastic and relies on an epigenetic mechanism (Kafsack et al., 2014).

The transmission process from human to human through mosquitos' bites involves several stages that are related to the parasite life cycle. *P. falciparum* life cycle includes many phases that take place inside the mosquito and inside the human host and are summarized in Fig. 6.1 (Bousema and Drakeley, 2011). The mosquito, when taking blood from an infected human through a bite, takes gametocytes too. Once in the mosquito midgut, gametocytes give rise to male and female *gametocytes* that can fuse and form a *zygote*. This zygote develops until forming an *oocyst* that will give rise to thousands of *sporozoites*. These *sporozoites* are the parasite forms transmitted to humans when the mosquito bites again. Once in the human, the majority of sporozoites migrate to the liver, where they invade liver cells in order to proliferate and form *schizonts*. These schizonts give rise to *merozoites* that migrate to the bloodstream, where they proliferate by invading red blood cells (RBC). This drives

the fever episodes characteristics of malaria. In addition, these merozoites convert into sexual forms (i.e.*gametocytes*) at a very low proportion. Therefore, the parasite survival depends on a good transmission between the human host and a new mosquito, in order to abandon the human host before the parasite extermination by either the immune system or the host death due to the virulence of the disease.

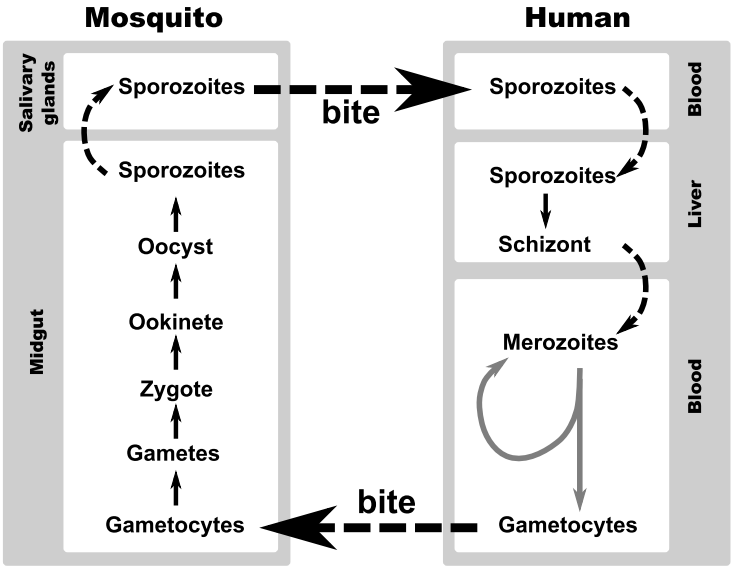

Figure 6.1 ***Plasmodium falciparum* life cycle involves two organisms: a mosquito and a human host.** Different parasite forms in the mosquito (left) and in the human host (right). Different localizations of the mosquito or in the human body are depicted with white boxes. Solid arrows (either black or grey) represent a development processes that result to a new parasite forms, while the dashed arrows represents process of migration, from one organ to another, or the process of transmission between the two hosts. Grey arrows denote the decision of the merozoites that takes place in the bloodstream. Adapted from (Bousema and Drakeley, 2011).

The main real data of gametocytes dynamics in human hosts is those collected by the US Public Health Service in the National Institute of Health Laboratories in Columbia, South Carolina and Milledgeville, Georgia, between 1940 and 1963, when malaria infection was used to treat neurosyphilis (Collins and Jeffery, 1999). Because of the difficulties in characterizing the parasite behaviour *in vivo* in the human host, the complex interaction between the parasite and the host immune system, and microscopy shortcommings to detect gametocytes, theoretical approaches are relevant too to understand the parasite decision of

becoming sexual. This sexual conversion decision has been indeed theoretically studied previously, pointing to competition between different parasite strains as the main factor that explains the low conversion rate (McKenzie and Bossert, 1998, 2005; Mideo and Day, 2008; Crooks, 2008). Crooks reviewed the main continuous-time models studied and concluded that a discrete-time approach is more accurate to describe the parasite dynamics (Crooks, 2008). Our study is focused on presenting a time-discrete model, which shares similarities with the one presented by Crooks, in order to evaluate the conversion probability that maximizes the gametocyte population and the probability of transmission according to new experimental data (Churcher et al., 2013).

6.2 The decision to become sexual and the maturation of gametocytes

The asexual cycle of parasite proliferation within the human lasts around 48 hours. During the cycle, inside a RBC, the parasite proliferates and gives rise to new identical asexual parasites that, once released, will be able to infect new RBC (Fig. 6.1). However, there is a decision that takes place during the asexual proliferation. The parasites inside the RBC can remain in the asexual form or can become sexually-committed. Regardless of the choice, the new parasites will be released by the RBC burst into the bloodstream and they will infect new RBCs. However, the sexually-committed parasites will not proliferate inside the new RBC and, instead of that, the RBC infected by the sexual committed parasite gives rise to a gametocyte (Bousema and Drakeley, 2011). Figure 6.2 illustrates this decision.

Each new gametocyte is temporarily sequestered away from the circulation in order to complete its maturation. This development results in a mature gametocyte that is re-released into the circulation and thereby it is susceptible to be transmitted to a mosquito. Hence, it takes some days (≈ 10) between the formation of an immature gametocyte and its development to become infectious to mosquitoes. Mature gametocytes eventually die, after some days (≈ 20) since their maturation. Cartoon of Fig. 6.3 shows both the decision and all these stages.

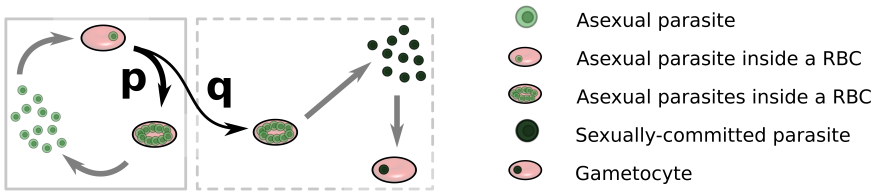

Figure 6.2 Malaria parasite decision in the bloodstream stage. Parasites remain at the asexual cycle (left rectangle), or start (with a conversion probability) a process that results in the gametocyte formation (right rectangle). The decision is depicted with black arrows. Grey arrows represent other steps such as the asexual cycle or the gametocyte formation.

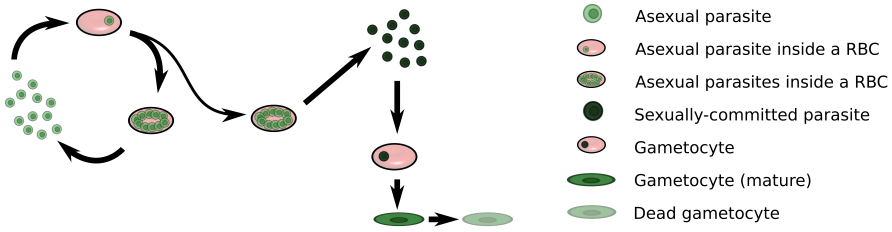

Figure 6.3 Some stages of the asexual and the sexual forms of the parasite. Different stages of the parasite in both cycles, the asexual proliferation cycle and the formation of the infectious (transmissible) parasite.

6.3 Model of the stochastic decision

Taking into account that the decision takes place in each asexual proliferation cycle, we choose each asexual cycle as the time unit of our model (discrete time model). We define as p the probability of remaining as an asexual parasite and q the probability of becoming a sexually-committed parasite ($p + q = 1$) (Fig. 6.2). Parasite population is described by three variables: the asexual parasites (A), the immature sexual parasites (S), and the mature sexual parasites (S^*) (Fig. 6.4).

The proliferation rate of the asexual parasites is given by R (Fig. 6.4). This is an effective proliferation rate that takes into account the asexual division rate inside the RBC and the death rate of asexual parasites. This death is produced by two main factors: immune system action on the infected RBC and

the death of the asexual parasite once it is released in the bloodstream. In this computational model, to take into account potential dispersion of R values, we define different values of R, each occurring with a certain probability associated. The proliferation value of each asexual parasite changes every cycle, according to the probability distribution of R values.

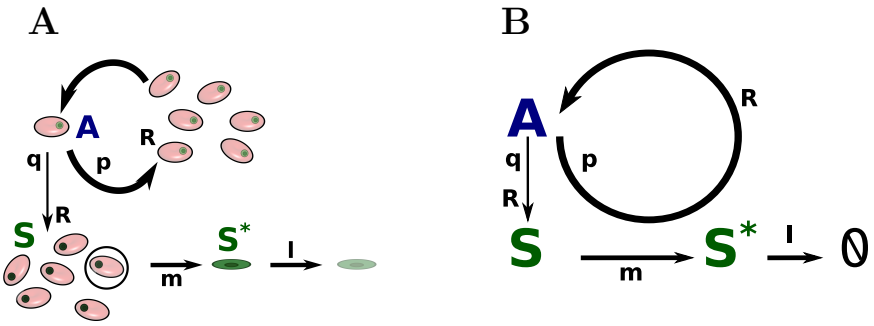

Figure 6.4 Asexual and sexual parasite model. The variables that describe the three parasite population are depicted: asexual (A), immature sexual (S,), and mature sexual (S^*) parasites. p and q probabilities describe the conversion decision. R is the proliferation rate, the number of asexual parasites generated by a single asexual parasite per cycle. m is the maturation time required for an immature sexual parasite to become mature. l is the life span of a mature sexual parasite. See the meaning of the cartoons of panel A in Fig. 6.3

A new immature sexual parasite is formed from an asexual precursor with a probability per cycle of q. In the stochastic simulations of the model, the conversion decision of each parasite is controlled by a random number generator. After some cycles (m), the gametocyte becomes mature and infectious. After l cycles in the bloodstream the mature sexual parasite dies. We call these two times, m and l, as *maturation time* and *life span* (Fig. 6.4). The stochastic numerical interpretation of the model also takes into account dispersion in the maturation time, m, and in the lifespan of each parasite l. The model confers to each new sexual parasite a value of m and l according to the following probability distribution

$$P(\langle X\rangle + k) = \frac{1}{\Delta X + 1}\left(1 - \frac{|k|}{\Delta X + 1}\right), \tag{6.1}$$

where $\langle X\rangle$ is the mean value of parameter m or l, ΔX the dispersion of the parameter (Δm or Δl), $k = \{k \in \mathbb{Z} | -\Delta X \geq k \leq \Delta X\}$. Notice that,

$$\sum_{-\Delta X}^{+\Delta X} P(\langle X \rangle + k) = 1\,. \tag{6.2}$$

According to the expression (6.1), m and l take integer values between $-\Delta m$ and $+\Delta m$ and $-\Delta l$ and $+\Delta l$ respectively. The probability reaches the maximum value in $m = \langle m \rangle$ and $l = \langle l \rangle$, respectively, and it decreases linearly for higher or lower values.

6.4 Transmission model

Churcher et al. (2013) have recently studied the relationship between gametocyte density (*P. falciparum*) in the human blood and the percentage of mosquitoes (*Anopheles gambiae*) that develop oocysts (see in Fig. 6.1 a reminder of oocysts). Their experimental work shows the relation between the density of gametocytes in blood and the probability of infecting a mosquito (transmission probability). According to their study, although the transmission probability increases with the density of gametocytes, the function that describes this dependency saturates at certain density.

Despite the fact that the experiments of Churcher et al. (2013) (see Fig. 1 of (Churcher et al., 2013)) reveal a high variability in the cases studied, we have qualitatively reproduced, according to their fitting, a function that describes the relationship between the gametocyte density and the probability of parasite transmission from the human bloodstream to the mosquito. The function that expresses this transmission probability (T) is,

$$T(S^*) = \begin{cases} 0.02\left(\tanh\left(\frac{S^*}{V_T} - 0.8\right) + 1\right), & \text{if} \quad \dfrac{S^*}{V_T} < 10 \\ 0.08\,\tanh\left(\dfrac{\frac{S^*}{V_T} - 250}{100}\right) + 0.12, & \text{if} \quad \dfrac{S^*}{V_T} \geq 10, \end{cases} \tag{6.3}$$

where V_t ($5 \cdot 10^6\,\mu l$) is the human blood volume. Figure 6.5 shows the transmission probability ($T(S^*)$) according to Eq. (6.3).

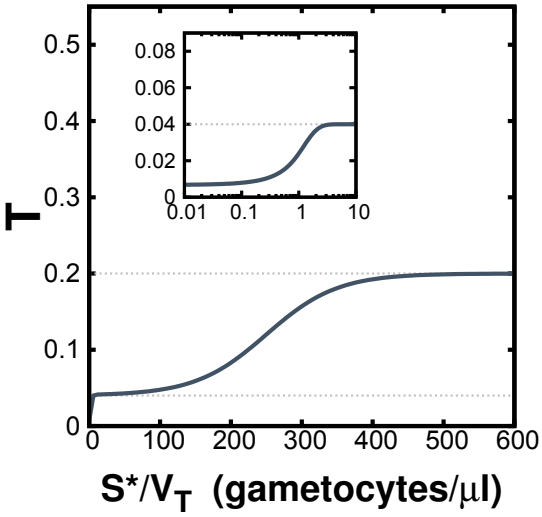

Figure 6.5 Transmission probability. Probability of transmission – of infecting a mosquito – (T) versus the mature gametocyte density (S^*/V_T) in the bloodstream of an infected human host. There are two saturation values (grey dashed lines). This function has been reproduced according to the Fig. 1 of (Churcher et al., 2013)).

6.5 Results

6.5.1 Dynamical regimes of the temporal evolution of the parasites

Taking into account the high number of parasites involved in a typical malaria infection (Bousema et al., 2006), we first evaluated the stochastic model of Section 6.3 analytically. Notice that the populations of parasites calculated by this analytical interpretation of the model can take non discrete values. However, we expect that the differences between both approaches are not relevant for large enough number of parasites.

$A(c)$ is the amount of asexual parasite at the c^{th} cycle. Initially, there are n asexual parasites ($A(0) = n$), which come from the liver stage. $g(c)$ is the number of immature sexual cells generated in the c^{th} cycle. The temporal evolution of these two variables, $A(c)$ and $g(c)$, is depicted in Table 6.1.

In this analytical approach of the stochastic model, we consider single, constant values of the maturation time (m), the life span (l) and the proliferation rate (R) without any dispersion.

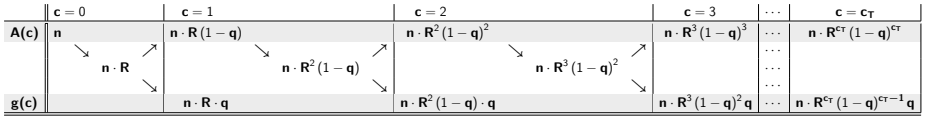

Table 6.1 Asexual parasites and immature sexual parasites generated per cycle. The table shows the number asexual parasites ($A(c)$) after each cycle (c). Furthermore, the number of immature sexual parasites ($g(c)$) produced in each cycle is also depicted.

According to Table 6.1, the number of asexual parasites in the c^{th} cycle is,

$$A(c) = n\,[R\,(1-q)]^{c} \tag{6.4}$$

The number of immature sexual parasites can be calculated with the following summation,

$$S^{*}(c) = \begin{cases} \displaystyle\sum_{i=1}^{c-m} g(i) & \text{if } \; c < l \\ \displaystyle\sum_{i=c-l}^{c-m} g(i) & \text{if } \; c \geq l, \end{cases} \tag{6.5}$$

which, according to the expression of $g(i)$ in Table 6.1, results into:

$$S^{*}(c) = \begin{cases} n\,q\,R\,\dfrac{1-[R\,(1-q)]^{(c-m)}}{1-R\,(1-q)} & \text{if } \; c < l \\ n\,q\,R\,\dfrac{[R\,(1-q)]^{(c-l-1)}\left\{1-[R\,(1-q)]^{(1+l-m)}\right\}}{1-R\,(1-q)} & \text{if } \; c \geq l \end{cases} \tag{6.6}$$

Equations 6.4 and 6.6 reveal that the dynamics of both the asexual and the sexual parasite population follows two regimes according to the values of R (proliferation rate) and q (conversion probability). Notice in Eqs. (6.4) and

(6.6) that $A(c)$ remains constant for $q = (1 - R^{-1})$ (i.e. $R(1 - q) = 1$). Furthermore, there is an exponential growth regime of $A(c)$ for $q < (1 - R^{-1})$, and an exponential decay regime for $q > (1 - R^{-1})$ (see Fig. 6.6). These two regimes (growth and decay) are also observed in the dynamics of the mature sexual cells, $S^*(c)$ (Fig. 6.6).

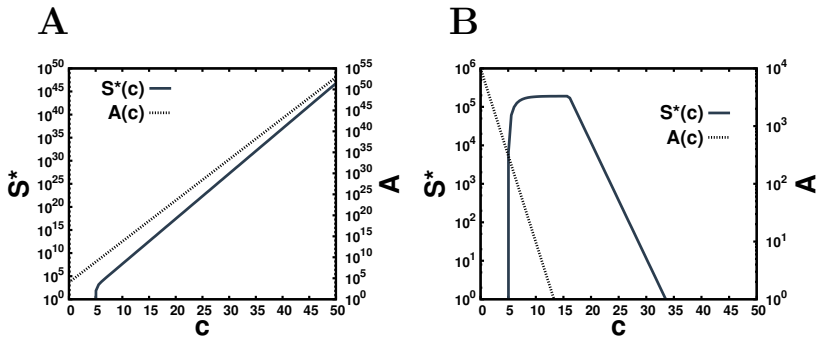

Figure 6.6 Two dynamical regimes for $A(c)$ and $S^*(c)$: growth and decay. (A) Dynamical evolution of asexual parasites (A) and mature sexual parasites (S^*) in an exponential growth regime: $q = 0.05 > (1 - R^{-1})$. (B) Dynamical evolution of asexual parasites (A) and mature sexual parasites (S^*) in an exponential decay regime: $q = 0.95 < (1 - R^{-1})$. Other parameter values: $n = 10^4$, $m = 5$, $l = 10$ and $R = 10$.

We can distinguish two phases in a typical infection of malaria: i) First, there is an exponential growth of the parasitemia (number of parasites in the bloodstream). ii) Due to the immune system response, the disease can reach a chronic phase where the parasitemia remains roughly constant and the symptoms are significantly reduced (Stone et al., 2015). While the first phase lasts a few days, the chronic phase can last some months, resulting in the host recovery. Despite we have distinguished these two phases for simplicity, the infection evolves in a continuous way from growth up to a kind of steady regime.

6.5.2 Optimal conversion probability to maximize the mature sexual parasites

The malaria parasites (e.g. *Plasmodium* falciparum) have evolved to guarantee their own survival. In this context, there is a crucial step in the parasite life cycle: the transmission from the human host to the mosquito. By this mechanism, the parasite avoids two catastrophic scenarios: its extermination by the

host immune system, and its ending with the host death. Taking into account that only the sexual parasites are able to infect a mosquito, this parasite form determines the viability of the parasite transmission from the human host to the mosquito. So, we consider that the strategy of the parasite for its survival and propagation lies in maximizing the amount of the parasites in its sexual form.

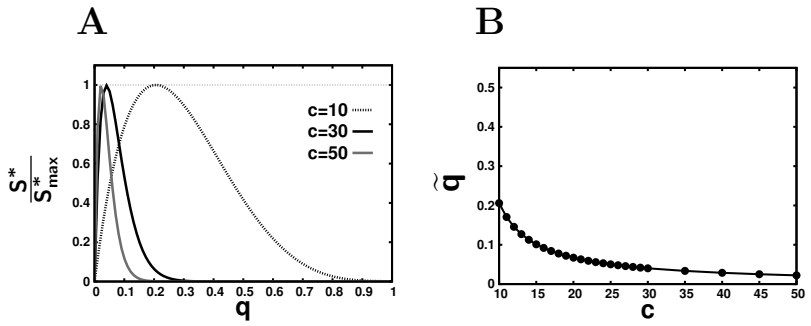

Figure 6.7 Optimal conversion probability value ($\widetilde{q}$) decreases with the cycle number (c). (A) Mature sexual parasites (S^*) for different conversion probability values (q). Three curves are depicted, for three values of cycles (c). S^* has been normalized with its maximum (S^*_{max}) in order to plot all the curves in the same axis. The conversion probability that maximizes each curve ($\widetilde{q}$) is: $\widetilde{q} = 0.2059$ ($c = 10$), $\widetilde{q} = 0.0402$ ($c = 30$), $\widetilde{q} = 0.0223$ ($c = 50$). (B) Optimal conversion probability, $\widetilde{q}$, versus the final cycle, c. Other parameter values: $n = 10^4$, $m = 5$, $l = 10$ and $R = 10$.

We explore the number of mature sexual parasites after a certain number of cycles for the different values of conversion probability, according to the Eq. (6.6) (Fig. 6.7). Figure 6.7A reveals that the amount of mature sexual parasites, S^*, exhibits an optimal behaviour with the conversion probability, q. Furthermore, the conversion probability that optimizes the number of mature sexual cells gets smaller as the number of cycles increases (Fig. 6.7B).

This result can be understood as follows: the optimal behaviour of the mature sexual parasites lies in the trade-off between the two extreme conversion probability values. For very low values of conversion probability, only a small proportion of asexual parasites becomes sexual and therefore there is small number of sexual parasites. But, in contrast, if the probability of conversion is high, we reduce the population of the asexual parasites that are, in fact, the responsible of the proliferation. This second consideration becomes more relevant for

long-term situations (i.e. large number of cycles) and so, these situations are optimized by lower probability values.

Notice from Fig. 6.7B that low values of conversion probability optimize the sexual parasite production for a very wide range of cycles. This values of q coincides with the low conversion probabilities found experimentally (Eichner et al., 2001).

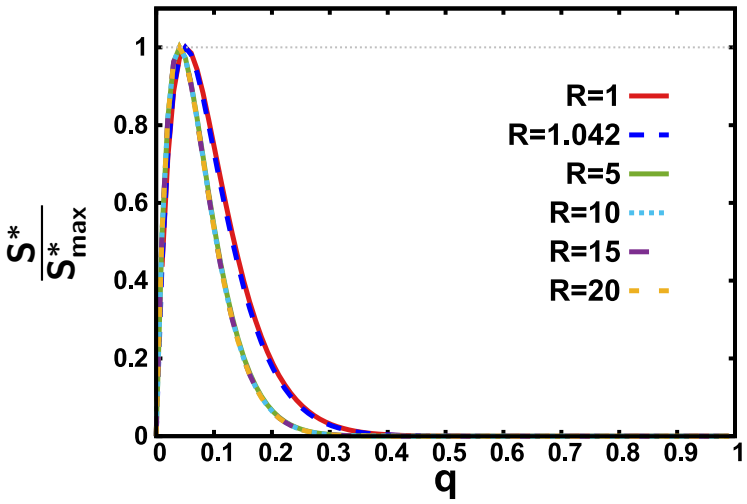

Figure 6.8 Optimal conversion probability value ($\widetilde{q}$) does not significantly depend on the proliferation, R. Mature sexual parasites (S^*) for different conversion probability (q). Six curves are depicted, for six values of proliferation (R). S^* has been normalized with its maximum (S^*_{max}) in order to plot all the curves in the same axis. The conversion probabilities that maximize each curve ($\widetilde{q}$) are: $\widetilde{q} = 0.0513$ ($R = 1$), $\widetilde{q} = 0.0503$ ($R = 1.042$), $\widetilde{q} = 0.0404$ ($R = 5$), $\widetilde{q} = 0.0402$ ($R = 10$), $\widetilde{q} = 0.0401$ ($R = 15$), $\widetilde{q} = 0.0401$ ($R = 20$). Other parameter values: $n = 10^4$, $m = 5$, $l = 10$ and $c = 30$.

Figure 6.8 shows how the optimal conversion probability does not significantly depend on the value of the proliferation, R. For all the values of proliferation explored, the optimal probability is between 0.051 and 0.04. Figure 6.8 displays the curves for two very low values of proliferation, $R = 1$ and $R = 1.042$, whose curves are slightly different to those of other proliferation values analysed. For $R = 1$, the parasite dynamics is in a decay regime for $q > 0$ (Fig. 6.6B). $R = 1.042$ has been chosen as an example in which the asexual parasite number, A, remains constant for $q = 0.04$ (compatible with the range of optimal conversion probabilities found). These low values of R are typically found in chronic stages

of the disease, where the parasitemia remains roughly constant. In contrast, values such as $R = 10$ drive the exponential growth of the initial phase of malaria.

6.5.3 Dispersion in parameters of the dynamics

Previous results have been generated through an analytical interpretation of the model (Eqs. (6.4) and (6.6)). In this interpretation, decision probabilities are implemented as ratios of population. Nevertheless, the probabilistic decision can also be simulated by a random number generator as Section 6.3 describes.

Numerical simulations can give rise to phenomena with low frequency such as parasite catastrophe. Taking into account that the production of asexual and sexual parasites depends on the population of asexual parasites, if parasite population goes to zero, it can not be restored. We call this as the *catastrophe situation*, and its probability is described by the following expression,

$$P_c(n, q, R) = \sum_{i=1}^{\infty} q^{A(i-1)} = \sum_{i=1}^{\infty} q^{n(R(1-q))^{i-1}}, \tag{6.7}$$

where i is the cycle. The probability of catastrophe at each cycle tends to zero for a realistic set of parameter values, (e.g. $q = 0.05$, $R = 10$, $n = 10^4$).

This numerical description also allows us to implement parasite-parasite variability in some parameters: R, m and l.

We have simulated the final mature sexual cells after 30 cycles for three different proliferation distributions that average the same value in Fig. 6.9. Every cycle, each asexual parasite proliferates with one value according to the distribution of probabilities (Fig. 6.9). For these three proliferation distributions, there are no significant differences neither between them nor with the curve calculated by Eq. (6.6).

Dispersion in maturation time and lifespan values follows a distribution according to the expression (6.1) (Fig. 6.10). Figure 6.10 reveals that dispersion in maturation time and lifespan values does not affect the number of the mature sexual cells.

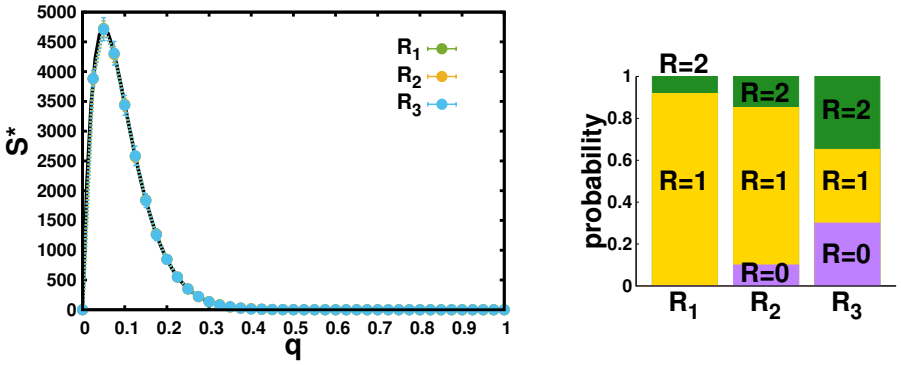

Figure 6.9 Numerical simulations with proliferation dispersion. (left) Mature sexual parasites (S^*) for different conversion probability values ($\boldsymbol{q}$) (left). Three curves, each for a different proliferation distribution (R_1, R_2, R_3, right panel) are depicted. All the proliferation distributions average the same value, $\langle R \rangle = 1.042$. The points correspond to averages over 100 repetitions, while lines are guides to the eye. Black line corresponds to the analytical curve calculated with Eq. (6.6). Other parameter values: $n = 10^4$, $m = 5$, $l = 10$ and $c = 30$. (right) Proliferation distributions as bar diagrams.

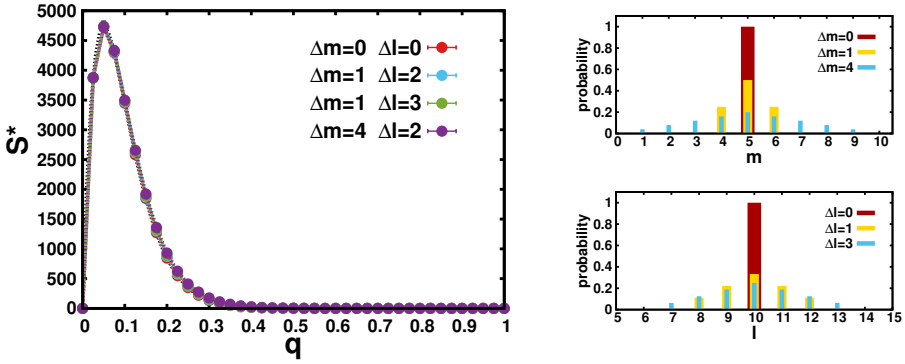

Figure 6.10 Numerical simulations with maturation time and lifespan dispersion. (left) Mature sexual parasites (S^*) for different conversion probability values ($\boldsymbol{q}$). Four curves, each for a different combination of maturation time and life span distributions (right panel). The points correspond to averages over 100 repetitions, while lines are guides to the eye. Black line corresponds to the analytical curve calculated with Eq. (6.6). Other parameter values: $n = 10^4$, $\langle m \rangle = 5$, $\langle l \rangle = 10$, $R_1 = 1.042$ and $c = 30$. (right) Distribution of maturation times (top) and lifespan distribution (bottom). These distributions are calculated through expression (6.1).

Results generated by this numerical interpretation of the model (see Figs. 6.9-6.10) are coherent with those produced by the analytical interpretation. The amount of parasites involved in the simulations is enough to describe the system with the Eqs. (6.4) and (6.6).

6.5.4 Malaria transmission for constant proliferation rates

We saw that, according to the two interpretations (numerical and analytical) of the model, low values of conversion probability (q) optimize the production of mature sexual parasite. In other words, the transmissible form of the parasite is favoured by high probability values of remaining asexual.

Despite the fact that mature sexual parasites (gametocytes) are required to infect a mosquito, the relationship between the gametocytes density in the bloodstream and the probability of infect a new mosquito is not linear (Churcher et al., 2013; Bousema et al., 2006; Schneider et al., 2007; Ouedraogo et al., 2009). According to recent experiments, the probability of infecting a mosquito saturates for a certain density of gametocytes in blood (Churcher et al., 2013).

Taking into account the hypotheses that the malaria parasite that is found nowadays is the one that has evolved to optimizes its host-to-host transmission (natural selection), we focus on this transmission variable instead of the gametocyte density in the bloodstream. These two variables – transmission and gametocyte density in blood – are related by a function such as those of the expression (6.3).

Figure 6.11 and 6.12 show both the transmission probability (T) and the mature sexual parasites (S^*) at each cycle for a constant value of proliferation.

Transmission diagram with a high proliferation that represents a malaria infection in the exponential growth phase ($R = 10$) reveals that there is a wide range of conversion probabilities that drive an equivalent parasite transmission (Fig. 6.11A). Significant differences between the amount of mature sexual parasites (6.11B) are screened by the saturation behaviour of the transmission probability function (Eq. (6.3)).

Malaria disease in a chronic phase is characterized by low proliferation values of merozoites. Figure 6.12 shows that the probability of transmission of all the

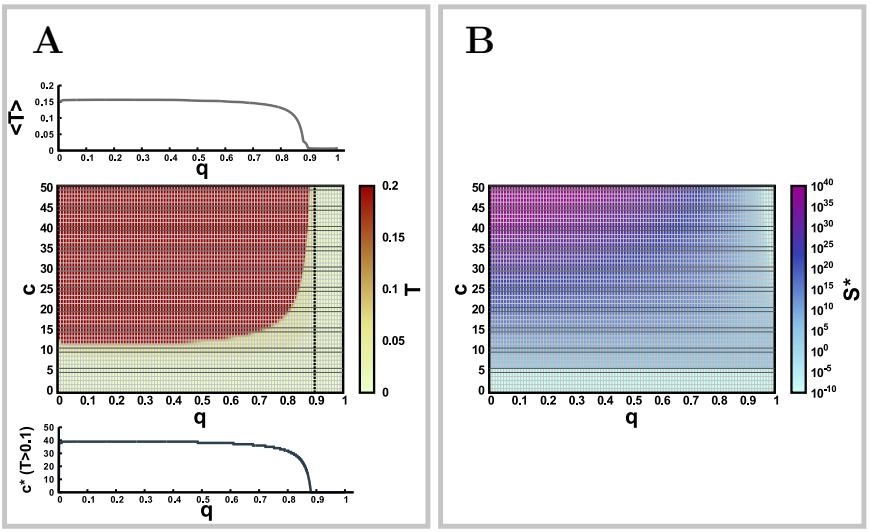

Figure 6.11 Malaria transmission by a constant proliferation rate of the exponential growth phase. (A) Average of the transmission probability (T) along 50 cycles ($\langle T \rangle$) (top). Transmission probability, T, at each cycle, c, for every conversion probability value, q (heatmap, middle). Dashed line corresponds to $q = (1 - R^{-1})$, which is the threshold of the conversion probability that determinates if the parasite population grows or decays. Number of cycles (c^*), of a total of 50, that exhibit a transmission probability of $T > 0.1$ (bottom). (B) Number of mature sexual parasites, S^*, at each cycle, c, for every conversion probability value, q (heatmap). Other parameter values: $n = 10^4$, $m = 5$, $l = 10$, $R = 10$.

cycles explored is negligible for a low proliferation rate ($R = 1.042$). Such low values of proliferation keeps the parasite population roughly constant (for low conversion probability values). So, the parasite requires a previous phase of exponential growth to reach a transmissible values of gametocyte density that will be kept during the chronic phase.

Consequently, constant proliferation rates do not select an optimal conversion probability, neither for low nor high proliferation values.

6.5.5 Malaria transmission for a proliferation that decays over time

In a normal malaria infection, once the parasites are released to the bloodstream from the liver, they grow exponentially due to a high proliferation. Each free

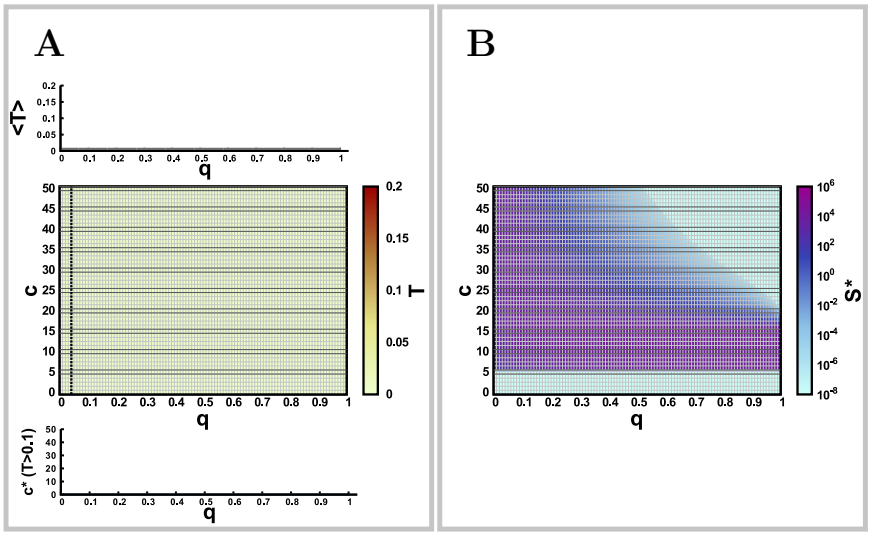

Figure 6.12 Malaria transmission by a constant proliferation rate of the chronic phase. (A) Average of the transmission probability (T) along 50 cycles ($\langle T \rangle$) (top). Transmission probability, T, at each cycle, c, for every conversion probability value, q (heatmap, middle). Dashed line corresponds to $q = 1 - R^{-1}$, which is the threshold of the conversion probability that determinates if the parasite population grows and the decays (see Section 6.5.1). Number of cycles (c^*), of a total of 50, that exhibit a transmission probability of $T > 0.1$ (bottom). (B) Number of mature sexual parasites, S^*, at each cycle, c, for every conversion probability value, q (heatmap). Other parameter values: $n = 10^4$, $m = 5$, $l = 10$, $R = 1.042$.

asexual parasite can give rise up around 20 parasites inside a RBC and, once these are released, around 10 of these parasites will infect a new RBC (Eichner et al., 2001).

The fast parasitemia growth during the first malaria infection stage can provoke the death of the host if his immune system does not respond fast enough. However, the effective proliferation rate decays after some cycles due to both the resources reduction – available RBC – and the immune system response. This proliferation reduction gives way to the host recovery or the chronic stage of the disease. This chronic stage – that can last up to some months – is characterized by a long period where the parasitemia remains roughly constant (Stone et al., 2015).

We have modelled these different stages of the malaria through a proliferation rate that evolves as an exponential decay function (Expression (6.8) and Fig.

6.13). The system spends the first cycles (c_m) with R_0 proliferation rate and then, it decays exponentially – with λ exponential decay parameter – until R_f proliferation rate ($R_f < R_0$).

$$R(c) = \begin{cases} R_0 & \text{if} \quad c < c_m \\ (R_0 - R_f)e^{-\lambda(c-c_m)} + R_f & \text{if} \quad c \geq c_m \end{cases} \tag{6.8}$$

Results of Fig. 6.13 show that, for a decreasing proliferation, the transmission is favoured for low conversion probability values such as those observed in nature (Eichner et al., 2001). Furthermore, the number of infectious cycles decreases as the decay constant increases. Hence, a faster response of the immune system of the host shortens the infection of the host, as it is expected.

Summarizing, the low conversion probability values observed in malaria infections increase the number of cycles at which the parasite can be transmitted to a mosquito. So, malaria parasite would have been selected by the pressure of the evolution in order to exhibit these low conversion probabilities to increase the chance of completing its life cycle and avoiding its death due to either the host death or the host recovery.

6.6 Discussion

The decision of remaining in the asexual cycles or becoming sexually-committed in malaria blood stage is a good example of cell autonomous decision making. Each parasite chooses its fate regardless of the other parasites choice. This decision is driven by a stochastic mechanism (Kafsack et al., 2014). The ratio between the parasites in the asexual form and in the sexual form is rather fixed and controlled by this stochastic mechanism. This population ratio – determined by the decision probability – has pressumably evolved to optimize the adaptation and survival of the parasite.

We implemented a stochastic model for parasite dynamics with two interpretations: a numerical interpretation, and an analytical one. The results revealed that the sexual parasite population is maximum for low conversion probability values, such as those observed in nature (Eichner et al., 2001). However, due to the saturation profile of the transmission function, transmission rates are similar

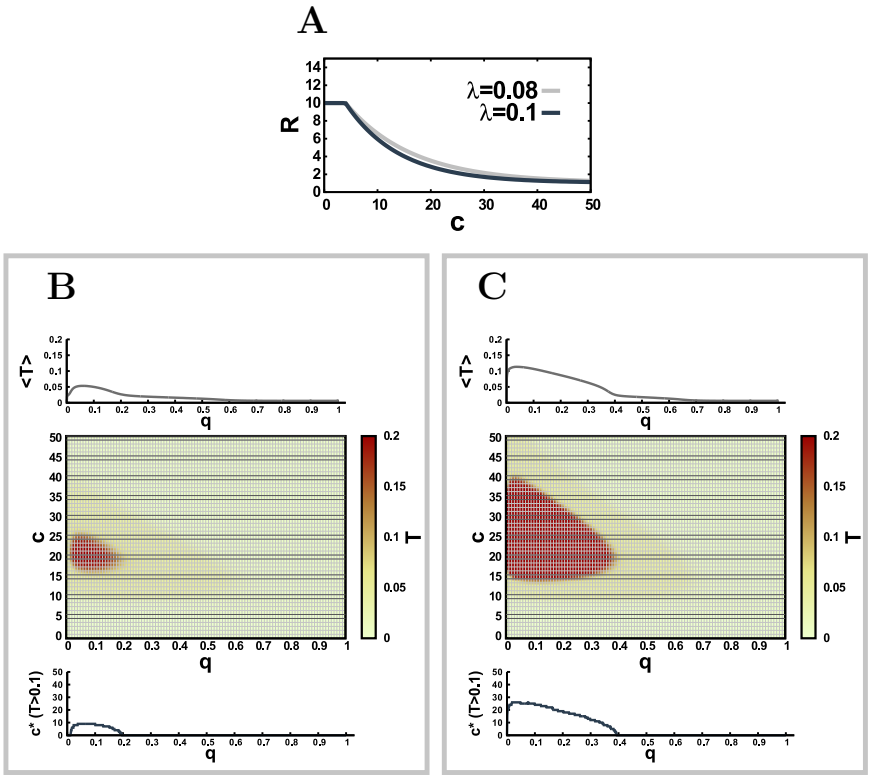

Figure 6.13 Malaria transmission by a proliferation rate that decays over time. (A) Proliferation rate evolving as an exponential decay. There are depicted two values of exponential decay constant: $\lambda = 0.1$ (dashed line) and $\lambda = 0.08$ (solid line). Other parameters: $c_m = 4$, $R_0 = 10$ and $R_f = 1.042$. (B) Average of the transmission probability (T) along 50 cycles with a proliferation rate that decays with $\lambda = 0.1$ ($\langle T \rangle$) (top). Transmission probability, T, at each cycle, c, for every conversion probability value, q (heatmap, middle). Number of cycles (c^*), of a total of 50, that exhibit a transmission probability of $T > 0.1$ (bottom). (C) Average of the transmission probability (T) along 50 cycles with a proliferation rate that decays with $\lambda = 0.08$ ($\langle T \rangle$) (top). Transmission probability, T, at each cycle, c, for every conversion probability value, q (heatmap, middle). Number of cycles (c^*), of a total of 50, that exhibit a transmission probability of $T > 0.1$ (bottom). Other parameter values: $n = 10^4$, $m = 5$, $l = 10$, $c_m = 4$, $R_0 = 10$ and $R_f = 1.042$.

for a very wide range of conversion probabilities. This range becomes strongly reduced, involving low conversion probabilities only, when the proliferation rate decays over time. This exponential decay can be explained by the action of the immune system, that brings the infection to a chronic phase that gives place, eventually, to the host recovery.

The model, despite its simplicity, explains a benefit of low conversion rates, and suggests a scenario of evolution of malaria parasite, that has developed an accurate strategy of adaptation during thousands of years of evolution. However, several factors of the parasite dynamics can be taken into account in order to check and refine the model.

The decay in proliferation is mainly caused by the effect of the immune system. This decay could be modelled by a parasite-population-dependent function, that decreases with the amount of asexual parasites (A) – instead of with the cycle number (c). This relationship between the proliferation rate and the number of asexual parasites could be described by a function that decreases and saturates for a certain population value. The immune system could respond more aggressively as the number of parasites gets higher. Also a delay between the presence of the parasite in the bloodstream and the response of the immune system can be included in the model. These considerations a priori do not favour the low conversion rates of the decision, because these rate values give rise to higher values of asexual parasites. However, the dynamics of the immune system is very complex. For instance, the strategy of the parasite consists in expressing one of up to 60 antigenic molecules on the infected RBC membrane. Each parasite can stochastically change of antigenic variation in order to evade the specific immune response (Recker et al., 2011; Coleman et al., 2014).

Other theoretical studies point to the competence between different parasite varieties in a multiple infection scenario as the explanation to the low conversion rate values (McKenzie and Bossert, 1998, 2005; Mideo and Day, 2008). De Moraes et al. (2014) found a reason by which multiple infections are so frequent. The study reveals that the parasite modifies the host odours in order to attract the mosquitoes. This mechanism not only enhances the parasite transmission, but also favours multiple infections, as a side effect. However, regardless of this hypothesis, our study revealed for first time that multiple infections are not required to explain the advantages of low values of conversion

rates. Only a proliferation decay over time - which is reasonable due to immune system effect - is sufficient to explain these low values.

Some aspects of the parasite dynamics are still unknown and a further study is required. Besides the difficulty of this system, that interacts with such a complex system as the immune system, we also have problems in collecting experimental data from infected humans. Despite the fact that some variants of the parasite infect other organisms, such as rodents, the differences between these variants and *P. falciparum* are relevant enough to not extrapolate their results to the human variety.

Part III

SUMMARY OF RESULTS AND OUTLOOK

Chapter 7

Conclusions

In this chapter we summarize the main conclusions of the results presented in the previous chapters and the perspectives these results open. The specific discussion of these results can be found in the last section of each chapter.

In this thesis we addressed the study of the dynamics of decision making from different points of view. On the one hand, we evaluated different theoretical scenarios of decision making processes. These studies focused on well-known types of interactions (or circuit architectures) taking place in cells but not on a specific biological process. We evaluated both cell-autonomous decisions, where each cell decides its fate regardless of the choice of other cells, and non-cell-autonomous decisions in which cells of a tissue that interact collectively choose between different spatial patterns. In this last case, we focused on the dynamics of cell-interactions mediated by Notch signaling pathway. For these theoretical scenarios, we have characterized cellular decision processes not only by the different responses that the system is able to perform, but also by the probability of selecting each choice. Our analysis focused on how the final selection depends on the dynamical mechanism that induces the decision. In the last chapter of this thesis, we focused on a specific biological context and decision: the decision to become sexual that takes place during the life cycle of the parasite that causes malaria in humans. In this case, we have not studied the mechanism that controls the probabilities involved in the decision, but the impact that the probability values have on the functionality of the system.

There are four common ingredients in our studies on theoretical scenarios for decision making. The first one is multistability. Considering that a decision making is a process in which a system responds differently to the same stimuli and under the same conditions, more than one stable solution available to the system is required. These solutions can be either cell states or tissue patterns. The second common ingredient is that this multistability is generated by non-linear interactions between two elements that conform the network motif known as toggle switch with auto-activation. These interactions determine which and how many solutions are available to the system. The third ingredient is that we interpreted the inducers of the cellular decisions as signals that change some parameters of the system dynamics. By changing these parameters, the phase space and attractors of the system also change. We showed that the dynamical description of the system during the signal effect helps to understand the final selection of the system. We analysed the phase spaces, the parameter spaces and the time scales involved in the selection of the different system fates. Finally, the fourth ingredient in common is the presence of intrinsic stochasticity in the dynamics. Since a cellular decision selects different cell/tissue states under the same signal, stochasticity is a very relevant ingredient. This stochasticity is considered to arise from low copy numbers of the species involved in cellular reactions and thermal fluctuations. Cells make their decisions in such a fluctuating environment.

Finally, as indicated, we studied a particular example of cell-autonomous decision making that is involved in the transmission of malaria disease. Malaria host-to-host propagation depends on a stochastic parasite decision that takes place in the bloodstream of the infected human. We proposed an explanation to the strategy that the parasite performs in order to optimize its transmission. Despite the importance of its propagation, the probability that the parasite adopts its transmissible form is very low. We showed that, counter-intuitively, low probability values of becoming transmissible maximize the time during which the host remains infectious when the proliferation rate of the parasite decays over time (e.g. due to the immune response of the host).

7.1 Cell-autonomous decision making

We studied cellular decision making of cell populations where each cell decides regardless the choices of the other cells. Results revealed that the dynamical behaviour generated by the signal that induces the decision determines its properties. Some examples of these features are: the time at which the decision takes place, the role of stochasticity on the decision, the existence of one or several precursor states, the memory conferred to previous decisions and the capability to integrate over time or show optimal behaviours. We studied two elemental decisions in order to characterize the interplay between the dynamics of the inductor mechanisms and the properties of these decisions. These features can be understood from the phase space changes directed by the signal and by taking into account that dynamics are stochastic.

The cell-autonomous decisions we studied are driven by transient step-like function signals that are described by three components: (1) the type of phase change the signal drives, (2) the *signal strength* which controls the asymmetry of phase space generated by the signal, and the (3) *signal duration* which determines the time during which the signal generates this new (and constant during the action of the signal) dynamical scenario. This type of signal characterization was previously used by other authors (Guantes and Poyatos, 2008). Other authors have also addressed more complex signals in which a single parameter controls both the asymmetry and duration (Nené et al., 2012).

We defined the state of cells in terms of the state of two variables interacting through the network motif toggle switch with auto-activation. A phenomenological stochastic model, based on the deterministic dynamics by (Guantes and Poyatos, 2008), was used, and a potential scenario of it in terms of molecular reactions was discussed at the light of the adiabatic approximation.

We started the study of cell-autonomous decision making with a simple decision where each cell of an homogeneous population, upon the action of a transient signal, has the chance to change of state. We showed that this decision can be driven by two types of signals that differ in the stability regime generated during their effect. We called these signals *monostable* and *multistable*, and we keep this nomenclature in this section. Monostable signals reduce all the attractors of the initial stability regime (three stable states, in our study) to a single one. So, the transition between states and thereby the decision involves a bifurcation

(pitchfork). The second signal type (multistable signals) does not modify the number of attractors, but reduces the stochastic stability of the precursor state enabling stochastic transitions from it to a new state.

Our study focused on how the probability of the decision, measured in terms of frequencies of transition to the new state, depends on the dynamical mechanism that induces it, and hence on these two types of signals. We showed that for both types of signals this probability can behave rather similarly, with threshold-like behaviours, to changes in the signal strength. Hence, by measuring ratios of cell populations and by applying modifications of the signal strength we would be unable to unravel which dynamical mechanism is taking place in the decision. The dynamical mechanism is revealed and becomes relevant when populations of cells in one state are removed. The dynamical mechanism also settles down when the decision takes place: right after the signal disappears and at the same time for all the population (monostable signals) or at different times for each cell while the signal acts (multistable signals).

We also showed that the probability of the decision can show a non monotonic behaviour with the duration of the signal, such that the maximal probability can occur for intermediate time signal durations. This can happen only for monostable signals. In addition, this maximal probability can be ≤ 1. This provides a mechanism for ensuring two cell states in the population, whatever the duration of the signal. This mechanism can be an interesting strategy to be used by cells for which it is advantageous to live within heterogeneous cell populations.

As expected, fluctuations – determined by the effective volume of the system – affect differently the probability threshold for these two types of transient signals. Noise enables and facilitates changes of state in multistable signals by reducing the stability of the initial state against fluctuations. In contrast, fluctuations smooth the relationship between the probability of changing of state and the signal strength of monostable signals, while the threshold at which there is a 50% chance to change does not vary.

The decision that results from several signals also exhibits different properties according to the dynamical mechanism of these signals. Due to the asymmetry of the stochastic switching of the multistable signals, the resultant decision integrates the differentiation induced by each of these signals. By contrast,

the total final population that has changed of state only depends on the last monostable signal when several of these signals are applied. This result arises from the fact that monostable signals erase the cell state induced by previous decisions, enabling any cell state to be precursor of the other one. In contrast, multistable signals lock the state of one cell population, which could be viewed as a committed or differentiated state. The number of attractors and their basins of attraction during the signal effect explain this different behaviour in front of multiple signals.

Based on these results, we may propose that monostable signals fit better our understanding of cellular decision making in bacteria, were cell state changes are reversible and where ensuring heterogeneous populations of cells in different states are relevant strategies for survival. In contrast, multistable signals could be more associated to developmental processes in which irreversibility is present.

We have also studied a decision type that involves three different cell states. In this decision, each cell of an homogeneous population chooses between three cell fates: the precursor state, and two new differentiated states. This decision is produced by a signal that generates a bistable regime: the attractor of the precursor state disappears and each attractor of the stability regime generated by the signal corresponds to one differentiated state. The value of the attractors and their basins is controlled by the strength of the signal. The signal duration determines the transient time during which the signal is acting.

We described the decision by two choices: the *Differentiation choice*, that expresses the final population of cells that has chosen one of the two differentiated states; and the *Asymmetric choice*, that describes the ratio of cells that has selected a certain differentiated state over all the differentiated population. We use the term differentiated population since if the cells of the precursor state are removed from an heterogeneous population generated by a first bistable signal, a second bistable signal can not restore the missed cell type. Hence, only one cell state acts as a precursor cell type.

We showed that these choices are controlled very differently and as a result are made at different times, being first made the asymmetric choice. The differentiation ratio is determined, mainly, by the signal duration, while the asymmetric ratio is controlled by the signal strength. In both cases, the relationship between the ratio and the associated signal parameter exhibits a threshold-like

behaviour. In addition, the asymmetric choice is significantly more dependent on fluctuations. Noise affects this ratio by increasing the heterogeneity of the final differentiated population. In other words, noise tends to equalise the population of both differentiated states.

If multiple signals of identical signal strength are applied to an homogeneous population, the total differentiated population integrates the effect of each individual signal but keeps fixed the proportions, within it, of subpopulations in each differentiated state. If the signals that take place differ in the signal strength, the first signal is the one that determines the final asymmetric ratio in a higher degree.

Together, these results show that the two choices involved in this cellular decision making process can be well decoupled, both in time and in their regulation. This may provide potential ways to flexibly modulate each of them.

7.2 Pattern selection

We have studied a decision where a cell tissue chooses between different spatial patterns. These patterns are described by the spatial distribution of different cell types. We defined this problem as pattern selection. The inducer of the decision are signals that are defined as parameter changes. According to how parameters change over time and space, the probability of selecting each pattern after the decision varies (Palau-Ortin et al., 2015).

We focused the study on the type of cell communication mediated by Notch signaling pathway. The communication occurs between adjacent cells. Each cell inhibits the production of the state variable of the neighbouring cells in a so-called lateral inhibition system. Besides, each cell self-activates the production of its own state variable, describing a toggle switch motif with positive auto-regulation. Herein, the two variables involved in this motif are the concentration of the cell and the concentration of the neighbour.

It has been proved in previous studies that these interactions give rise to multiple pattern solutions when the dynamics are deterministic (Formosa-Jordan and Ibañes, 2014). Three of them are: the homogeneous (where all the cells

are identical), the *salt-and-pepper* (where cells of one type are completely surrounded by cells of a second type), and the stripes solution (where rows of two different cell types are alternated). Which of these three patterns is stable depends on the values of the parameters that define the interactions of the system (Formosa-Jordan and Ibañes, 2014). We evaluated the stability of these solutions to large perturbations of the state. We also analysed the stability of these different patterns in front of different levels of intrinsic noise.

We tackled the problem of which signals enable to select one pattern solution and not another one and with what probability (Palau-Ortin et al., 2015). These signals change the value of two parameters related with the interaction inside the cell (cis interaction) and the lateral inhibition between neighbouring cells (trans interaction). Three main scenarios were built: A first scenario where the parameter change affects all the cells of the tissue at the same time (global path); a second scenario where only a subset of cells change their parameters over time (local path); and a third scenario where the parameters do not only change over the time, but also across the space (spatio-temporal path).

The first scenario sets a mechanism by which a certain pattern solution arises in all the tissue at the same time. Results of this scenario confirmed that to select a pattern distinct from the initial one, it is required a destabilization of the initial solution. This can be achieved by the transient exploration of regions in the parameter space where the initial solution is not stable and the final pattern solution is stable. These results are in agreement with what we know from cell-autonomous decision making (Huang et al., 2007; Guantes and Poyatos, 2008; Nené et al., 2012). As for these decisions, the probability of selecting a new pattern solution depends on the time during which the initial solution is being destabilized as a threshold-like function.

In the second scenario we studied the selection driven by signals that only act in a small cluster of cells. This signals are able to select a new pattern if it is stable and able to invade the initial one. The selection of the new pattern takes place in a small region and spontaneously propagate to cover the whole tissue. If the cluster of cells visits the new pattern solution during the signal effect, the new solution is able to nucleate there and propagate. Our results revealed that, a tissue initially at an homogeneous solution can select another solution if the cluster of cells transiently takes the value of another homogeneous solution (with different concentration value). In this case, the new pattern arises in the

cells of the tissue that are in contact with the cells of the cluster by a boundary effect that drives a large perturbation of the initial state. The selection studied in this scenario depends on the cluster size and it depends on this size differently in both cases exposed.

The third scenario exemplifies how a certain pattern solution can be induced progressively over time and space by a signal (induced propagation). This spatio-temporal signals are able to select pattern solutions that can not be spontaneously selected. We showed that the stripe pattern can be selected by parameter changes that evolve according to a propagating front. Furthermore, the velocity of this front affects the probability of selecting this less spontaneous pattern. Our results revealed that there is an optimal range of velocity of propagation that optimizes the probability of selection of the stripe pattern.

7.3 Malaria parasite strategy for host-to-host transmission

Finally, we have characterized a particular example of cellular decision making that takes place in the life cycle of the parasite that causes the malaria disease. Malaria is a disease that affects humans and requires mosquitoes to act as a vector to propagate the infection from an infected human to another. Hence, the transmission from a human host to a mosquito is a crucial step in the parasite survival. In this step, the transmissible form of the parasite is called *gametocyte* and corresponds to a sexual form of the parasite arising stochastically from an asexual form (*merozoite*) in the bloodstream of the human (Kafsack et al., 2014). The parasite, in the asexual form, highly proliferates. The probability of becoming a gametocyte (conversion rate) takes very low values that are counter-intuitive considering the high importance of the parasite transmission for its own survival.

We have made a discrete-time stochastic model that describes the dynamics of the merozoite and gametocyte populations. The unit of time has been chosen one proliferation cycle. The model confirmed that low conversion rates maximize the number of gametocytes after many number of cycles. We have shown that this result does not depend on the dispersion of some parameters involved

in the dynamics (proliferation rate, maturation time, lifespan), nor strongly on the proliferation rate.

Despite the fact that the transmission probability (from human host to mosquito) depends on the amount of gametocytes in human blood, this relationship saturates at certain gametocytes density value (Churcher et al., 2013). We also evaluated the number of cycles at which the human host is infectious. Our model revealed that, if the proliferation rate decays over time (as a consequence of the immune system response), low conversion rates maximize the number of cycles at which the human host remains infectious.

Previous theoretical works pointed as the competence in multiple infections as the justification of low conversion rates. However, our study does not require this ingredient to explain why the parasite has evolutionary selected this conversion values. According to our model, this values maximizes the infectivity of the human host in a proliferation rate decay scenario.

7.4 Future perspectives

In this thesis we have presented two mechanisms that, although both drive the same cell-autonomous decision, this decision behaves differently according to the mechanism that induces it. Our results suggest observables and experiments that could be performed in biological decisions to unveil the dynamical mechanism that induces them. They also reveal how different properties of the cell population can be controlled by signals. This cross-communication between the theory and the experimental data could help us to built a complete idea about the correlation between the general mechanism that induces a decision and the features of this decision.

We focused our work of cell-autonomous decisions in signals that affect the cells transiently. We can extend this study to other signals such as permanent signals with a continuous profile or fluctuating signals that may model a fluctuating environment. Also other genetic circuits can be analysed to explore if the features of these mechanisms do not depend on the genetic circuit. Finally, since many cellular decision making processes take place in proliferating cells, the dynamics of cell growth and cell division could be taken into account.

We have described a cell-autonomous decision that involves three cell types. Our work sets how the different signal parameters control the different choices involved in this decision. We may also study different mechanisms that induce the same decision such as a stochastic switching mechanism. Also decisions with more cell types involved could be characterized from the same point of view.

We extended the problem of cellular decision making to non-autonomous decisions. Taking into account that our work poses general mechanisms, we could connect this theoretical results to what can be found experimentally. Our model takes into account interactions between first neighbouring cells. However, we could also consider longer cell-to-cell communication (e.g., due to filopodia). In this scenario, the number of pattern solutions may increase and, consequently, the problem of selecting a certain solution by a signal could be more challenging.

In the last chapter of the thesis, we have showed that the strategy of the parasite that causes malaria can be explained by considering a proliferation rate that decays over time. We could extend our model in different directions. We can include a dependency between the proliferation rate and the number of parasites. This consideration would include the response of the immune system as a function that increases with the amount parasites in the bloodstream. On the other hand, it is well known that the parasite evades the immune system by changing the antigenic varieties that expresses while it is inside a red blood cell. The switching between the different antigenic varieties can be included in the model as it is a relevant strategy of its survival. Finally, since previous studies have pointed the competition in a multiple infection scenario as the main reason for the strategy of the parasite transmission, this scenario may be also considered in our model.

Appendix A

Thesis summary (in Catalan)

A.1 Introducció

En aquesta tesi abordem el concepte de *presa de decisions cel·lulars* des d'una perspectiva teòrica. Dins del marc de la Biologia de Sistemes (Alon, 2007b), pretenem dilucidar quins mecanismes generals estan implicats en la presa decisions cel·lulars i com les propietats són afectades per la dinàmica d'aquests mecanismes.

Les cèl·lules, ja sigui com a organismes unicel·lulars, o bé formant part de d'organismes multicel·lulars, han de realitzar diverses funcions (v.g. sintetitzar cert enzim, dividir-se o diferenciar-se en cert tipus de cèl·lula) que, tot sovint, venen determinades pels estímuls o les condicions de l'entorn que perceben (Alberts et al., 2008). En aquest marc, podem definir com a "presa de decisions cel·lulars" aquells processos mitjançant el quals les cèl·lules escullen una resposta en un escenari en el que diverses d'aquestes en són potencialment accessibles (Losick and Desplan, 2008; Balazsi et al., 2011). D'aquesta manera, l'opció escollida per la cèl·lula es governada per un mecanisme probabilístic. Cal diferenciar aquests processos d'aquelles que, produint també una canvi de comportament en la cèl·lula, ho fan de manera unívoca davant d'una condició de l'entorn o d'un estímul concret. Considerant que aquests canvis cel·lulars no

generen una varietat de respostes, no podem parlar estrictament d'ells com el producte d'una decisió cel·lular.

Aquests règims de funcions desenvolupades per una cèl·lula, i que canvien d'acord amb el seu entorn, podem ser definits com a *estats cel·lulars*. D'aquesta manera, una decisió cel·lular descriu el canvi d'estat d'una cèl·lula cap a un altre entre diversos de possibles. Tenint en compte que les proteïnes són les encarregades de desenvolupar la majoria de funcions de les cèl·lules, i que la síntesis d'aquestes ve determinada per l'expressió genètica (Alberts et al., 2008), els estats cel·lulars poden ser alternativament identificats pels perfils d'expressió d'una cèl·lula.

En tota cèl·lula, la síntesi de cada proteïna ve determinat per la regulació del gen que codifica aquesta proteïna. Entre diversos elements que poden estar implicats en aquesta regulació, hi trobem els factors de transcripció. Els factors de transcripció són proteïnes que, individualment o en forma de complex, interactuen amb la lectura de la informació genètica i en regulen la seva expressió, ja sigui promovent-la (activant) o bloquejant-la (inhibint). D'aquesta manera, el perfil d'expressió d'una cèl·lula ve controlat per complexes xarxes d'interaccions. Anàlisis topològics d'aquestes xarxes genètiques han revelat l'existència de circuits genètics amb arquitectures recurrents. Cadascuna d'aquestes arquitectures s'anomenen *motius de xarxa*, i el seu aïllament i estudi pot ser fonamental per a entendre el comportament d'alguns processos biològics (Alon, 2007b). En aquesta tesi hem aprofundit en la modelització d'un exemple de motius de xarxa (Capítol 2). Aquest circuit genètic descriu dos gens que interactuen inhibint-se mútuament (inhibició mútua) i que en promouen la seva pròpia expressió (auto-activació).

Una de les propietats emergents que ha estat caracteritzades en diversos motius de xarxa n'és la *multiestabilitat*. El principal origen d'aquesta rau en la no-linealitat de interaccions que s'esdevenen entre els diferents elements del circuit genètic. Donat que en una decisió cel·lular es plantegen més d'una resposta, la multiestabilitat és un dels principals ingredients per a entendre aquests processos.

A més de la multiestabiltat, les decisions cel·lulars requereixen d'un mecanisme probabilístic que les doti de la capacitat d'escollir entre aquestes diverses respostes davant d'un mateix escenari. La font d'aquesta estocasticitat és la

naturalesa discreta de les reaccions moleculars i les fluctuacions tèrmiques de l'entorn en el que aquestes tenen lloc (Elowitz et al., 2002).

La metodologia utilitzada per a l'elaboració d'aquesta Tesi s'ubica dins del marc de la Dinàmica de Sistemes (Strogatz, 1994), recorrent a conceptes com ara el d'atractor, d'espai de fases o de conca d'atracció, entre d'altres. En el nostre estudi associem els diferents estats cel·lulars implicats en la decisió amb els atractors estables de la dinàmica del sistema. D'acord amb aquesta interpretació, una decisió cel·lular dóna lloc a una transició entre atractors. Un dels mecanismes capaç impulsa-ne aquestes transicions és el d'un canvi transitori o permanent del règim d'estabilitat del sistema (nombre d'atractors i les seves conques d'atracció). Definim com a "senyal" aquell component del sistema que controla de manera dinàmica algun dels paràmetres de la interaccions entre els components d'una cèl·lula. Aquests senyals poden modificar el règim d'estabilitat del sistema i, així, impulsar-ne una decisió (Guantes and Poyatos, 2008; Nené et al., 2012).

Els algoritmes utilitzats per a descriure les dinàmiques temporals dels esdeveniments biològics analitzats en aquesta Tesi responen a descripcions deterministes (Ruge-Kutta de quart ordre) o estocàstiques (Equacions de Langevin, algorisme de Gillespie i cadenes de Markov) (Wilkinson et al., 2006).

En els Capítols 3 i 4 hem estudiat decisions en les que cada cèl·lula escull una estat cel·lular independentment de la tria de la resta de cèl·lules de la població (*decisions cel·lulars autònomes*). També hem estudiat l'escenari en el que la decisió es presa de forma col·lectiva per tota la població o teixit (Capítol 5). Aquestes decisions (*decisions cel·lulars no autònomes*) requereixen de mecanismes de comunicació entre les cèl·lules i estan típicament orientades a la formació de patrons espaial de respostes. Finalment, en el Capítol 6 hem estudiat la repercussió que el caràcter probabilístic d'una decisió concreta pot tenir en la viabilitat d'un organisme. El sistema d'estudi triat ha estat el del paràsit responsable de la malaria en humans.

A.2 Resum dels resultats

En els Capítols 3 i 4 de la Tesi s'ha abordat l'estudi de dues decisions autònomes. Wl Capítol 3 se centra en la caracterització de la decisió simple mitjançant

la qual cada cèl·lula escull entre canviar d'estat o romandre en l'estat inicial (decisió de dos estats). En el Capítol 4 s'estén l'estudi a una decisió en la que hi ha un tercer estat implicat (decisió de tres estats). D'aquesta manera, cada cèl·lula tria entre romandre en l'estat inicial, o canviar d'estat cap a un dels dos de nous.

Hem estudiat aquestes dues decisions autònomes en l'escenari de dos gens que s'auto-activen i que interactuen entre sí d'acord a una inhibició mútua. El mecanisme inductor de la decisió és un senyal transitòria amb un perfil d'esgraó que modifica, transitòriament, el règim d'estabilitat del sistema. Aquest senyal ve descrita per tres components: (1) El nombre d'atractors generats (*estabilitat del senyal*); (2) la asimetría d'aquests atractors (*força del senyal*); i (3) el temps durant el qual es produeix aquest canvi d'atractors (*duració del senyal*). També hem explorat l'efecte de l'aplicació seqüencial de varis senyals.

Els resultats del Capítol 3 ens han mostrat que una decisió cel·lular pot estar estar generada per mecanismes dinàmics diferents, que generin diferents règims d'estabilitat. D'acord amb el mecanisme dinàmic implicat, la dependència de la decisió amb els paràmetres de la senyal pot exhibir comportaments notablement diferents. D'aquesta manera, podem establir una relació entre les propietats de la decisió i la dinàmica que subjuga al mecanisme inductor.

En el Capítol 4 ens hem centrat en una decisió amb tres estats cel·lulars involucrats. Hem dividit la decisió en dues tries: la tria de canviar d'estat en front de mantenir-lo (tria de diferenciar-se); i l'elecció de, un cop una cèl·lula ha decidit abandonar l'estat inicial, escollir un dels nous estats en front l'altre (tria asimètrica). Aquesta caracterització de la senyal ens ha permès observar comportaments clarament diferenciats entre aquestes dues tries que, en conjunt, defineixen la decisió total.

Quan les cèl·lules implicades en una decisió estan dotades de comunicació entre elles, les decisions poden estar lligades a les decisions de les altres cèl·lules de la població (o teixit). En Capítol 5 hem estudiat un sistema on les interaccions entre cèl·lules tenen lloc a primeres veïnes. Cada cèl·lula inhibeix la producció d'una proteína de les seves veïnes (*inhibició lateral*) al mateix temps que n'auto-activa la producció pròpia (auto-activació). Aquest tipus d'interaccions poden donar lloc a diverses distribucions espaials (patrons). En aquesta tesi hem

abordat la qüestió de com una senyal duu al sistema a seleccionar un d'aquests patrons enlloc d'un altre, i amb quina probabilitat.

En aquest context de selecció de patrons, hem estudiat tres tipus de senyals que ens defineixen tres escenaris diferents: un en el que totes les cèl·lules del teixit varien el valor dels seus paràmetres alhora (canvi global); un en el que només un subconjunt de cèl·lules del teixit es veu afectat per la senyal (canvi local); i un tercer escenari en el que el valor dels paràmetres del teixit canvien, no només amb al llarg del temps, sinó que també al llarg del teixit (canvi espaial i temporal). Els tres escenaris ens han revelat com la selecció final del teixit depèn de les característiques de cada senyal en cadascun dels tres escenaris.

Finalment, en el Capítol 6 hem estudiat el cas d'una decisió estocàstica en la que es té coneixement de la seva probabilitat associada (Kafsack et al., 2014). Es tracta d'una decisió que té lloc durant el cicle vital del paràsit responsable de causar la malària en humans. Aquest paràsit utilitza els mosquits com a vector de transmissió entre humans. Precisament durant la fase en la que el paràsit es troba en el torrent sanguini de l'hoste humà, aquest es pot presentar en dues formes: una forma asexual amb la capacitat de proliferar, i una forma sexual (gametòcit) que no prolifera però que és capaç de transmetre's a un nou mosquit (que piqui a l'humà infectat). Cada paràsit en la forma asexual pot decidir diferenciar-se en gametòcit. Tot i que la transmissió de la infecció és un pas crucial per a la propagació i supervivència del paràsit, la probabilitat de convertir-se en gametòcits és molt baixa. El nostre estudi ha mostrat que, en un escenari en el que el ritme de proliferació dels paràsits asexuals decau amb el temps (degut, per exemple, al sistema immunitari), aquests valors baixos de probabilitat de conversió maximitzen el nombre de cicles durant els quals l'hoste humà roman infecciós.

Bibliography

M. Acar, A. Becskei, and A. van Oudenaarden. Enhancement of cellular memory by reducing stochastic transitions. *Nature*, 435(7039):228–232, 2005.

M. Acar, J. T. Mettetal, and A. van Oudenaarden. Stochastic switching as a survival strategy in fluctuating environments. *Nat. Genet.*, 40(4):471–475, 2008.

G. K. Ackers, A. D. Johnson, and M. A. Shea. Quantitative model for gene regulation by lambda phage repressor. *Proc. Natl. Acad. Sci. U.S.A.*, 79(4): 1129–1133, 1982.

D. Adalsteinsson, D. McMillen, and T. Elston. Biochemical network stochastic simulator (bionets): software for stochastic modeling of biochemical networks. *BMC bioinformatics*, 5(1):24, 2004.

D. D. Álamo and F. Schweisguth. Notch signalling: Receptor Cis-inhibition to achieve directionality. *Curr Biol*, 19(16):R683–R684, 2009.

B. Alberts, A. Johnson, J. Lewis, M. Raff, R. K., and W. P. *Molecular Biology of the Cell*. New York: Garland Science, 5th edition, 2008.

U. Alon. Network motifs: theory and experimental approaches. *Nat. Rev. Genet.*, 8(6):450–461, 2007a.

U. Alon. *Introduction to systems biology. Design principles of biological circuits*. Chapman & Hall/CRC, 2007b.

E. R. Andersson, R. Sandberg, and U. Lendahl. Notch signaling: simplicity in design, versatility in function. *Development*, 138(17):3593–3612, 2011.

S. Artavanis-Tsakonas, M. Rand, and R. Lake. Notch signaling: cell fate control and signal integration in development. *Science*, 284(5415):770, 1999.

P. Ashwin and A. Zaikin. Pattern selection: the importance of "how you get there". *Biophys. J.*, 108(6):1307–1308, 2015.

N. Q. Balaban, J. Merrin, R. Chait, L. Kowalik, and S. Leibler. Bacterial persistence as a phenotypic switch. *Science*, 305(5690):1622–1625, 2004.

G. Balazsi, A. van Oudenaarden, and J. J. Collins. Cellular decision making and biological noise: from microbes to mammals. *Cell*, 144(6):910–925, 2011.

O. Barad, E. Hornstein, and N. Barkai. Robust selection of sensory organ precursors by the Notch-Delta pathway. *Curr Opin Cell Biol*, 23(6):663–7, 2011.

B. L. Bassler and R. Losick. Bacterially speaking. *Cell*, 125(2):237–246, 2006.

H. J. Beaumont, J. Gallie, C. Kost, G. C. Ferguson, and P. B. Rainey. Experimental evolution of bet hedging. *Nature*, 462(7269):90–93, 2009.

A. Becskei and L. Serrano. Engineering stability in gene networks by autoregulation. *Nature*, 405(6786):590–593, 2000.

U. S. Bhalla, P. T. Ram, and R. Iyengar. Map kinase phosphatase as a locus of flexibility in a mitogen-activated protein kinase signaling network. *Science*, 297(5583):1018–1023, 2002.

J. T. Bousema, P. Schneider, L. C. Gouagna, C. J. Drakeley, A. Tostmann, R. Houben, J. I. Githure, R. Ord, C. J. Sutherland, S. A. Omar, and R. W. Sauerwein. Moderate effect of artemisinin-based combination therapy on transmission of Plasmodium falciparum. *J. Infect. Dis.*, 193(8):1151–1159, 2006.

T. Bousema and C. Drakeley. Epidemiology and infectivity of Plasmodium falciparum and Plasmodium vivax gametocytes in relation to malaria control and elimination. *Clin. Microbiol. Rev.*, 24(2):377–410, 2011.

O. Carrillo, M. Ibañes, J. García-Ojalvo, J. Casademunt, and J. Sancho. Intrinsic noise-induced phase transitions: Beyond the noise interpretation. *Pysical Review E*, 67:046110, 2003.

H. H. Chang, P. Y. Oh, D. E. Ingber, and S. Huang. Multistable and multistep dynamics in neutrophil differentiation. *BMC Cell Biol.*, 7:11, 2006.

H. H. Chang, M. Hemberg, M. Barahona, D. E. Ingber, and S. Huang. Transcriptome-wide noise controls lineage choice in mammalian progenitor cells. *Nature*, 453(7194):544–547, 2008.

T. S. Churcher, T. Bousema, M. Walker, C. Drakeley, P. Schneider, A. L. Ouedraogo, and M. G. Basanez. Predicting mosquito infection from Plasmodium falciparum gametocyte density and estimating the reservoir of infection. *Elife*, 2:e00626, 2013.

M. Cohen, M. Georgiou, N. L. Stevenson, M. Miodownik, and B. Baum. Dynamic filopodia transmit intermittent Delta-Notch signaling to drive pattern refinement during lateral inhibition. *Dev Cell*, 19(1):78–89, 2010.

M. Cohen, B. Baum, and M. Miodownik. The importance of structured noise in the generation of self-organizing tissue patterns through contact-mediated cell-cell signalling. *J R Soc Interface*, 8:787–798, 2011. doi: {10.1098/rsif.2010.0488}.

B. I. Coleman, K. M. Skillman, R. H. Jiang, L. M. Childs, L. M. Altenhofen, M. Ganter, Y. Leung, I. Goldowitz, B. F. Kafsack, M. Marti, M. Llinas, C. O. Buckee, and M. T. Duraisingh. A Plasmodium falciparum histone deacetylase regulates antigenic variation and gametocyte conversion. *Cell Host Microbe*, 16(2):177–186, 2014.

J. R. Collier, N. A. Monk, P. K. Maini, and J. H. Lewis. Pattern formation by lateral inhibition with feedback: a mathematical model of Delta-Notch intercellular signalling. *J Theor Biol*, 183(4):429–46, 1996.

W. E. Collins and G. M. Jeffery. A retrospective examination of sporozoite- and trophozoite-induced infections with Plasmodium falciparum: development of parasitologic and clinical immunity during primary infection. *Am. J. Trop. Med. Hyg.*, 61(1 Suppl):4–19, 1999.

F. Corson and E. D. Siggia. Geometry, epistasis, and developmental patterning. *Proc. Natl. Acad. Sci. U.S.A.*, 109(15):5568–5575, 2012.

L. Crooks. Problems with continuous-time malaria models in describing gametocytogenesis. *Parasitology*, 135(8):881–896, 2008.

M. Cross and H. Greenside. *Pattern formation and dynamics in nonequilibrium systems*. Cambridge University Press New York, 2009.

E. H. Davidson. Emerging properties of animal gene regulatory networks. *Nature*, 468(7326):911–920, 2010.

C. M. De Moraes, N. M. Stanczyk, H. S. Betz, H. Pulido, D. G. Sim, A. F. Read, and M. C. Mescher. Malaria-induced changes in host odors enhance mosquito attraction. *Proc. Natl. Acad. Sci. U.S.A.*, 111(30):11079–11084, 2014.

M. Eddison, I. L. Roux, and J. Lewis. Notch signaling in the development of the inner ear: lessons from Drosophila. *Proc Natl Acad Sci USA*, 97:11692–11699, 2000.

M. Eichner, H. H. Diebner, L. Molineaux, W. E. Collins, G. M. Jeffery, and K. Dietz. Genesis, sequestration and survival of Plasmodium falciparum gametocytes: parameter estimates from fitting a model to malariatherapy data. *Trans. R. Soc. Trop. Med. Hyg.*, 95(5):497–501, 2001.

M. B. Elowitz, A. J. Levine, E. D. Siggia, and P. S. Swain. Stochastic gene expression in a single cell. *Science*, 297(5584):1183–1186, 2002.

B. Ermentrout. Stripes or spots? nonlinear effects in bifurcation of reaction-diffusion equations on the square. *Proceedings: Mathematical and Physical Sciences*, 434(1891):413–417, 1991.

J. E. Ferrell. Bistability, bifurcations, and waddington's epigenetic landscape. *Current Biology*, 22(11):R458–R466, 2012.

J. E. Ferrell and E. M. Machleder. The biochemical basis of an all-or-none cell fate switch in Xenopus oocytes. *Science*, 280(5365):895–898, 1998.

U.-M. Fiuza, T. Klein, A. M. Arias, and P. Hayward. Mechanisms of ligand-mediated inhibition in Notch signaling activity in Drosophila. *Dev Dyn*, 239 (3):798–805, 2010.

R. J. Fleming, K. Hori, A. Sen, G. V. Filloramo, J. M. Langer, R. A. Obar, S. Artavanis-Tsakonas, and A. C. Maharaj-Best. An extracellular region of Serrate is essential for ligand-induced Cis-inhibition of Notch signaling. *Development*, 140(9):2039–49, 2013.

P. Formosa-Jordan and M. Ibañes. Diffusible ligand and lateral inhibition dynamics for pattern formation. *J Stat Mech*, P03019, 2009.

P. Formosa-Jordan and M. Ibañes. Competition in Notch signaling with Cis enriches cell fate decisions. *PLoS ONE*, 9(4):e95744, 2014.

P. Formosa-Jordan, M. Ibañes, S. Ares, and J. Frade. Regulation of neuronal differentiation at the neurogenic wavefront. *Development*, 139(13):2321–2329, 2012.

P. Formosa-Jordan, M. Ibañes, S. Ares, and J.-M. Frade. Lateral inhibition and neurogenesis: novel aspects in motion. *Int J Dev Biol*, 57(5):341–50, 2013.

D. Frigola, L. Casanellas, J. Sancho, and M. Ibañes. Asymmetric stochastic switching driven by intrinsic molecular noise. *PLoS ONE*, 7(2):e31407, 2012.

J. Garcia-Ojalvo. Physical approaches to the dynamics of genetic circuits: a tutorial. *Contemporary Physics*, 52(5):439–464, 2011.

C. Gardiner. *Stochastic processes in physics and chemistry*. Springer, 3rd edition, 2005.

A. Gierer and H. Meinhardt. A theory of biological pattern formation. *Kybernetik*, 12(1):30–39, 1972.

Gilbert, SF. *Developmental Biology*. Sinauer Associates, 10th edition, 2006.

D. Gillespie. Exact stochastic simulation of coupled chemical reactions. *J Phys Chem*, 81(25):2340–2361, 1977.

D. Gillespie. The chemical langevin equation. *J. Chem. Phys.*, 113:297, 2000.

T. G. Graham, S. M. Tabei, A. R. Dinner, and I. Rebay. Modeling bistable cell-fate choices in the Drosophila eye: qualitative and quantitative perspectives. *Development*, 137(14):2265–2278, 2010.

J. B. Green and J. Sharpe. Positional information and reaction-diffusion: two big ideas in developmental biology combine. *Development*, 142(7):1203–1211, 2015.

R. Guantes and J. F. Poyatos. Multistable decision switches for flexible control of epigenetic differentiation. *PLoS Comput. Biol.*, 4(11):e1000235, 2008.

C. A. Guerra, R. E. Howes, A. P. Patil, P. W. Gething, T. P. Van Boeckel, W. H. Temperley, C. W. Kabaria, A. J. Tatem, B. H. Manh, I. R. Elyazar, J. K. Baird, R. W. Snow, and S. I. Hay. The international limits and population at risk of Plasmodium vivax transmission in 2009. *PLoS Negl Trop Dis*, 4(8): e774, 2010.

H. Hamada, M. Watanabe, H. E. Lau, T. Nishida, T. Hasegawa, D. M. Parichy, and S. Kondo. Involvement of Delta/Notch signaling in zebrafish adult pigment stripe patterning. *Development*, 141(2):318–24, 2014.

P. Heitzler and P. Simpson. Altered epidermal growth factor-like sequences provide evidence for a role of Notch as a receptor in cell fate decisions. *Development*, 117(3):1113–23, 1993.

T. Hong, J. Xing, L. Li, and J. J. Tyson. A mathematical model for the reciprocal differentiation of t helper 17 cells and induced regulatory t cells. *PLoS computational biology*, 7(7):e1002122, 2011.

T. Hong, J. Xing, L. Li, and J. J. Tyson. A simple theoretical framework for understanding heterogeneous differentiation of cd4+ t cells. *BMC systems biology*, 6(1):66, 2012.

S. Huang. Reprogramming cell fates: reconciling rarity with robustness. *Bioessays*, 31(5):546–560, 2009.

S. Huang, Y. P. Guo, G. May, and T. Enver. Bifurcation dynamics in lineage-commitment in bipotent progenitor cells. *Dev. Biol.*, 305(2):695–713, 2007.

K. Ishimatsu, T. Hata, A. Mochizuki, R. Sekine, M. Yamamura, and D. Kiga. General applicability of synthetic gene-overexpression for cell-type ratio control via reprogramming. *ACS synthetic biology*, 3(9):638–644, 2013.

T. L. Jacobsen, K. Brennan, A. M. Arias, and M. A. Muskavitch. Cis-interactions between Delta and Notch modulate neurogenic signalling in Drosophila. *Development*, 125(22):4531–40, 1998.

B. F. Kafsack, N. Rovira-Graells, T. G. Clark, C. Bancells, V. M. Crowley, S. G. Campino, A. E. Williams, L. G. Drought, D. P. Kwiatkowski, D. A. Baker, A. Cortes, and M. Llinas. A transcriptional switch underlies commitment to sexual development in malaria parasites. *Nature*, 507(7491):248–252, 2014.

T. Kalmar, C. Lim, P. Hayward, S. Munoz-Descalzo, J. Nichols, J. Garcia-Ojalvo, and A. Martinez Arias. Regulated fluctuations in nanog expression mediate cell fate decisions in embryonic stem cells. *PLoS Biol.*, 7(7):e1000149, 2009.

S. Kauffman. Homeostasis and differentiation in random genetic control networks. *Nature*, 224(5215):177–178, 1969a.

S. A. Kauffman. Metabolic stability and epigenesis in randomly constructed genetic nets. *J. Theor. Biol.*, 22(3):437–467, 1969b.

D. B. Kearns and R. Losick. Cell population heterogeneity during growth of Bacillus subtilis. *Genes Dev.*, 19(24):3083–3094, 2005.

A. Koseska, A. Zaikin, J. Kurths, and J. García-Ojalvo. Timing cellular decision making under noise via cell-cell communication. *PLoS ONE*, 4(3):e4872, 2009.

A. Kuchina, L. Espinar, J. Garcia-Ojalvo, and G. M. Suel. Reversible and noisy progression towards a commitment point enables adaptable and reliable cellular decision-making. *PLoS Comput. Biol.*, 7(11):e1002273, 2011.

L. Lebon, T. V. Lee, H. Jafar-Nejad, D. Sprinzak, and M. B. Elowitz. Fringe proteins modulate Notch-ligand Cis and Trans interactions to specify signaling states. *eLife Sciences*, 3, 2014.

K. Lewis. Persister cells, dormancy and infectious disease. *Nat. Rev. Microbiol.*, 5(1):48–56, 2007.

C.-M. Lin, T. X. Jiang, R. E. Baker, P. K. Maini, R. B. Widelitz, and C.-M. Chuong. Spots and stripes: pleomorphic patterning of stem cells via p-erk-dependent cell chemotaxis shown by feather morphogenesis and mathematical simulation. *Dev Biol*, 334(2):369–82, 2009.

D. Lopez, H. Vlamakis, and R. Kolter. Generation of multiple cell types in Bacillus subtilis. *FEMS Microbiol. Rev.*, 33(1):152–163, 2009.

R. Losick and C. Desplan. Stochasticity and cell fate. *Science*, 320(5872):65–68, 2008.

M. Lu, M. K. Jolly, R. Gomoto, B. Huang, J. Onuchic, and E. Ben-Jacob. Tristability in cancer-associated microrna-tf chimera toggle switch. *The Journal of Physical Chemistry B*, 117(42):13164–13174, 2013.

D. K. Lubensky, M. W. Pennington, B. I. Shraiman, and N. E. Baker. A dynamical model of ommatidial crystal formation. *Proc Natl Acad Sci USA*, 108(27):11145–50, 2011.

H. Maamar and D. Dubnau. Bistability in the Bacillus subtilis K-state (competence) system requires a positive feedback loop. *Mol. Microbiol.*, 56(3): 615–624, 2005.

H. Maamar, A. Raj, and D. Dubnau. Noise in gene expression determines cell fate in Bacillus subtilis. *Science*, 317(5837):526–529, 2007.

C. K. Machens, R. Romo, and C. D. Brody. Flexible control of mutual inhibition: a neural model of two-interval discrimination. *Science*, 307(5712):1121–1124, 2005.

L. Marcon and J. Sharpe. Turing patterns in development: what about the horse part? *Curr Opin Genet Dev*, 22(6):578–84, 2012.

M. N. McClean, A. Mody, J. R. Broach, and S. Ramanathan. Cross-talk and decision making in map kinase pathways. *Nature genetics*, 39(3):409–414, 2007.

F. E. McKenzie and W. H. Bossert. The optimal production of gametocytes by Plasmodium falciparum. *J. Theor. Biol.*, 193(3):419–428, 1998.

F. E. McKenzie and W. H. Bossert. An integrated model of Plasmodium falciparum dynamics. *J. Theor. Biol.*, 232(3):411–426, 2005.

Meinhardt, H. *Models of biological pattern formation*. London Academic Press, 1982.

H. M. Meyer and A. H. Roeder. Stochasticity in plant cellular growth and patterning. *Front Plant Sci*, 5:420, 2014.

N. Mideo and T. Day. On the evolution of reproductive restraint in malaria. *Proc. Biol. Sci.*, 275(1639):1217–1224, 2008.

T. Mikeladze-Dvali, M. F. Wernet, D. Pistillo, E. O. Mazzoni, A. A. Teleman, Y. W. Chen, S. Cohen, and C. Desplan. The growth regulators warts/lats and melted interact in a bistable loop to specify opposite fates in Drosophila R8 photoreceptors. *Cell*, 122(5):775–787, 2005.

A. C. Miller, E. L. Lyons, and T. G. Herman. Cis-inhibition of Notch by endogenous Delta biases the outcome of lateral inhibition. *Curr Biol*, 19(16): 1–6, 2009.

P. Mombaerts. Odorant receptor gene choice in olfactory sensory neurons: the one receptor-one neuron hypothesis revisited. *Curr. Opin. Neurobiol.*, 14(1): 31–36, 2004.

L. G. Morelli, K. Uriu, S. Ares, and A. C. Oates. Computational approaches to developmental patterning. *Science*, 336(6078):187–191, 2012.

I. Mueller, M. R. Galinski, J. K. Baird, J. M. Carlton, D. K. Kochar, P. L. Alonso, and H. A. del Portillo. Key gaps in the knowledge of Plasmodium vivax, a neglected human malaria parasite. *Lancet Infect Dis*, 9(9):555–566, 2009.

J. Murray. *Mathematical Biology*. Springer, New York, 2002.

Y. Narui and K. Salaita. Membrane tethered delta activates notch and reveals a role for spatio-mechanical regulation of the signaling pathway. *Biophys. J.*, 105(12):2655–2665, Dec 2013.

N. R. Nene and A. Zaikin. Interplay between path and speed in decision making by high-dimensional stochastic gene regulatory networks. *PLoS ONE*, 7(7): e40085, 2012.

N. R. Nené and A. Zaikin. Decision making in noisy bistable systems with time-dependent asymmetry. *Phys. Rev. E*, 87:12715, 2013.

N. R. Nené, J. Garca-Ojalvo, and A. Zaikin. Speed-dependent cellular decision making in nonequilibrium genetic circuits. *PLoS ONE*, 7(3):e32779, 2012.

J. Neves, G. Abelló, J. Petrovic, and F. Giraldez. Patterning and cell fate in the inner ear: a case for Notch in the chicken embryo. *Dev Growth Differ*, 55 (1):96–112, 2012.

A. C. Oates, L. G. Morelli, and S. Ares. Patterning embryos with oscillations: structure, function and dynamics of the vertebrate segmentation clock. *Development*, 139(4):625–39, 2012.

O'Dea, R. D. and King, J. R. Multiscale analysis of pattern formation via intercellular signalling. *Math Biosci*, 231(2):172–185, 2011.

O'Dea, R. D. and King, J. R. Continuum limits of pattern formation in hexagonal-cell monolayers. *J Math Biol*, 64(3):579–610, 2012.

A. L. Ouedraogo, T. Bousema, P. Schneider, S. J. de Vlas, E. Ilboudo-Sanogo, N. Cuzin-Ouattara, I. Nebie, W. Roeffen, J. P. Verhave, A. J. Luty, and R. Sauerwein. Substantial contribution of submicroscopical Plasmodium falciparum gametocyte carriage to the infectious reservoir in an area of seasonal transmission. *PLoS ONE*, 4(12):e8410, 2009.

D. Palau-Ortin, P. Formosa-Jordan, J. M. Sancho, and M. Ibañes. Pattern selection by dynamical biochemical signals. *Biophysical journal*, 108(6):1555–1565, 2015.

V. Panin, V. Papayannopoulos, R. Wilson, and K. Irvine. Fringe modulates Notch-ligand interactions. *Nature*, 387(6636):908–912, 1997.

T. J. Perkins and P. S. Swain. Strategies for cellular decision-making. *Mol. Syst. Biol.*, 5:326, 2009.

J. Petrovic, P. Formosa-Jordan, J. Luna-Escalante, G. Abelló, M. Ibañes, J. Neves, and F. Giraldez. Ligand-dependent Notch signaling strength orchestrates lateral induction and lateral inhibition in the developing inner ear. *Development*, 141:2313–2324, 2014.

B. Pfeuty. Dynamical principles of cell-cycle arrest: Reversible, irreversible, and mixed strategies. *Physical Review E*, 86(2):021917, 2012.

B. Pfeuty and K. Kaneko. The combination of positive and negative feedback loops confers exquisite flexibility to biochemical switches. *Physical biology*, 6 (4):046013, 2009.

C. S. Rao and A. P. Arkin. Stochastic chemical kinetics and the quasi-steady-state assumption: Application to the Gillespie algorithm. *J Chem Phys*, 118 (11):095105, 2003.

M. Recker, C. O. Buckee, A. Serazin, S. Kyes, R. Pinches, Z. Christodoulou, A. L. Springer, S. Gupta, and C. I. Newbold. Antigenic variation in Plasmodium falciparum malaria involves a highly structured switching pattern. *PLoS Pathog.*, 7(3):e1001306, 2011.

P. Rue and J. Garcia-Ojalvo. Modeling gene expression in time and space. *Annu Rev Biophys*, 42:605–627, 2013.

K. Sakamoto, O. Ohara, M. Takagi, S. Takeda, and K. Katsube. Intracellular cell-autonomous association of Notch and its ligands: A novel mechanism of Notch signal modification. *Dev Biol*, 241(2):313–326, 2002.

I. Salazar-Ciudad, J. Jernvall, and S. A. Newman. Mechanisms of pattern formation in development and evolution. *Development*, 130(10):2027–2037, 2003.

P. Schneider, J. T. Bousema, L. C. Gouagna, S. Otieno, M. van de Vegte-Bolmer, S. A. Omar, and R. W. Sauerwein. Submicroscopic Plasmodium falciparum gametocyte densities frequently result in mosquito infection. *Am. J. Trop. Med. Hyg.*, 76(3):470–474, 2007.

R. Schwanbeck, S. Martini, K. Bernoth, and U. Just. The Notch signaling pathway: molecular basis of cell context dependency. *Eur. J. Cell Biol.*, 90 (6-7):572–581, 2011.

H. Shoji, Y. Iwasa, and S. Kondo. Stripes, spots, or reversed spots in two-dimensional turing systems. *J Theor Biol*, 224(3):339–350, 2003.

D. S. A. Simakov and L. M. Pismen. Discrete model of periodic pattern formation through a combined autocrine-juxtacrine cell signaling. *Phys Biol*, 10 (4):046001, 2013.

C. Sokolik, Y. Liu, D. Bauer, J. McPherson, M. Broeker, G. Heimberg, L. S. Qi, D. A. Sivak, and M. Thomson. Transcription factor competition allows embryonic stem cells to distinguish authentic signals from noise. *Cell Syst*, 1 (2):117–129, 2015.

D. Sprinzak, A. Lakhanpal, L. Lebon, L. A. Santat, M. E. Fontes, G. A. Anderson, J. Garcia-Ojalvo, and M. B. Elowitz. Cis-interactions between Notch and Delta generate mutually exclusive signalling states. *Nature*, 465(7294): 86–90, 2010.

D. Sprinzak, A. Lakhanpal, L. LeBon, J. Garcia-Ojalvo, and M. B. Elowitz. Mutual inactivation of Notch receptors and ligands facilitates developmental patterning. *PLoS Comput. Biol.*, 7(6):e1002069, 2011.

W. Stone, B. P. Goncalves, T. Bousema, and C. Drakeley. Assessing the infectious reservoir of falciparum malaria: past and future. *Trends Parasitol.*, 31 (7):287–296, 2015.

M. Strasser, F. J. Theis, and C. Marr. Stability and multiattractor dynamics of a toggle switch based on a two-stage model of stochastic gene expression. *Biophysical journal*, 102(1):19–29, 2012.

S. Strogatz. *Nonlinear dynamics and chaos (with applications to physics, biology, chemistry, and engineering)*. Westview Press, 1994.

G. M. Suel, J. Garcia-Ojalvo, L. M. Liberman, and M. B. Elowitz. An excitable gene regulatory circuit induces transient cellular differentiation. *Nature*, 440 (7083):545–550, 2006.

G. M. Suel, R. P. Kulkarni, J. Dworkin, J. Garcia-Ojalvo, and M. B. Elowitz. Tunability and noise dependence in differentiation dynamics. *Science*, 315 (5819):1716–1719, 2007.

T. Tian and K. Burrage. Stochastic models for regulatory networks of the genetic toggle switch. *Proc. Natl. Acad. Sci. U.S.A.*, 103(22):8372–8377, 2006.

A. Turing. The chemical basis of morphogenesis. *B Math Biol*, 52(1):153–197, 1952.

J. J. Tyson and B. Novak. Functional motifs in biochemical reaction networks. *Annu Rev Phys Chem*, 61:219–240, 2010.

J. J. Tyson, K. C. Chen, and B. Novak. Sniffers, buzzers, toggles and blinkers: dynamics of regulatory and signaling pathways in the cell. *Curr. Opin. Cell Biol.*, 15(2):221–231, 2003.

N. Van Kampen. *Handbook of Stochastic Methods for Physics, Chemistry, and the Natural Sciences*. North-Holland Personal Library, 3rd edition, 2007.

D. Vasiliauskas, R. Johnston, and C. Desplan. Maintaining a stochastic neuronal cell fate decision. *Genes Dev.*, 23(4):385–390, 2009.

B. Verd, A. Crombach, and J. Jaeger. Classification of transient behaviours in a time-dependent toggle switch model. *BMC systems biology*, 8(1):43, 2014.

C. H. Waddington. *The strategy of the genes*. George Allen & Unwin, 1957.

H. Wearing and J. Sherratt. Nonlinear analysis of juxtacrine patterns, 2001.

M. Weber and J. Buceta. Noise regulation by quorum sensing in low mRNA copy number systems. *BMC Syst Biol*, 5:11, 2011.

M. Weber and J. Buceta. Dynamics of the quorum sensing switch: stochastic and non-stationary effects. *BMC Syst Biol*, 7:6, 2013.

S. L. Werner, D. Barken, and A. Hoffmann. Stimulus specificity of gene expression programs determined by temporal control of ikk activity. *Science*, 309 (5742):1857–1861, 2005.

M. F. Wernet, E. O. Mazzoni, A. Celik, D. M. Duncan, I. Duncan, and C. Desplan. Stochastic spineless expression creates the retinal mosaic for colour vision. *Nature*, 440(7081):174–180, 2006.

K. Wiesenfeld and F. Moss. Stochastic resonance and the benefits of noise: from ice ages to crayfish and SQUIDs. *Nature*, 373(6509):33–36, Jan 1995.

D. J. Wilkinson, A. Johnson, J. Lewis, M. Raff, R. K., and W. P. *Stochastic modelling for systems biology.* Capman & Hall/CRC, London, 2006.

C. P. Wolk. Heterocyst formation. *Annu. Rev. Genet.*, 30:59–78, 1996.

L. Wolpert. Positional information and the spatial pattern of cellular differentiation. *J. Theor. Biol.*, 25(1):1–47, 1969.

L. Wolpert. Positional information and pattern formation. *Curr. Top. Dev. Biol.*, 6(6):183–224, 1971.

K.-F. Wong and X.-J. Wang. A recurrent network mechanism of time integration in perceptual decisions. *The Journal of neuroscience*, 26(4):1314–1328, 2006.

W. Xiong and J. E. Ferrell. A positive-feedback-based bistable 'memory module' that governs a cell fate decision. *Nature*, 426(6965):460–465, 2003.